THE UNIVERSITY OF CHICAGO

THE ROLES OF THE PLANAR CELL POLARITY MOLECULES PRICKLE1A AND PRICKLE1B IN ZEBRAFISH CRANIAL NEURAL CREST

A DISSERTATION SUBMITTED TO

THE FACULTY OF THE DIVISION OF THE BIOLOGICAL SCIENCES

AND THE PRITZKER SCHOOL OF MEDICINE

IN CANDIDACY FOR THE DEGREE OF

DOCTOR OF PHILOSOPHY

COMMITTEE ON DEVELOPMENT, REGENERATION, AND STEM CELL

BIOLOGY

BY

KAMIL AHSAN

CHICAGO, ILLINOIS

DECEMBER 2018

TABLE OF CONTENTS

LIST OF FIGURES

SUPPLEMENTAL FILES

Supplemental files available upon request. Please contact kamilahsan@uchicago.edu to request.

ACKNOWLEDGMENTS

For my deep and abiding love for Developmental Biology, I am grateful to all my teachers and colleagues, past and present. My professors at the *Lahore University of Management Sciences* (LUMS), particularly Dr. Muhammad Tariq, laid the seeds for my curiosity. It is remarkable how rigorous and well-rounded my undergraduate training was at LUMS. I had the fortune of being surrounded by the most ambitious—and to this day, the smartest—peers I've ever met. I have never worked harder than I did then.

The single best decision I made during graduate school was to join Dr. Victoria Prince's lab. Her down-to-earth sensibility has proven to be the most crucial aspect of my relationship with her. She has given me lessons of academic practice I value most: on honesty, stamina, curiosity, and an almost-unheard-of willingness to let me chart my own path. I hope more scientists—in the rapidly-changing academic market—heed her example. Thank you, too, to Dr. Robert Ho for being a sort of deputy advisor to me, and to all those in the Prince and Ho labs, including Alana, Crystal, Lindsey, Haley, Adam, Erin, Sarah, Violet, Stephanie, Jessie, Gökhan, and Vish. Thank you Noor, for constantly putting me at ease, thank you Christina for making work the best part of my day; thanks, both of you, for being the best collaborators and friends I could ask for. Thank you Ana: I've met my match in you. Thank you Manny for generosity of spirit; never change. Thank

you to my lightning-in-a-bottle crew: Chris, Claire, and Younan. I'm very lucky to have you.

Thank you to my thesis committee: my chair, Dr. Edwin Munro, Dr. Clifton Ragsdale, Dr. Richard Fehon, and Dr. Ankur Saxena for demanding more from me than one would from a known imposter. When I asked them to be part of my committee, in a state of blind ambition, I asked those who I felt would be tough on me. And while that has occasionally led to some consternation on my part, it turns out my initial instinct was the right one. Thank you all, for asking the right questions, and demanding the answers from me. Ed, thank you for maintaining a healthy skepticism—as it should be. Rick, thank you for giving me the gift of Planar Cell Polarity. Cliff, thank you for being my advocate when I wanted to work on neural crest, and thank you for *not* being my advocate when I wanted to work on Rest. And thank you, Ankur, for all the above, and for having my back.

Thank you, as well, to my numerous communities on and off campus. To faculty in the *Committee on Development, Regeneration & Stem Cell Biology,* especially Dr. Edwin (Chip) Ferguson and Dr. Sally Horne-Badovinac. I have also had the luxury of being a part of another academic collective: *the Committee on Historical & Conceptual Studies of Science*. Thanks to my MA advisor, Dr. Fredrik Albritton Jonsson. Thank you to my fellow graduate student workers in the Graduate Student Union (GSU) for giving shape

to the word ‘solidarity’. Thanks to my closest comrades: Sharvari, Sneha, Susie, Sally, Yana, Mario, Mashail, Maira, Mohsin, Katie, Usama, and Benjamin.

Thank you to the family I have chosen, and have spent far too much time away from: Zoya, Wijdan, Wafa, Mehek, Nimra, Mehru, Hassan, Kanwal, Maheen, Anum, Haris, Zain, Nayab, and Aisha. I love you all. Thank you for constantly commenting on how voracious my ambitions are, and then reminding me that it’s a good thing.

And finally, thank you to the family I’ve been born into. My mother, for holding out an umbrella over me through my breezy life while standing in the rain. My older sister and brother, Nadia and Omar, for giving me a template of selfhood. And thank you to my brother-in-law, Faisal, and my beautiful niece, Lyla. You are all the warmth I will ever need.

Here we go round the prickly pear.

ABSTRACT

In this dissertation, I will discuss my investigation into the roles of two molecules, zebrafish Prickle1b and Prickle1a, part of a suite of proteins called Planar Cell Polarity (PCP) proteins, in the specific context of a multipotent stem cell population, the neural crest. Neural crest cells have been likened to metastatic cancer cells in how they invade regions of the developing embryo by traversing large distances and subsequently differentiating into many different cell types. PCP proteins are known to behave in a variety of different contexts in both *Drosophila melanogaster* and vertebrate model systems, and although two other PCP proteins have been investigated in the cranial sub-population of the migrating neural crest in vertebrates, this is the first investigation into the roles of the *pk1* paralogous genes, or any PCP genes, broadly during neural crest development including well before crest cells begin their migration. I demonstrate that not only are zebrafish Pk1b and Pk1a required for cranial neural crest migration, they are additionally required in a process that precedes migration: an epithelial-to-mesenchymal transition (EMT) that occurs in neural crest cells and many other cell types in both vertebrate and invertebrate developing embryos. EMT allows neuroepithelial cells within the developing neural tube to transition to cells that lie outside the neural tube and eventually migrate away to different locations in developing embryos. By showing that the zebrafish PCP Pk1 proteins regulate specific morphological transitions during EMT

that are required for neural crest cells to migrate away from their initial location, as well as during migration itself, at least partly through the regulation of the levels of two members of the Cadherin-family of adhesion molecules, I demonstrate roles for the PCP Pk1 molecules broadly during neural crest development through a hitherto-unrecognized function of PCP signaling during the process of EMT.

CHAPTER 1

THE NEURAL CREST AND PLANAR CELL POLARITY

1.1 Introduction to the neural crest

1.1.1 The evolution and development of neural crest

The neural crest (NC) is an embryonic, transient, multipotent cell population that is capable of giving rise to numerous different cell types, including the cartilage and bone of the craniofacial skeleton, melanocytes, smooth muscle, and components of the peripheral nervous system including sensory, enteric, and sympathetic neurons as well as glia (Fig 1.1). As a result, neural crest cells (NCCs) contribute to a great deal of the vertebrate body plan (Donoghue et al., 2008; Hall, 2000; Le Douarin and Kalcheim, 1999), and are critical to the evolution of the vertebrate cephalic region (Gans and Northcutt, 1983). The cephalic neural crest, or the cranial neural crest, is the subject of this dissertation.

The neural crest is unique to vertebrates, although it shares certain cell types with non-vertebrate chordates (Bronner and LeDouarin, 2012; Green et al., 2015). For instance, in the tunicate *Ciona intestinalis*, the melanocyte lineage arises from cells at the margins of the neural plate, and expresses genes that are known to be part of the neural crest specification module in vertebrate model systems, like Snail, Twist, Ets, FoxD as well as Wnt-signaling broadly (Abitua et al., 2012). Further, misexpression of Twist could 'reprogram' these melanocyte precursors into ectomesenchymal-like cells. To my knowledge, these melanocyte precursors are the closest homologs to the vertebrate neural

crest that have been demonstrated in non-vertebrate systems, suggesting that both a melanocyte precursor and the gene regulatory network (GRN) operating in the

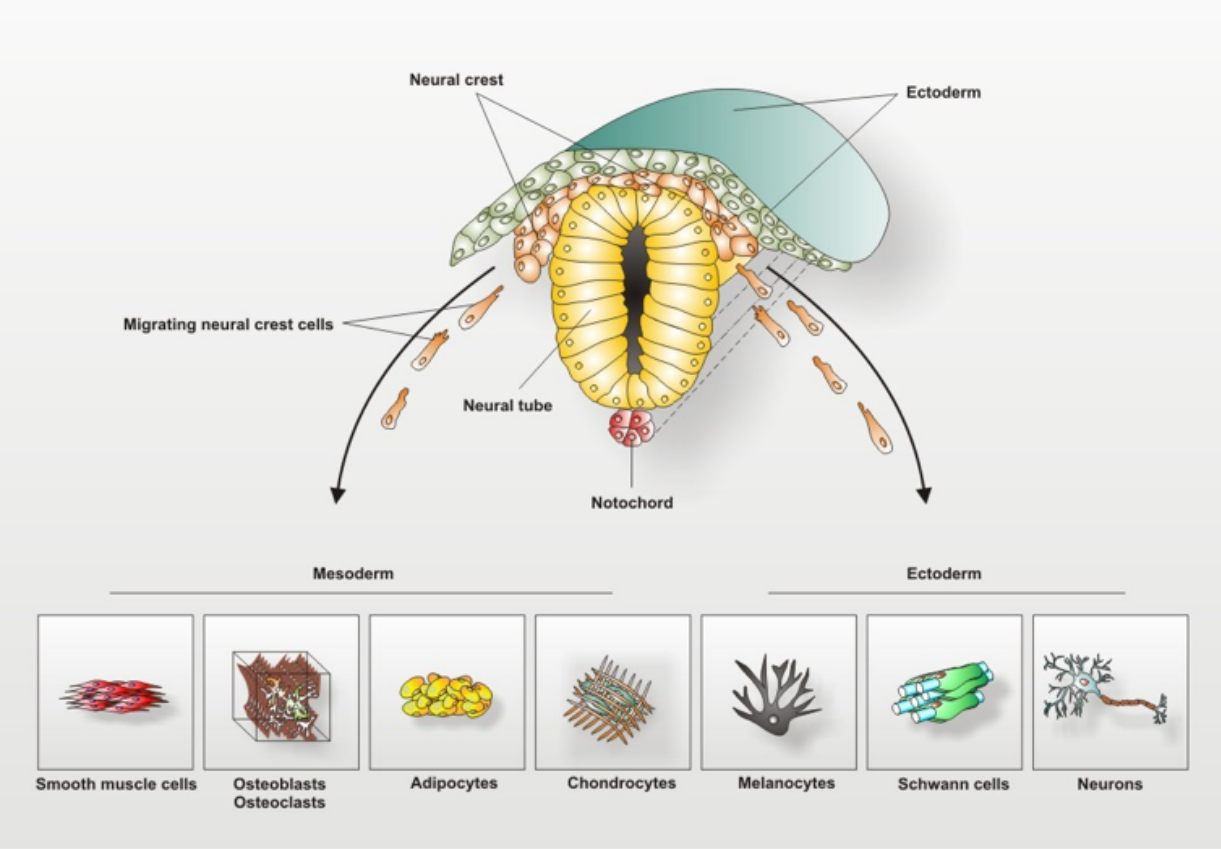

Fig. 1.1: The neural crest and its derivatives

melanocyte precursor were present in the last common ancestor of tunicates and vertebrates. Similar to the seemingly-sudden appearance of neural crest in vertebrates which has now been revised due to new observations in tunicates, neurogenic placodes have also long been thought to be a vertebrate innovation, and like with neural crest, the tunicate *Ciona intestinalis* seems to have a "proto-placodal ectoderm" with expression of the transcription factor Six1/2 (the mutation of Six1, in humans, causes craniofacial

defects (Ruf et al., 2004)) and its co-factor Eya which are known to be required as part of the regulatory module of neurogenic placodes in vertebrates (Abitua et al., 2015; Steventon et al., 2014). Regardless, it still seems that the vertebrate lineage saw an extensive addition of roles and properties to neural crest precursors at nearly every axial level, thus allowing for bona fide neural crest which can give rise to the structural elements of the head, peripheral nervous system, pigment cells etc. thus imbuing the neural crest with a far more extensive developmental potential—and migratory ability—than in pre-vertebrate forms (Green et al., 2015).

The historical discussion around neural crest has, thus, been characterized by its unique and innovative properties. Noden and Schneider (2006) state that since their discovery, NCCs have moved from the "category of renegade intra-embryonic wanderers to achieve rebel status" (Noden and Schneider, 2006). Indeed, the neural crest is often referred to as the 'fourth germ layer' or the 'ectomesenchyme' (Hall, 2000) because of the derived cell types it forms that were traditionally thought to arise from the ectoderm or mesoderm. As stated above, it has been studied extensively in part because of its developmental plasticity (Le Douarin et al., 2004) but also because both the migration and gene regulatory networks of NCCs have been likened to metastatic cancer cells (Gallik et al., 2017; Gupta and Massague, 2006; Maguire et al., 2015). Indeed, some cancerous cell types share a common gene regulatory network with neural crest: during melanoma initiation

for instance, cells begin to express genes characteristic of undifferentiated neural crest cell identity (Kaufman et al., 2016).

The neural crest arises from the regions bordering the neural plate and is specified at this border region prior to neurulation, the subject of the next section (Fig. 1.2). Briefly, during neurulation, the neural plate undergoes convergence movements, which in teleost embryos drive formation of the neural keel which subsequently produces the neural rod. The neuroepithelial cells then align at the midline to ultimately produce a lumen and the fully formed neural tube (Fig. 1.2) (Clarke, 2009). The neural crest lies at the interface of the developing neural tube and the overlying ectoderm, residing in and migrating from the dorsal aspect of the neural tube (Figs. 1.1, 1.2) over large distances in the embryo along stereotypic pathways (Bronner and LeDouarin, 2012; Theveneau and Mayor, 2011a). Many of these key observations regarding the neural crest were first made using seminal transplantation experiments, both in amphibian embryos (Hörstadius, 1950) and later using quail-chick chimeras (Le Douarin, 1973). These studies established the stereotypic pathways NCCs follow, as well as the cell fates of the NCCs at their target locations.

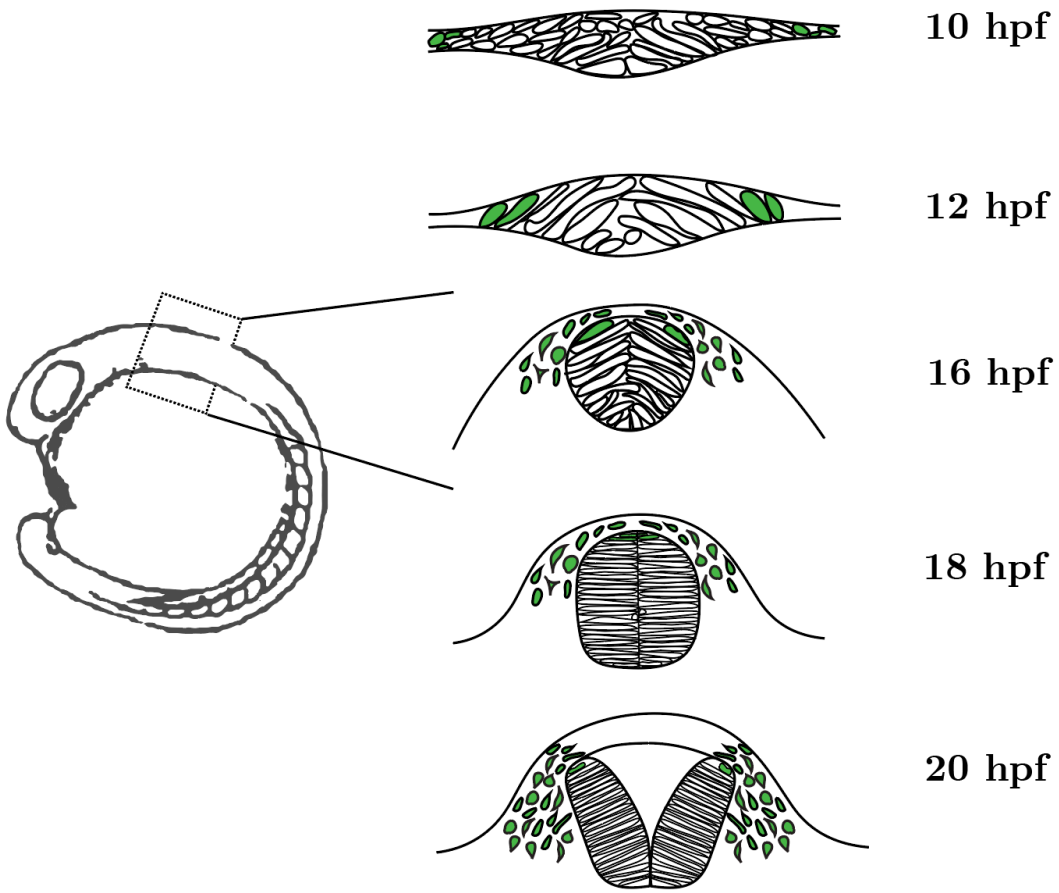

Fig. 1.2: Zebrafish neurulation and cranial neural crest development. Each panel schematizes transverse sections through the hindbrain of the embryo. As stated in the text, neurulation in teleosts differs from the process in amniote vertebrates: Convergence drives the thickening of the neural plate in the ventral direction producing a neural keel, a bonafide midline is then formed, and subsequently the lumen opens. Cells colored green indicate NCCs present at the border of the neural plate, which will migrate from dorsal positions staring as early as the 12 hours post-fertilization (hpf) stage and continuing through 16 hpf and beyond, when the neural keel and then tube have formed.

Due to extensive study of the neural crest and the gene regulatory network that regulates its development (Sauka-Spengler and Bronner-Fraser, 2008), the development of the neural crest can be roughly sub-divided into five key phases: *induction* at the neural plate border, *specification* to establish the pool of NC progenitor cells, an *epithelial-to-mesenchymal transition* (EMT) from the neuroepithelial cells of the neural tube (a process which is sometimes used interchangeably with the term *delamination* which refers to the more general movement of the population of NCCs out of and away from the neural tube), *migration* of NCCs through specific microenvironments and with the help of particular guidance cues, and finally *differentiation* into numerous cell types to form tissues and organs. I will deal with EMT and migration in more detail in the subsequent section.

Two considerations are integral at the outset. The first is that each of these processes has been ascribed slightly differing definitions in different contexts (Theveneau and Mayor, 2012). Further, owing to the gene regulatory pathways that are common to multiple processes during NC development (Simoes-Costa and Bronner, 2015), it is sometimes unclear where the distinction between the end of one process and the beginning of another is set.

The second consideration is that these processes show clear variation both in different organisms and along the antero-posterior axis. Cephalic, or cranial, neural crest follows a

different migratory pattern as compared to the trunk neural crest because of different tissue environments along the axis (Lallier et al., 1992). Further, cranial and trunk neural crest have significantly different differentiation potentials (Huang et al., 2016b). Many of the differences have been found in the gene regulatory programs regulating cranial and trunk neural crest (Simoes-Costa and Bronner, 2015). Indeed, even genes that are commonly-expressed in both cranial and trunk neural crest, often have different regulatory regions acting in each location (Barembaum and Bronner, 2013; Betancur et al., 2010; Simoes-Costa et al., 2014; Simoes-Costa et al., 2012; Tahtakran and Selleck, 2003): the marker Sox-10 for instance, is driven by enhancers specific to the cranial or trunk neural crest as early as the specification of the neural crest, and remains expressed throughout migration (Betancur et al., 2010).

1.1.2. Neurulation and neural crest development

Neurulation is the process by which morphogenetic movements result in the formation in the embryo of the neural tube, which gives rise to the brain and spinal cord. Broadly speaking, the process of neurulation in vertebrates has been described as consisting of two types of neurulation. There is primary neurulation where an organized epithelial substrate thickens to form the neural plate and subsequently folds and rolls up to create a neural tube, and secondary neurulation where mesenchymal cells condense to form a rod and subsequently an epithelial tube from the tail bud to form the posterior neural tube (Colas

and Schoenwolf, 2001; Criley, 1969; Griffith et al., 1992; Lowery and Sive, 2004; Schoenwolf, 1984; Schoenwolf and Delongo, 1980; Schoenwolf and Larsen, 2009). However, this process is highly variable among vertebrates (Colas and Schoenwolf, 2001; Lowery and Sive, 2004). One point at which there is a high level of variability is the way in which the open neural tube is formed (Davidson and Keller, 1999; Morriss-Kay et al., 1994; Peeters et al., 1998). In *Xenopus* embryos, for instance, the open neural tube is formed by a 'smooth rolling' of the epithelium (Davidson and Keller, 1999; Lowery and Sive, 2004). In chick, however, depending on anteroposterior locations, cells can become wedge-shaped and form 'hinge points' such that the resulting neural tube has a diamond-shaped lumen that is comparatively larger than the lumen in another species as well as the lumen in the spinal cord region which is slit-like (Schoenwolf and Delongo, 1980; Smith and Schoenwolf, 1991).

However, neurulation in teleosts occurs differently than in other vertebrates (Lowery and Sive, 2004). In teleosts, in both the brain and trunk region, first a neural keel is formed that subsequently develops a lumen (Fig. 1.2) (Geldmacher-Voss et al., 2003; Reichenbach et al., 1990; Schmitz et al., 1993). In contrast to amniotes, teleost embryos do not form the central lumen by the folding of the epithelial sheet. Instead, cells in the neural rod primordium rearrange and 'cavitate' to form a hollow tube (Fig. 1.2) (Clarke, 2009). Because of the major differences in neurulation in teleosts compared to other vertebrates,

it has historically been difficult to ascribe neurulation at any point along the anteroposterior axis to either primary or secondary neurulation (Geldmacher-Voss et al., 2003; Kimmel et al., 1995; Lowery and Sive, 2004; Miyayama and Fujimoto, 1977; Reichenbach et al., 1990; Strahle and Blader, 1994).

I will deal with the process of neurulation in teleosts chronologically. Work largely in zebrafish as a model organism for teleosts has shown that neurulation begins around 10 hpf. First, the columnar epithelial sheet that forms the neural plate at 10 hpf (Fig. 1.2) thickens, with convergence movements driving its expansion in the ventral direction to form the neural keel. At approximately 16 hpf, the neural keel condenses into a solid neural rod with a distinct midline (Clarke, 2009; Lowery and Sive, 2004). At late neural keel and neural rod stages, cells orient predominantly horizontally along the mediolateral axis and perpendicular to the dorsoventral axis (Fig. 1.2) (Clarke, 2009; Lowery and Sive, 2004). Subsequently, polarized cells divide in a mirror-symmetric fashion such that daughter cells intercalate into opposite sides of the developing neural tube (Clarke, 2009; Tawk et al., 2007). This mirror-symmetric division is termed the "C-division" and it ensures that daughter cells carry mirror-image morphology and apico-basal polarity in such a manner so as not to lie across the midline (Ciruna et al., 2006; Clarke, 2009; Tawk et al., 2007).

Importantly, these cells are polarized *prior* to division using key polarity molecules. Pard3, for instance, localizes to the cleavage furrow and is inherited by both daughter cells—in this way, Pard3 is required for one daughter cell to intercalate into the "contralateral" neuroepithelium (Tawk et al., 2007). Further, neural progenitors also require Wnt/PCP molecules to polarize along the anteroposterior axis. It has been shown that in zebrafish embryos mutant for the PCP gene *vangl2* (trilobite mutants), neural keel cells do not polarize in the mirror-symmetric manner *at the midline* and instead ectopically divide mirror-symmetrically on either side of the midline, causing neural tube defects. PCP signaling is thus required for polarized cell division and rearrangement in order for the subsequent formation of the lumen (at anterior locations) to take place (Ciruna et al., 2006; Lowery and Sive, 2004; Tawk et al., 2007).

The emergence of the neural crest is contemporaneous with the process sketched above. Neural crest cells are 'induced' as early as 12 hpf, at the 'border' between the neural ectoderm that forms the neural plate and the non-neural ectoderm which lies more laterally and ventrally (Baker and Bronner-Fraser, 1997; Klymkowsky et al., 2010; Milet and Monsoro-Burq, 2012; Schilling and Kimmel, 1994). Fate maps of zebrafish cranial neural crest using fluorescent dyes showed that neural crest cells are segmentally-restricted depending on the location on the anteroposterior axis from which they arise (Schilling and

Kimmel, 1994), migrating in streams towards the pharyngeal arches with very little mixing between pharyngeal arch compartments.

As the neural keel develops and a midline is formed, neural crest cells are 'induced' from neural crest precursors in the dorsal neuroepithelium on either side of the midline (Fig. 1.2) (Jimenez et al., 2016; Klymkowsky et al., 2010; Kulesa et al., 2010; Schilling and Kimmel, 1994). Though neural crest cells originate at lateral positions from the neural plate border as early as 12 hpf, a large proportion of neural crest cells originate from the dorsal-most neural tissue at later stages. Thus, cranial neural crest cells migrate in successive waves towards their ventral targets (Jimenez et al., 2016; Schilling and Kimmel, 1994). The specific origins and targets of the streams in the cranial region are detailed further in section 1.1.2.

Following a brief overview and introduction to the neural crest, I will subsequently describe the processes of EMT and migration of cranial neural crest in zebrafish embryos, in more detail. Here, I have dealt with Planar Cell Polarity (PCP) with regards to its roles in neurulation alone. Further sections in this chapter will detail the roles of PCP in zebrafish in other contexts, and I will describe models connecting PCP to neural crest.

In Chapters 2 and 3, I will demonstrate the roles of two key polarity genes—the Planar Cell Polarity (PCP) genes *prickle1a* and *prickle1b*—in the zebrafish cranial neural crest that arises from the forebrain, midbrain and hindbrain regions of the neural tube and migrates along specific pathways: the frontonasal process in the head, as well as in streams towards the pharyngeal arches (also referred to as branchial arches in other organisms) (Creuzet, 2009a, b; Le Douarin et al., 2007; Le Douarin et al., 2012). In Chapter 2, I will demonstrate how Prickle1b and Prickle1a are required for cranial neural crest migration, as well as for conferring polarity to migrating NCCs. Subsequently, in Chapter 3, I will explore how prior to this migration, NCCs must undergo EMT, and that Prickle1a and Prickle1b are required in EMT as well. For the purposes of the Introduction, I now turn to providing an overview of EMT and migration.

1.2 The sequential stages of EMT and migration in neural crest development

1.2.1 Epithelial-to-mesenchymal transition (EMT)

Across vertebrate model systems, following specification, the neural crest undergoes the process of epithelial-to-mesenchymal transition (EMT) before migrating. The transition involves multiple steps. In both cranial and trunk regions, the nascent neural crest cells first detach from the apical midline of the dorsal neuroepithelium of the neural tube (Le Douarin and Kalcheim, 1999). Following apical detachment, NCCs undergo a

morphological transition from an epithelial cell to a mesenchymal cell: a transition that involves a suite of regulatory transcription factors and other molecules (Simoes-Costa and Bronner, 2015). In recent years, EMT has been studied extensively because of the key role it plays in collective cell migration, morphogenesis, and cancer (Friedl and Gilmour, 2009; Friedl and Wolf, 2003; Gallik et al., 2017; Lee et al., 2006; Thompson and Williams, 2008). Nonetheless, EMT is an immensely complex process: one which involves changes in cell adhesion, the extracellular matrix, a breach of the basal lamina, the extension of protrusions such as filopodia and pseudopodia, as well as directed migration (Erickson and Perris, 1993; Halloran and Berndt, 2003; Savagner, 2001), indicating the extent to which EMT and migration are interlinked.

A number of events accompany the complex process of EMT. One key event that has been greatly studied is the acquisition of motile, mesenchymal morphology due to the loss of high affinity adherens junctions and the loss of apico-basal polarity proteins from tightly-packed epithelial cells (Ahlstrom and Erickson, 2009; Hay, 2005; Simoes-Costa and Bronner, 2015; Thiery and Sleeman, 2006). However, despite changes in the expression of adhesion proteins, apico-basal polarity proteins and cell-cell junctions, the process of EMT involves many of the same transcriptional regulators that specify neural crest—such as the family of Snail and Twist proteins, as well as Sip1 and FoxD3 (Cheung et al., 2005;

Thiery and Sleeman, 2006). Wnt signaling has also been implicated during EMT, in the regulation of Snai1/2 (Vallin et al., 2001).

A common thread in the process of EMT is the regulation of the Cadherin family of adhesion proteins, which many of the key EMT factors are known to regulate (Theveneau and Mayor, 2011a). For instance, in avian NC, Snail2 is known to regulate Cadherin-6B (Coles et al., 2007), and FoxD3 and Sox-10 have been found to regulate Cadherin-7 (Cheung et al., 2005), and the Wnt pathway to regulate Cadherin-11 (Chalpe et al., 2010). However, much of the knowledge about the temporal sequence of events leading to cadherin regulation is both organism- and axial level-specific (Cousin, 2017; Taneyhill and Schiffmacher, 2017).

Nowhere is this more obvious than the regulation of two key Cadherin molecules which have long been thought to play a pivotal role in EMT: the classical type-I cadherins E-Cadherin and N-Cadherin. For the purposes of clarity, I will focus here on studies done in zebrafish, while noting the studies that call the broad consensus in the field into question. The canonical model of EMT with regards to E-Cad and N-Cad has been one of a 'switch' from epithelial cells expressing high levels of E-Cad and low levels of N-Cad to migratory mesenchymal cells expressing high levels of N-Cad and low levels of E-Cad (Piloto and Schilling, 2010; Powell et al., 2015; Scarpa et al., 2015)—a model that was

first demonstrated in a number of cancerous cell types (Friedl and Gilmour, 2009; Gavert et al., 2008; Grunert et al., 2003; Wheelock et al., 2008). These studies were complemented by similar studies on neural crest in frog, chick, and mouse models (Taneyhill and Schiffmacher, 2017).

The binary model of cadherin switching as a way to 'switch' from the epithelial to mesenchymal morphology has been called into question for two primary reasons. First, EMT and migration are known to require more cadherins than merely E-Cad and N-Cad. For instance, Cadherin-6 (Cdh6) has been reported to be essential for EMT (Clay and Halloran, 2014). The authors showed that prior to EMT, there is a downregulation of N-Cad and an upregulation of Cdh6. They also showed that Cdh6 promotes the regulation of apical detachment as well as the spatiotemporal dynamics of F-actin and active Rho GTPase. As mentioned earlier, Cadherin-7 and Cadherin-11 have also been shown to have roles in EMT and migration, albeit in chick, rat, and frog model systems. Furthermore, a recent study in *Xenopus* showed that E-Cad is required for migration as well as membrane protrusion (Huang et al., 2016a). Thus, even taking into account context-specific differences, it seems unlikely that an E-Cad to N-Cad switch is sufficient for EMT across model systems.

Second, as EMT processes are investigated in more detail, the canonical model in which EMT constitutes a singular morphological transition—largely derived from earlier classifications (Hay, 2005) as well as the commonly-held notion that mesenchymal cells migrate individually through the extracellular matrix (Acloque et al., 2009)—has been called into question. From investigations on different collective cell migration processes, such as mammalian wound healing, zebrafish lateral line cells, *Drosophila* tracheal cells, cancer cell types, and neural crest cells, a collective understanding that the characteristics of epithelial and mesenchymal cells are not mutually exclusive has led to two hypotheses: a 'spectrum' model wherein cells can occupy any number of states along a spectrum from epithelial to mesenchymal morphologies (Campbell and Casanova, 2016), and a 'continuum' model which postulates that as cells move from exhibiting epithelial markers (such as intact tight and adherens junctions and established apico-basal polarity) to mesenchymal markers (a lack of junctions and a shift from apico-basal polarity to front-back polarity) they can take on different morphologies, some of which are more energetically stable and others which are more energetically 'metastable' (Nieto et al., 2016).

The postulation of a 'metastable', and transitory state during EMT, has been suggested predominantly in literature on metastatic carcinoma cells (Savagner, 2001, 2010). The free energy landscape of cells undergoing EMT has been modeled using thermodynamic and

kinetic considerations for lung and pancreatic cancer cells undergoing EMT, with the intermediate states corresponding to ATP production within the cells (Zadran et al., 2014). Carcinoma cells with hybrid characteristics of both 'epithelial' and 'mesenchymal' were thus suggested as 'metastable' owing both to their transitory morphology (Lee et al., 2006), as well as their thermodynamic instability. The body of work referenced for both the 'spectrum' and 'continuum' models indicates the growing understanding that EMT is a highly plastic and stochastic process wherein cells can take on morphologies that cannot be ascribed as entirely epithelial or entirely mesenchymal.

The detailed process of EMT in different systems is beginning to be described far better due to advances in *in vivo* imaging modalities. For zebrafish cranial neural crest cells, the morphological transitions have recently been well-described although they have not yet been fully adopted by the field at large. Two studies found that during EMT, NCCs first detach from the apical midline where they initially have an elongated morphology (Berndt et al., 2008). Subsequently, these NCCs round up and form membrane-based blebs—rounded bulges on one side of the cell—before transitioning to a filopodial and lamellipodial-based morphology and migrating using frequent but transient contacts with neighboring cells in streams (morphological transitions shown in Fig. 1.4) (Berndt et al., 2008; Clay and Halloran, 2014). F-actin was found to localize differently in filopodia and

blebs; the disruption of myosin-II, Rho-GTPase and Rho-kinase (ROCK) was found to inhibit EMT, indicating central roles for each.

Although the studies demonstrated the varied morphologies NCCs undergo *en route* to fully-migratory mesenchymal cells using confocal microscopy, they did not report the

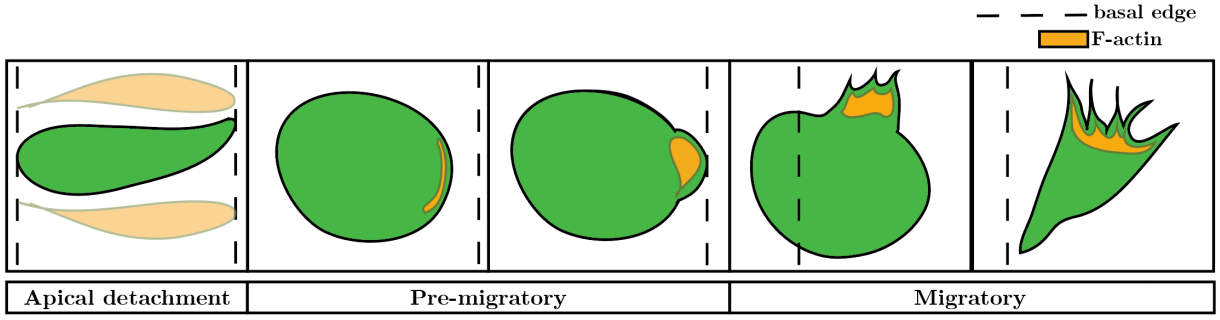

Fig. 1.3: Morphological changes during EMT. In the panel on the right, a neuroepithelial cell within the neural tube is detaching from the apical (left dotted line) surface. Following apical detachment, NCCs round up and form blebs before actively migrating laterally into streams (dotted line in pre-migratory and migratory panels is the basal edge of the neuroepithelium. Once cells move past the basal edges of the neuroepithelium—the 'sides' of the neural tube in a dorsal view—cell move ventrally (in a dorsal view, into the plane of the page). These cells are actively migratory because they have developed the highly-filopodial and lamellipodial-based morphology characteristic of migrating mesenchymal NCCs.

---

migratory potential of the transitional bleb-based cells (Fig 1.4, third panel). However, in zebrafish primordial germ cells (PGCs), bleb-based protrusions dependent on Cdc42 were found in migrating cells and were also found to be integral for cell motility and migration

toward a target (Goudarzi et al., 2017). These findings demonstrate that bleb-based cells are capable of motility. In the context of PGCs, these bleb-based morphologies are also capable of directed migration, however our observations in zebrafish neural crest (Chapter 3), as well as previous reports (Berndt et al., 2008; Clay and Halloran, 2014), indicate that the bleb-based morphologies are a transitional stage before the filopodial- and lamellipodial-based mesenchymal cells capable of directed migration (Fig. 1.4).

Subsequent to EMT, actively protrusive mesenchymal cells move out of the domain of the dorsal neural tube and through the extracellular matrix toward their targets. How zebrafish cranial NCC migration occurs—the mechanisms by which cells respond to cues in their environment, and the contacts they establish with neighboring cells in a stream—is the subject of the next section.

1.2.2 Migration

As the cranial NCCs move away from the neuroepithelium in a 'continuous wave' (Theveneau and Mayor, 2012), they begin to migrate in distinct streams (Hall and Hall, 2009; Le Douarin and Kalcheim, 1999). NCCs from the forebrain and anterior midbrain contribute to the frontonasal primodium of the face (Dee et al., 2013; Knight and Schilling, 2006). Three streams of NCCs migrate to and fill the pharyngeal arches: the mandibular (first) stream), hyoid (second) stream, and the post-otic streams that lead to the formation

of the ceratobranchials I-V (Schilling and Kimmel, 1994). The arches are filled progressively, with the first stream formed by cells from the posterior midbrain and the anterior hindbrain, the latter of which is segmented into compartments called rhombomeres—rhombomere-1 (r1) and rhombomere-2 (r2), in particular, contribute to the first stream (Fig. 1.4). While the region adjacent to r3 is a NC-free zone, NCCs from r3 contribute to both the first and second streams along with r4 and some NCCs from r5 which also contributes to the third, post-otic, stream along with r6. Lastly, r7 and r8 fill the fourth pharyngeal arch. The NC-free zones adjacent to r3 and r5 restrict NCC movement to streams on either side of these rhombomeres partly due to local inhibitory signals and physical barriers such as the otic vesicle adjacent to r5 (Farlie et al., 1999; Lumsden et al., 1991; Trainor et al., 2002), events that are largely conserved across vertebrate species (Kulesa et al., 2010). Cranial NCCs do not however only invade the pharyngeal arches: at post-otic levels along the antero-posterior axis, a population of cardiac NCCs migrate to the developing heart (not shown in Fig. 1.4) (Kirby and Hutson, 2010).

The migration of NCCs to these regions within the vertebrate embryo is critical for the development of many tissues and organs. Much of the cartilage and bone structure of the head, neck, and jaw are formed by NCCs (Couly et al., 1993; Evans and Noden, 2006; Gross and Hanken, 2005; Hanken and Gross, 2005; Helms et al., 2005; Helms and

Schneider, 2003). Cranial NCCs also contribute to the cranial nerves and ganglia, pigment cells, the dermis of the head, the ocular and periocular structures, smooth muscles, and the connective tissue of blood vessels (Creuzet et al., 2005; Creuzet, 2009a, b; Hall and Hall, 2009).

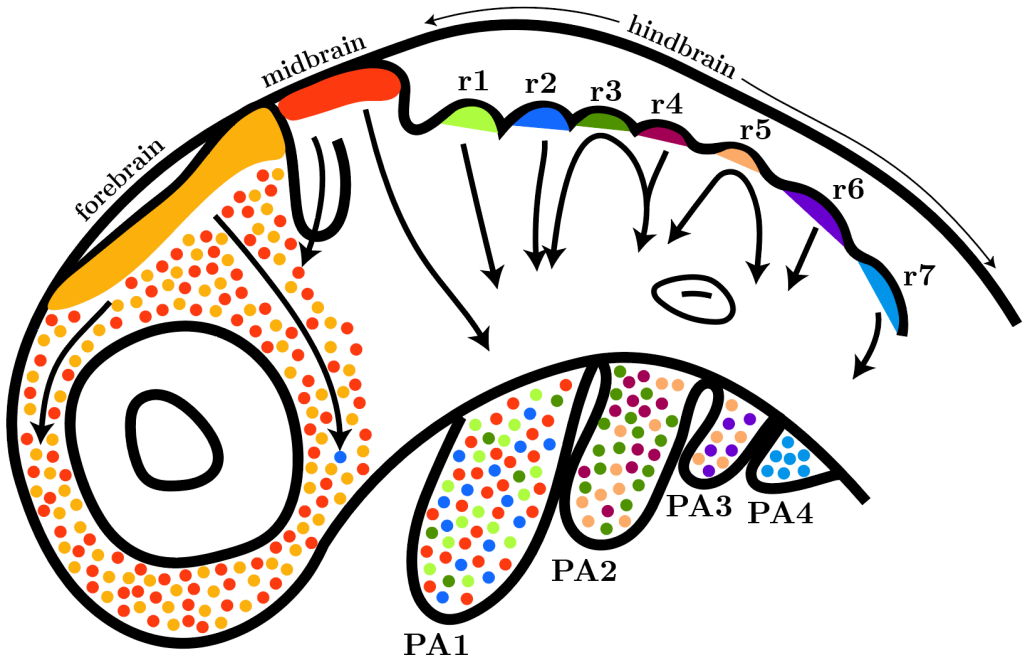

Fig. 1.4 The streams of migrating cranial neural crest cells in zebrafish embryos. Color-coded streams originating from the forebrain, midbrain, and hindbrain are indicated, with the rhombomeres (segments) of the hindbrain indicated from r1 to r7. NCCs from the forebrain and anterior midbrain contribute to the frontonasal process in the anterior-most region of the embryo, whereas NCCs from the posterior midbrain and r1 contribute to the first (mandibular) pharyngeal arch (PA1). Regions directly adjacent to r3 and r5 are NCC-free zones, however NCCs from r3 and r5 contribute to two arches by

Fig. 1.4 continued: migrating first anteriorly or posteriorly and then laterally. NCC populations are shown using color-coded circles to indicate origin.

In some cases—for instance the extent to which the skeletal structures at the back of the neck and jaw are NC-derived or mesoderm-derived—the specific derivatives of neural crest are either unclear or have important species-specific differences (Theveneau and Mayor, 2011b). Regardless, the development of these structures in each species investigated, depends on the stereotypic migration of NC streams. While defects in induction, specification, and proliferation can lead to a variety of dysplasias such as Treacher Collins syndrome (Trainor, 2010; Walker and Trainor, 2006), defects in NC migration often lead to general malformations such as cleft lip, cleft palate, a lack of pigmentation, abnormal ear development and other defects found in Waardenburg, DiGeorge and Goldenhar syndromes (Jones, 1990; Le Douarin and Kalcheim, 1999; Schoenwolf and Larsen, 2009; Wurdak et al., 2006). Further, because of the elements linking the migration of metastatic cancer cells and that of NCCs, there has been much historical focus on this aspect of NC development (Gallik et al., 2017; Maguire et al., 2015).

As discussed earlier, in zebrafish, cranial NCCs migrate in 'waves'. A large proportion of neural crest cells start migrating at approximately 16 hpf from the dorsal aspect of the neural tube, from where they move ventrolaterally to occupy the pharyngeal arches (Fig.

1.5). However, a recent study that uses a transgenic line marking *snai1b* with a fluorescent reporter—a gene encoding a transcription factor that is expressed both in premigratory cells before and during EMT as well as migrating cells—has indicated that there are at least two populations of cranial NCCs that delaminate from different regions in the embryo (Jimenez et al., 2016). The study was motivated by the observation that there are no reported instances of the disruption of a single pathway leading to NCCs remaining trapped within the neural tube. Using the *Tg[snai1b:GFP]* line, the authors demonstrated that there is an earlier population of NCCs that delaminates from ectoderm adjacent to the neural keel and thus lies laterally to the later population of NCCs within the neural rod that delaminates dorsally as previously described. This finding demonstrates that rather than migrating as merely a 'continuous wave' from the dorsal aspect of the neural tube, cranial NCCs deploy more than one spatiotemporal mode of migration.

As with specification and EMT, a number of molecular players during NCC migration are shared with previous phases in NC development. One of these is Sox10—a member of the SoxE family of transcription factors—which is driven by another member of the family and neural crest specifier gene Sox9, also expressed throughout migration (Betancur et al., 2010; Simoes-Costa et al., 2014). Furthermore, other factors such as FoxD3 (Simoes-Costa et al., 2012; Stewart et al., 2006) are also commonly expressed throughout

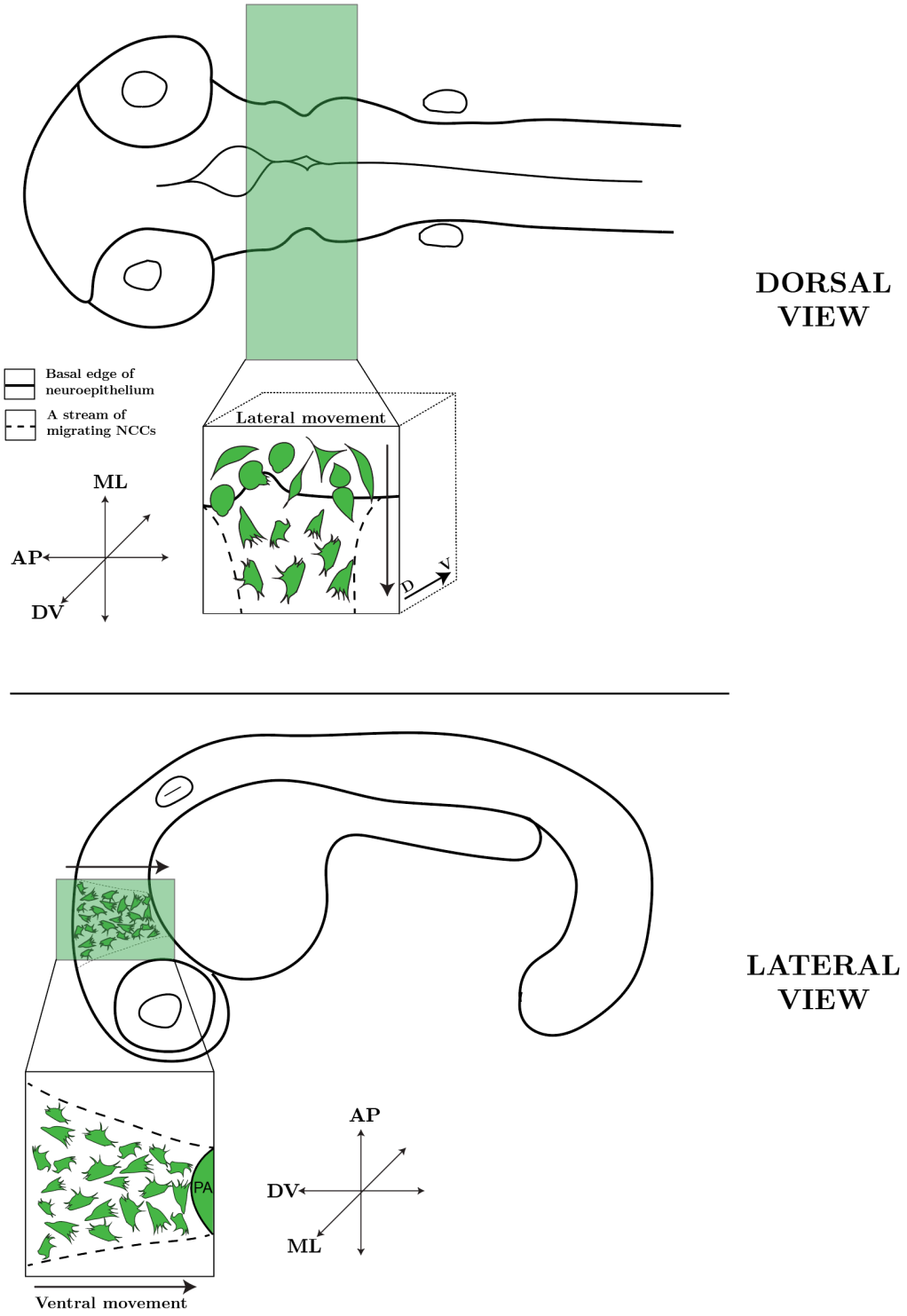

Fig. 1.5: Ventrolateral migration of cranial neural crest cells towards the pharyngeal arches. Above is a dorsal view which shows the initial lateral migration of neural crest cells past the basal edge of the

Fig. 1.5 continued: neuroepithelium, after which they move ventrally (into the plane of the page). In a lateral view, NCCs can be seen moving from their dorsal positions into ventral ones (closer to the yolk) to 'home in' to their pharyngeal arch targets.

---

development, and indeed a migratory NCC gene regulatory network (GRN) has been identified that involves many neural crest specifier genes, including Ets1 and Myb, in regulating many of the genes in the migratory NC module (Simoes-Costa and Bronner, 2015; Simoes-Costa et al., 2014). Each of the aforementioned molecules is known to be required in zebrafish cranial neural crest. Migratory NCCs are subject to different environmental signals than NCCs undergoing induction, specification or EMT as they interact not only with other NCCs but a large number of different microenvironments depending on where they are targeted. The semaphorin class of secreted and membrane proteins and their neuropilin receptors have long been known to play crucial roles for cranial NC migration. Several molecules of class 3 semaphorins and their corresponding receptors are required to keep the zones adjacent to r3 and r5 NC-free in chick, mouse, and zebrafish by acting as repulsive cues, with NCCs expressing the neuropilin receptors as surrounding tissues secrete semaphorin ligands (Eickholt, 2008; Eickholt et al., 1999; Gammill et al., 2007; Gammill et al., 2006; Osborne et al., 2005; Yu and Moens, 2005). The extensive work on semaphorins and neuropilins, both *in vitro* and *in vivo*, has

demonstrated that sempahorin signaling is often used as an inhibitory cue to keep NCCs in streams.

In addition, the transmembrane Ephrin ligands and Eph receptors also play roles in both sorting NCCs into streams and preventing mixing of NCCs into inappropriate streams, (Adams et al., 2001; Davy et al., 2004; Mellott and Burke, 2008). While Slit/Robo signaling has been implicated in the formation of cranial sensory ganglia (Shiau and Bronner-Fraser, 2009) and in trunk NCC migration in chick (Jia et al., 2005) and mouse (De Bellard et al., 2002), there are no reported roles for the signaling pathway in zebrafish cranial NC. Further, intriguing studies on chemoattraction of cranial NCCs into branchial arches have been conducted. Using both *in vivo* work in chick and *in silico* modeling, the Kulesa group showed that the vascular endothelial growth factor (VEGF), which is expressed in the ectoderm of branchial arches, is critical for NCC migration and also to confer 'trailblazer' identity onto cells at the front of an invading NCC stream (McLennan et al., 2015b; McLennan et al., 2010). Based on profiling of mRNA expression levels in different cell populations and computational modeling, the 'trailblazer' model proposes that the directional information is specific to the leading cells of a given stream, in the form of a specific molecular signature (McLennan et al., 2015a).

VEGF is not the only chemokine proposed to play a role in NC migration, however: another study in zebrafish showed that stromal cell-derived factor-1b (Sdf1b) acts as a chemokine, and along with its receptor CXCR4A, it is important for cranial NCC migration with Sdf1b expressed in pharyngeal arch endoderm and CXCR4A in cranial NCCs (Olesnicky Killian et al., 2009). In chick, differential expression of the chemoattractant Sdf1 and CXCR4 have also been shown to be required for NCC migration to the dorsal root ganglia and sympathetic ganglia (Kasemeier-Kulesa et al., 2010), as well as the dorsal aorta and sympatho-adrenal system (Saito et al., 2012). Finally, most critically, Sdf1 has also been demonstrated as a chemokine for the 'chase-and-run' mechanism by which NCCs 'chase' placodal cells, and along with the repulsive cues set up by contact-inhibition of locomotion (discussed subsequently) segregate placodes and allow NCCs to migrate in streams (Theveneau et al., 2013).

Further important work involving guidance cues and chemoattraction involves the findings in *Xenopus* that NCCs require the extracellular matrix molecule Versican in two ways. First, by inhibiting migration in certain parts of the embryo, Versican establishes exclusionary boundaries that allow it to 'confine' NCCs and forces them to migrate in coordinated streams. Second, these restrictive boundaries subsequently, simulated *in silico*, enhance collective migration in turn (Szabo et al., 2016). Thus, Versican, by setting up exclusionary boundaries acts as a guidance cue for NCCs. Importantly for our work is

the fact that morpholino knockdown targeted against Versican is sufficient to block NCC migration; that a single guidance cue is sufficient to block NCC migration suggests cross-talk with other chemokines.

Altogether, the molecular signatures of migrating NCCs indicates that: 1, there are important context-specific differences, and 2, that NCC migration uses attractive and repulsive guidance cues to allow NCCs to be condensed into pharyngeal arches. The holistic, tissue-level modes by which cranial NCCs migrate, however, is not 'settled' in any model organism.

The Kulesa group's studies on 'trailblazer' identity constitute a model of cranial NCC migration, albeit one with data exclusively in chick embryos. This has been contradicted by another group which shows that in both chick and zebrafish embryos, cranial NCCs do not require leader cells and that all cells have similar migratory capacities and can rearrange to be at the leading edge at any point (Richardson et al., 2016).

Another prevailing model for how neural crest cells migrate and invade regions of the developing embryo is termed 'contact-inhibition of locomotion' (CIL), a type of migration first reported in 1976 for chick fibroblast cells (Abercrombie and Heaysman, 1976). The Mayor group has proposed a model which maintains that highly-protrusive neural crest

cells contact one another, activate non-canonical Wnt/PCP signaling at the point of contact, and subsequently reorient their protrusions to migrate away from each other (Fig. 1.8) (Carmona-Fontaine et al., 2008). Both *in vitro* and *in vivo* in *Xenopus* and zebrafish embryos, the authors found that although NCCs reorient when they meet other NCCs, when NCCs meet another cell type, they invade the tissue similar to metastatic cancer cells (Szabo and Mayor, 2016). Inhibition of non-canonical Wnt signaling abolishes CIL. In subsequent studies, it was reported that the switch from E-Cad to N-Cad was necessary for EMT to complete and CIL to begin as cells begin to migrate (Scarpa et al., 2015). This model for reorientation of protrusions upon contact, along with inhibitory cues in the microenvironment through which NCCs migrate, provides a mechanism for directional NCC migration towards their specific targets.

The model of CIL, which is dealt with in more detail in the next section, is very appealing as a mechanism to describe the interactions of cells both with each other and with their surrounding milieu in order to be restricted to and migrate in streams. However, it is not thought of as the definitive model that describes migration across different spatial and temporal contexts, at different axial levels, and most importantly, across vertebrate species. A recent report, using *in vivo* imaging of the chick neural crest has shown that chick cranial NCCs do not use CIL in migration, suggesting that a role for CIL may not be conserved for all vertebrates (Genuth et al., 2018).

In this study, I use cranial NCCs in the developing zebrafish embryo as a model to query the requirement of PCP signaling in collective NC migration, whether it uses mechanisms identified in CIL or not (PCP in CIL is discussed in more detail in section 1.4). Critically, CIL both *in vitro* and in *Xenopus* has largely been described as a 'switch' from epithelial cell morphology to mesenchymal cell morphology. The authors of the report connecting EMT and CIL treat the two processes as discrete and binary (Scarpa et al., 2015), and not, as other reports suggest, as a spectrum of cell morphologies and behaviors, expression levels of adhesion properties and dynamic F-actin accumulation in protrusions that are not as simple as the orientation of protrusions of one NCC away from a recently-contacted NCC (Berndt et al., 2008; Clay and Halloran, 2014; Coles et al., 2007; Genuth et al., 2018; reviewed in Halloran and Berndt, 2003; reviewed in Le Douarin et al., 2004).

Resolving the uncertainty regarding EMT and cell migration will require a more in depth analysis of the cell behaviors and the molecules that control them. As I describe in Chapter 3, I find that the process of morphological change from a neuroepithelial cell to a highly-protrusive mesenchymal cell accords with previous findings (reviewed in Campbell and Casanova, 2016; Nieto et al., 2016) on morphological transitions for NCCs, with intermediate states that require PCP to confer polarity to NCs in EMT. However, in addition to the role for PCP Prickle1 molecules in EMT, subsequent defects in migration

due to deficiencies in the core Planar Cell Polarity molecule Prickle1 seem to suggest a CIL-like mode of migration. Planar cell polarity is the subject of the next two introductory sections.

1.3 Introduction to Planar Cell Polarity

1.3.1 PCP in *Drosophila melanogaster*

Planar polarity, a feature of multicellular tissues whereby cells coordinate with their neighbors to establish tissue-level polarity, was first discovered in *Drosophila* where epidermal cells, for instance, were polarized in the plane of the epithelium. In *Drosophila melanogaster*, the suite of proteins responsible for establishing this form of polarity, henceforth referred to as the core Planar Cell Polarity (PCP) proteins, were identified in screens and epistasis experiments where the loss of asymmetric alignment of hairs and bristles in epithelial tissues such as the surfaces of the wing or abdomen was associated to the loss of these proteins (Gubb and Garcia-Bellido, 1982; Shulman et al., 1998; Wong and Adler, 1993). The phenotypes associated with the loss of one or more of the core PCP proteins were swirling, randomized patterns where tissue-level polarity orthogonal to the apicobasal axis was lost (reviewed in Adler, 2002).

Principally, processes that implicate PCP implicate some or all of the proteins. These include the Wnt receptor Frizzled (Fz), thought to be the key receptor for the PCP pathway but not necessarily in a Wnt-dependent manner (Axelrod, 2001; Axelrod and McNeill, 2002; Lawrence et al., 2002). Other core PCP proteins include the cytoplasmic PDZ-domain protein Disheveled (Dvl or Dsh) which associates with Fz to mediate PCP signaling (Axelrod, 2001; Klingensmith et al., 1994), the cytoplasmic LIM-domain protein Prickle (Gubb et al., 1999; Tree et al., 2002), the membrane protein Strabismus (Stbm), also known as Van Gogh (Vangl in vertebrate contexts) (Taylor et al., 1998), the seven-pass transmembrane cadherin-domain protein Starry Night, also known as Flamingo and Celsr (Usui et al., 1999), and the cytoplasmic ankyrin-repeat protein Diego (Feiguin et al., 2001) among others.

Importantly, in the context of Drosophila epithelial sheets it was discovered that the core PCP proteins, save for Flamingo, localize asymmetrically, and this is required for the establishment of global Planar Polarity (Fig. 1.5 shows proximal/distal localization of Fz, Dsh, Stbm, and Pk) (Axelrod, 2001; Bastock et al., 2003; Das et al., 2004; Strutt, 2001; Tree et al., 2002; reviewed in Zallen, 2007), with Van Gogh and Prickle localizing to proximal surfaces and Frizzled and Disheveled on distal surfaces (Fig. 1.5). Genetic and molecular studies established a series of targeting, recruitment and feedback mechanisms allowing for stable asymmetries to be formed. For instance, genetic analyses and

visualization of endogenous protein levels showed that Prickle and Frizzled can interact across cell boundaries on proximal and distal sides, respectively (Tree et al., 2002) and that Prickle is capable of amplifying asymmetries via a feedback mechanism through its intercellular interaction with Strabismus and intra-cellular interaction with Frizzled. Furthermore, Frizzled seems to act through Diego to promote the clustering of Flamingo (Feiguin et al., 2001), and Diego and Prickle can compete for binding to Disheveled thereby allowing for the modulation and stabilization of Frizzled-Disheveled complexes at the distal surface (Das et al., 2004; Jenny et al., 2005).

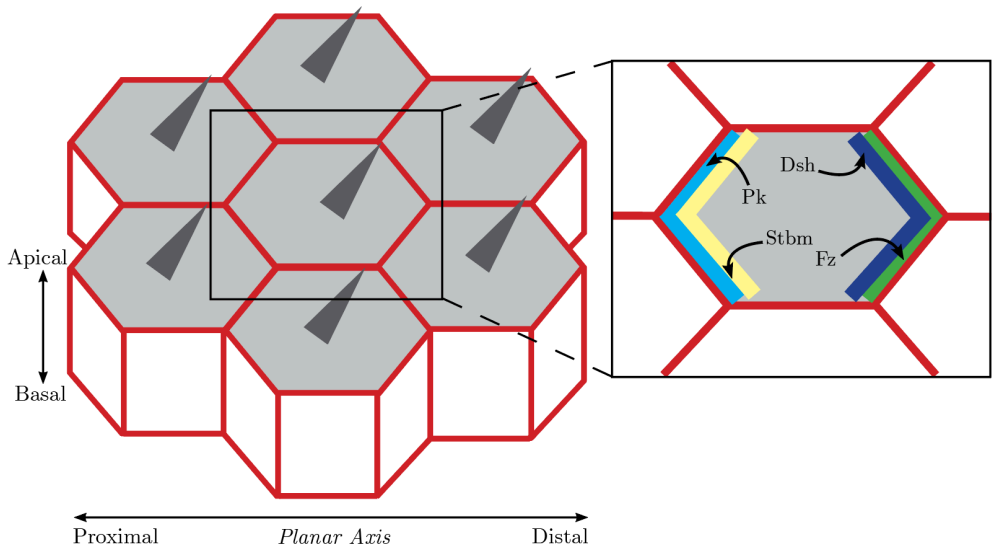

Fig. 1.6: Core PCP proteins and their localization in Drosophila epithelia

It has also been demonstrated in *Drosophila* that the two isoforms of the endogenous prickle gene—Prickle and Spiny-legs (Sple)—are both critical to establish tissue polarity,

in a level-dependent manner such that when both are absent the whole body surface is affected, however critically, isoform-specific mutations showed them to work in mutually exclusive tissues (Gubb et al., 1999; Lin and Gubb, 2009). Further quantitative analysis, *in silico* modeling, and imaging dynamic expression of the isoforms showed not only that they work in an antagonistic fashion to each other (if the isoforms are 'swapped', tissue polarity is found to be reversed), but also that the two isoforms control how the 'core' PCP module temporally couples (i.e. works in tandem with) the Fat/Dachsous PCP module (Merkel et al., 2014). There are mechanisms that have been elucidated showing how the isoforms work with both modules (Ambegaonkar and Irvine, 2015; Ayukawa et al., 2014), which I shall not detail here. However, specifically regarding the functions of the two isoforms, it has been found—largely through genetic analysis—that Pk and Sple affect the direction of tissue polarity by controlling the apical microtubule network thereby controlling the directionality of vesicle traffic (Olofsson et al., 2014; Strutt et al., 2013), and establishing tissue polarity by amplifying the asymmetries of other core PCP proteins. Since then, it has been found that Pk and Sple affect issue polarity both in microtubule-dependent and microtubule-independent manners: for instance, in the distal part of the wing (D-wing) and the posterior part of the abdomen (P-abd), the isoforms affect polarity without affecting microtubule polarity (Sharp and Axelrod, 2016).

The significance of these recent studies in *Drosophila* for Prickle homologs in vertebrates lies in the possibility of conserved function: it is a formal possibility, for instance, that the multiple Prickle homologs in vertebrates could behave similarly to the Pk and Sple isoforms, both by acting antagonistically in the same process, and to function earlier than other PCP molecules, thus amplifying their asymmetry. However, this function could also be lost, as in vertebrates there are no *prickle* gene homologs with more than one known transcript that encodes a functional protein (isoforms).

1.3.2 PCP in vertebrates

Similar to *Drosophila*, vertebrate epithelia also require PCP proteins for planar polarization of epithelial structures, such as the skin, tracheal cells, sensory organs, as well as the neuroepithelium (reviewed in Hale and Strutt, 2015). Many of these PCP-based structures rely on microtubule-based ciliated structures, the directionality and polarization of which is crucial in, for instance, inner ear development in vertebrates where orthologs of PCP genes present in *Drosophila* play key roles in the polarization of cells (Curtin et al., 2003; Montcouquiol and Kelley, 2003). PCP asymmetries underlie the asymmetric positions of cilia (Borovina et al., 2010; Hashimoto et al., 2010). This regulation of the cytoskeleton by PCP proteins has been observed in many different PCP contexts.

Thus, while the role of PCP proteins in the polarization of a plane of epithelial cells remains largely conserved in vertebrates, PCP proteins in vertebrates also have key roles in the migratory behaviors of epithelial, mesenchymal, and neuronal cells (reviewed in Davey and Moens 2017). What is key to note is that each of the core PCP proteins have orthologs in vertebrate genomes but their number differs between species; in zebrafish, for instance, owing to whole-genome duplication (Hurley et al., 2007), there are five known orthologs of *Drosophila prickle* (*prickle1a, prickle1b, prickle2a, prickle2b, and prickle3*). Several orthologs have thus far remained unstudied, however those that have been studied show a striking degree of conservation of the complex sets of interactions, feedback mechanisms and asymmetries to the *Drosophila* wing and abdomen (Butler and Wallingford, 2015; Chu and Sokol, 2016; Ciruna et al., 2006; Davey and Moens, 2017; Hashimoto et al., 2010; Vladar et al., 2012).

PCP in vertebrates was first implicated in the convergence extension movements of cells of the neuroepithelium and mesoderm during gastrulation and neurulation, a role that has been demonstrated in *Xenopus*, chick, zebrafish and mouse models (Heisenberg et al., 2000; Jessen et al., 2002; Sepich et al., 2011; Takeuchi et al., 2003; Veeman et al., 2003; Wallingford et al., 2000; Wang et al., 2006; Yin et al., 2008). As discussed earlier, PCP signaling is also required during neurulation for the polarization of neural progenitors. In the zebrafish neural keel, loss of *vangl2* resulted in the loss of polarization of keel cells

thus inhibiting the intercalation of daughter cells into the neuroepithelium on either side of the midline resulting in neural tube defects (Clarke, 2009). It was also found that cell division is coupled to neural tube morphogenesis (Ciruna et al., 2006). In subsequent studies, it has been found that the loss of PCP proteins disrupts the processes of apical constriction, medial intercalation and neighbor exchange by affecting actomyosin contractility (Nishimura et al., 2012; Ossipova et al., 2014; Yen et al., 2009). By establishing asymmetric localization in neuroepithelial progenitors (Ciruna et al., 2006; McGreevy et al., 2015; Nishimura et al., 2012; Ossipova et al., 2015; Roszko et al., 2009), PCP proteins have been found to regulate actomyosin contractility through RhoGTPases and Rho-associated proteins, including ROCK, that drive apical constriction (Nishimura and Takeichi, 2008) or adaptors such as Daam1, a formin homology protein that directs the nucleation and elongation of actin filaments as well as linking PCP proteins to RhoA (Habas et al., 2001; Nishimura et al., 2012)

Critically, PCP proteins have also been implicated in contexts which do not strictly involve the polarization of cell sheets and instead involve more 3D processes: for instance in the migration of facial branchiomotor neurons (Bingham et al., 2002; Glasco et al., 2012; Jessen et al., 2002; Mapp et al., 2011; Mapp et al., 2010; Qu et al., 2010; Rohrschneider et al., 2007; Wada et al., 2006), in organizing the sensory cells of the inner

ear (reviewed in May-Simera and Kelley, 2012; Rida and Chen, 2009), and in neural crest, to which we now turn.

1.4 Planar Cell Polarity acts in contact-inhibition of locomotion in migrating neural crest

The finding that PCP plays a role in neural crest is relatively recent. As mentioned earlier, PCP molecules have been found to be required for the behavior associated with contact-inhibition of locomotion (CIL): in particular, the molecules Frizzled (Fzd) and Disheveled (Dsh) have been implicated in CIL. These studies showed that when migrating NCCs come into contact, Fzd and Dsh are localized at the point of contact, and subsequently

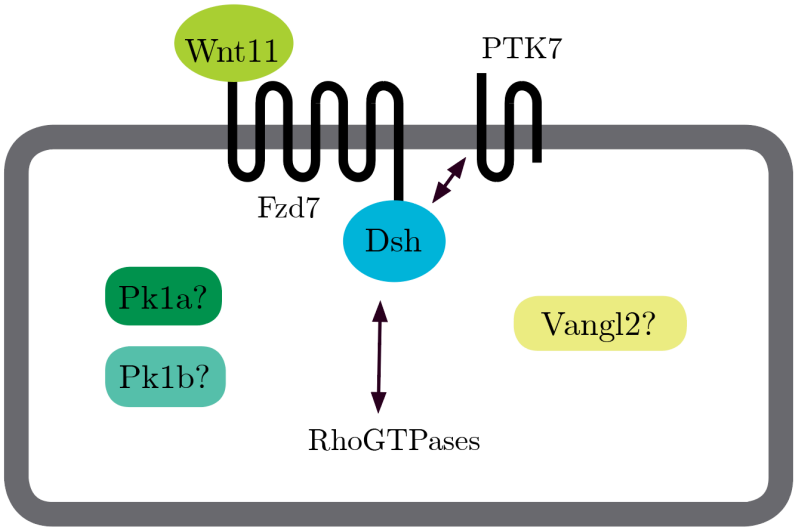

Fig. 1.7: PCP proteins and other important regulators previously implicated in neural crest migration.

they activate RhoA at the lagging edge of a migrating cell and Rac1 at the leading edge of the cell (Carmona-Fontaine et al., 2008; Matthews et al., 2008). De Calisto et al. (2005) reported the first results showing a role for non-canonical Wnt/PCP signaling in NCC migration—in particular, in *Xenopus laevis* embryos, and specifically implicating Wnt11, Frizzled-7 (Fzd7), and Disheveled (Dsh) (Fig. 1.7) (De Calisto et al., 2005). The ligand Wnt11, was found to be expressed in ectoderm adjacent to the presumptive neural crest which expressed the Wnt receptor and core PCP molecule Frizzled-7 (Fzd7). Using various mutants of Dsh, some of which disrupted canonical Wnt signaling and others which only disrupted non-canonical Wnt/PCP signaling, the authors found that the expression of a dominant negative Dsh-DEP+ form of Dsh which only disrupts non-canonical Wnt signaling was sufficient to block neural crest migration. Though the authors did not test other possible Wnt ligands, they found that Wnt11 was expressed adjacent to Slug-expressing neural crest cells. Although no Wnt11 receptor was known, from previous work, Fzd7 was the principal homolog of *Drosophila* Frizzled known to participate in Wnt/PCP signaling (Djiane et al., 2000; Medina et al., 2000), and Fzd7 was also found to be expressed in the right place at the right time for a role in neural crest migration. Using injection of dominant-negative Wnt11 (dnWnt11) mRNA, migration was blocked as with Dsh-DEP+ cells, a phenotype that was rescued by grafting a PCP-activating form of Dsh into dnWnt11-injected embryos. Finally, the authors showed that in Dsh-DEP+ embryos, neural crest cells showed far fewer protrusions than cells in control embryos. Thus, using

data from Wnt11, Fzd7 and Dsh alone, the authors concluded that non-canonical Wnt/PCP signaling was required for neural crest migration in *Xenopus* embryos. Also in *Xenopus* embryos, another group later found that the protein tyrosine kinase-7 (PTK7) recruits Dsh to the plasma membrane, and that this role is necessary for the activity of Dsh and neural crest migration (Shnitsar and Borchers, 2008).

In a subsequent study focused on the role of the proteoglycan Syndecan-4 (Syn4), the same group that first implicated Wnt11, Fz7, and Dsh, used FRET analysis to measure the activity of the small GTPases RhoA, Rac1, and Cdc42 (Matthews et al., 2008). Here, the group used the conclusions of the previous study to observe the effects of disruption of PCP in zebrafish embryos, as well as *in vitro* cultured *Xenopus* neural crest cells. In zebrafish embryos, the authors used embryos injected with the dominant-negative form of Dsh, Dsh-DEP+, as well as *trilobite*-mutant embryos (mutant for the gene *vangl2*, which encodes the core PCP component Vangl2 or Strabismus). In both cases, the authors used in situ hybridization for the pan-neural crest marker *crestin* to show that streams of trunk neural crest cells were blocked from migrating, though *trilobite*-mutant embryos showed a milder phenotype than Dsh-DEP+-injected embryos. Finally, using FRET both *in vitro* in cultured cells and *in vivo* in *Xenopus* embryos, the authors found that Dsh-DEP+-expressing cells showed a significant decrease in RhoA activity, but with no effect found on Cdc42 or Rac. Regardless, the authors concluded that because of the known crosstalk

between the small GTPases, it was likely that the PCP pathway—here assayed solely through the Dsh-DEP+ reagent—acted upstream of the small GTPases to promote RhoA activity, in a parallel pathway to Syn-4, which was found to inhibit Rac (Matthews et al., 2008).

Even with these two studies, a mechanism of action for the PCP molecules in neural crest migration was lacking. This was provided in a study published the same year as the Syn-4 study, through a mechanism called contact-inhibition of locomotion (CIL), first discovered in 1953 in cultured chick fibroblast cells (Abercrombie and Heaysman, 1953, 1954, 1976). Carmona-Fontaine et al. (2008) found that neural crest cells cultured *in vitro* displayed behavior consistent with CIL (Fig. 1.8), such that when two migrating neural crest cells from two different explants of neural crest cells (an 'explant confrontation assay') formed contacts, they collapsed their protrusions at the contact, and repolarized away from one another (Carmona-Fontaine et al., 2008). In contrast, explants of neural crest cells and mesodermal cells showed that NC cells instead invaded the mesodermal cells in a manner similar to metastatic carcinoma cells. Importantly, only the 'edge' or leader NC cells showed a high degree of persistence and capability to repolarize, whereas cells internal to the explant showed a lack of polarity and moved randomly (see internal and leading cells in Fig. 1.8). If the neighbors of internal NC cells were removed, those NC cells now had a free edge and behaved like leader cells. Knowing that NC migration

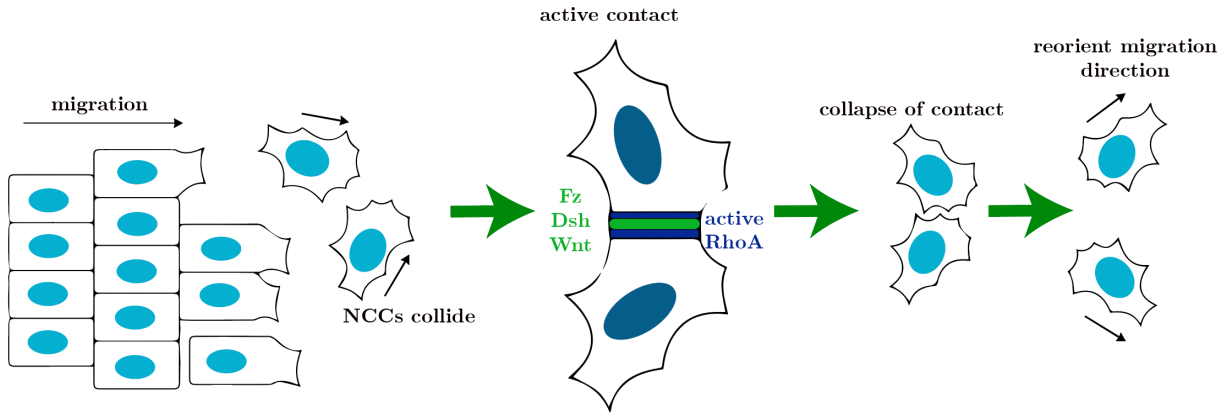

Fig. 1.8: PCP and the contact inhibition of locomotion (CIL) model for migrating neural crest. The process is as follows: leader cells in a stream show protrusive ability and are able to move away from each other. When NCCs collide and establish active contact, Wnt11, Fzd7, and Dsh are activated at the point of contact as is active RhoGTPase, which subsequently cause a collapse of contacts and repolarization of migration direction.

---

was predicated on cell-cell contact during migration at the leading edge, the authors then studied Dsh-DEP+-expressing NC cells and found that in contrast to control cells, Dsh-DEP+ NC cells all behaved like internal cells, did not repolarize, and instead crawled on top of one another (like invasive cells).

While this work was done *in vitro*, the authors did a limited number of *in vivo* experiments as well: they injected zebrafish embryos with the dominant-negative Dsh-DEP+ construct, the dominant-negative dnWnt11 construct, or with morpholinos targeted to both *vangl2*

(referred to as stb or strabismus) and *prickle1a* (i.e. morpholinos against *both* genes were injected into the same embryos). They then assayed the direction of NC cells immediately following collision with another cell, and found that in contrast to control cells, Dsh-DEP+, dnWnt11, and Stb/Pk1 MO NCCs did not change their direction of migration, though importantly *the speed of movement of the NC cells was not significantly altered.* Using fusion proteins for Fz7, Wnt11, and Dsh, the authors found each of them to be upregulated at the point of contact between two cells. Using FRET, they in turn showed that this also upregulated RhoA at the point of contact.

These studies, together, allowed for the development of a model whereby neural crest cells migrated using CIL, allowing cell contacts to be created, non-canonical Wnt/PCP signaling to be upregulated at the point of contact, as well as RhoA (see point of contact in Fig. 1.8). This in turn allowed cells to repolarize in a different direction (Mayor and Carmona-Fontaine, 2010; Mayor and Theveneau, 2014; Theveneau and Mayor, 2011a, b, 2012).

A number of problems remained for this model. CIL during directed migration did not seem sufficient to allow for NCCs to migrate in streams toward specific targets, and thus collective chemotaxis in conjunction with CIL was required (Theveneau et al., 2010). In a subsequent study, this research group resolved that problem to a degree by showing

that the extracellular matrix molecule Versican acts as a guiding cue that establishes exclusionary boundaries and inhibits NCC migration. The authors argued, using *in vitro, in vivo* and *in silico* methods, that *in vivo* confinement of neural crest cells in a specific area was dictated by the boundaries set up by Versican, and that NCCs were then able to migrate successfully towards their target using CIL (Szabo and Mayor, 2016; Szabo et al., 2016).

Further, at a few junctures, the authors used a *trilobite* mutant or morpholinos targeted to *both prickle1a* and *vangl2*. However, in the vast majority of experiments, the CIL model was drawn from observations only on Fzd7 and Dsh. A role for other core PCP molecules was not queried in the context of CIL, or neural crest migration—nor, critically, at any stages prior to migration. Other than in the context of CIL for Frizzled-7 and Disheveled, to our knowledge there has been no comprehensive analysis of other core PCP components in zebrafish neural crest.

In sum, in this chapter I have attempted to demonstrate that there is a gap in knowledge regarding the roles of Planar Cell Polarity molecules other than Frizzled and Disheveled in cranial NCC migration. Further, a role for PCP molecules has not been queried at other phases of NCC development except migration. In Chapters 2 and 3, I demonstrate that not only are the PCP proteins Prickle1b and Prickle1a required in zebrafish cranial neural

crest, as might be expected from previous findings—they are also required broadly in NCC development, and in particular in a key transition during EMT. Critically, PCP has never been implicated in EMT in any system prior to this study. Collectively, these chapters demonstrate a far broader role for the Prickle1 PCP molecules that could be anticipated from previous work.

CHAPTER 2

THE CORE PLANAR CELL POLARITY PROTEINS PRICKLE1A AND PRICKLE1B REGULATE POLARITY AND MIGRATION OF *DANIO RERIO* CRANIAL NEURAL CREST

2.1 ABSTRACT

As detailed in Chapter 1, the neural crest gives rise to diverse cell types including melanocytes, neurons and glia of the peripheral nervous system, and chondrocytes of the jaw and skull. Proper development of the cephalic region is dependent on the tightly regulated specification and migration of cranial neural crest cells (NCCs). Previously, the core PCP proteins Frizzled and Disheveled have been implicated in NCC migration in the particular mechanism of contact-inhibition of locomotion, but critically, other core PCP proteins—particularly the Prickle homologs—have not been queried in any depth.

In this chapter, I detail my investigation into the functions of the core PCP proteins Prickle1a and Prickle1b in zebrafish cranial NCC migration and polarity. First, I show that *prickle1b* and *prickle1a* are expressed in domains lateral to the neural tube, consistent with expression of pan-neural crest markers. Second, using analysis of *pk1a* and *pk1b* mutant embryos in both fixed whole-mount and live embryos imaged in dorsal views, I show that the genes share similar roles in facilitating cranial NCC migration. Disruption of either gene causes pre-migratory NCCs to cluster together at the dorsal aspect of the neural tube. Like wild-type NCCs, *pk1*-deficient NCC clusters exhibit high levels of motility. Unlike wild-type NCCs which move laterally, however, *pk1*-deficient NCCs exhibit aberrant directionality of movement, with NCCs moving in anterior directions.

Next, I show that *pk1*-deficient NCCs show polarities oriented along the AP axis unlike wild-type cells NCCs, which orient along the mediolateral axis, but critically, specimens double-heterozygous for both genes show a randomized polarity despite showing net anterior movement, indicating that polarity can be lost and decoupled from movement in these specimens, and further suggesting a specific type of dosage-specific redundancy in function for Pk1b and Pk1a.

Finally, I show that even as early as 12 hpf, *pk1*-deficient NCCs form clusters of cells that fail to break contact with each other, and that higher-order clusters (i.e. clusters consisting of three or more cells) exhibit a high degree of persistence in the wrong direction. Taken together, these results show that Pk1b and Pk1a are required for cranial NCC migration and establishment of polarity; in their absence, NCCs maintain the capacity for motility but are unable to sever contacts with each other, and migrate aberrantly in anterior directions. That defects are seen at multiple different stages of neural crest development, also suggests defects prior to the acquisition of 'migratory' morphology.

2.2 CONTRIBUTIONS

This chapter greatly benefitted from the work of individuals other than myself. Manuel Rocha and Noor Singh conducted the in situ hybridization experiments (Fig 2.1), as well as imaging of 18 hpf *Tg[-4.9sox10-EGFP]* embryos counterstained with DAPI (Fig. 2.3

panels A-C). Christina Huang, an undergraduate student, and I performed analysis of wild-type, *pk1b*-morphant, *pk1b*-mutant, *pk1a*-mutant, *vangl2*-morphant, and *pk1a*$^{-/-}$+ *pk1b-MO* fixed specimens at 24 hpf, as well as time-lapse imaging from 16 to 18 hpf together (Fig 2.3, panels D-I and Supplemental movies). This chapter is adapted from a manuscript currently under revision, coauthored with Christina Huang, Victoria Prince, Manuel Rocha and Noor Singh. Materials and methods are dealt with in Chapter 5.

2.3 INTRODUCTION

The neural crest is an embryonic, multipotent cell population that arises from the lateral edges of the developing neural plate, at the interface between neural and non-neural ectoderm (reviewed in Hall, 2000; Le Douarin and Kalcheim, 1999; Theveneau and Mayor, 2012). It is capable of giving rise to a large array of cell types that contribute to the vertebrate body plan (reviewed in Donoghue et al., 2008) including melanocytes, the neurons and glia of the entire peripheral nervous system, and in the cranial region only, the chondrocytes that form the bony elements of the jaw and skull. As a defining feature of the vertebrate phylum, neural crest has been key to the evolution of the complex vertebrate cephalic region (Gans and Northcutt, 1983).

Neural crest cells (NCCs) travel large distances through the developing embryo and display a migratory potential that has been likened to that of metastatic cancer cells

(reviewed in Gallik et al., 2017; Maguire et al., 2015). Like cancer cells, before NCCs migrate to colonize the embryo, they undergo an epithelial-to-mesenchymal (EMT) transition during which they lose their epithelial character (Kaufman et al., 2016), subsequent to which they migrate in streams—in the cephalic region, streams targeted toward specific pharyngeal arches originate from specific dorsal antero-posterior locations.

Many collective cell migration processes in vertebrates, including NCC migration, depend on Planar Cell Polarity (PCP) molecules (reviewed in Davey and Moens, 2017; Roszko et al., 2009). The non-canonical Wnt/PCP pathway influences cranial NCC migration in both *Xenopus* and zebrafish by mediating contact inhibition of locomotion (CIL) (Carmona-Fontaine et al., 2008; De Calisto et al., 2005; Matthews et al., 2008; Scarpa et al., 2015; Theveneau et al., 2010; Theveneau et al., 2013). Specifically, highly-protrusive migratory NCCs contact one another, activate the core PCP proteins Frizzled and Disheveled at the points of contact, and reorient their protrusions to migrate away from each other (Carmona-Fontaine et al., 2008; Scarpa et al., 2015; Szabo et al., 2016; Theveneau et al., 2013).

The core PCP protein Prickle (Pk) has not previously been comprehensively investigated in cranial neural crest development. However, several characteristics make it an attractive candidate for study. In *Drosophila*, Pk is required to amplify cellular asymmetries of other

core PCP proteins, and differential expression of Pk isoforms is critical for the establishment of tissue polarity (Ambegaonkar and Irvine, 2015; Merkel et al., 2014; Sharp and Axelrod, 2016; Tree et al., 2002; reviewed in Zallen, 2007). Additionally, in vertebrates, multiple orthologs of *Drosophila* Pk control the localization and dynamics of other core PCP proteins in morphogenesis and collective cell migration (reviewed in Davey and Moens, 2017; Jussila and Ciruna, 2017). Like other core PCP proteins, Pk1 molecules play roles in convergent extension during gastrulation and neurulation (Ciruna et al., 2006; Sepich et al., 2011; Veeman et al., 2003; Yin et al., 2008), in organizing the sensory cells of the inner ear (reviewed in May-Simera and Kelley, 2012; Rida and Chen, 2009), in the polarization of ciliated epithelia (Butler and Wallingford, 2015), and in the migration of facial branchiomotor neurons (Mapp et al., 2011; Mapp et al., 2010).

In this study, we present evidence of roles for the zebrafish Prickle1 paralogs, Prickle1b (Pk1b) and Prickle1a (Pk1a), in both EMT and NCC migration. Our investigation has utilized both our previously described *pk1b*$^{fh122/fh122}$ mutant (Mapp et al., 2011), and a new *pk1a*$^{ch105/ch105}$ mutant. Time-lapse imaging analysis revealed that disruption of either *pk1b* or *pk1a* causes pre-migratory NCCs to cluster with neighboring NCCs at the dorsal aspect of the neural tube, and adopt aberrant cell polarity and inappropriate motility along the anteroposterior (AP) axis of the dorsal neural tube. The two *pk1* paralogs function redundantly both in EMT and migration. Our findings demonstrate that the core

PCP Pk1 molecules are required in the regulation of cranial neural crest polarity and migration.

2.4 RESULTS

2.4.1 Disruption of *pk1b* and *pk1a* function alters cranial NCC disposition

Both zebrafish *pk1b* and *pk1a* paralogs are expressed in the developing nervous system (Carreira-Barbosa et al., 2003; Rohrschneider et al., 2007; Roszko et al., 2009; Veeman et al., 2003). Our previous in situ hybridization analysis has demonstrated that *pk1b* is expressed in the developing hindbrain by the 16 hpf stage, with elevated levels of expression in migrating facial branchiomotor neurons (FBMNs) (Rohrschneider et al., 2007). Similarly, *pk1a* expression has also been reported in the hindbrain (Carreira-Barbosa et al., 2003; Roszko et al., 2009). In both reports, expression can additionally be noted in domains immediately lateral to the developing hindbrain, suggesting that the *pk1* paralogs might also be expressed in cranial neural crest cells. To investigate cranial NCC expression in more detail, we performed in situ hybridization to investigate *pk1b* and *pk1a* expression at 24 hpf, and compared the expression patterns with that of the pan-neural crest marker *crestin* (Fig. 2.1). Although colorimetric in situ hybridization analysis does not provide single-cell resolution, both *pk1b* and *pk1a* are expressed in domains lateral to the anterior hindbrain and midbrain that overlap with expression of *crestin*. These results

indicate that *pk1b* and *pk1a* are expressed at an appropriate time and place to play a role in the development of cranial neural crest.

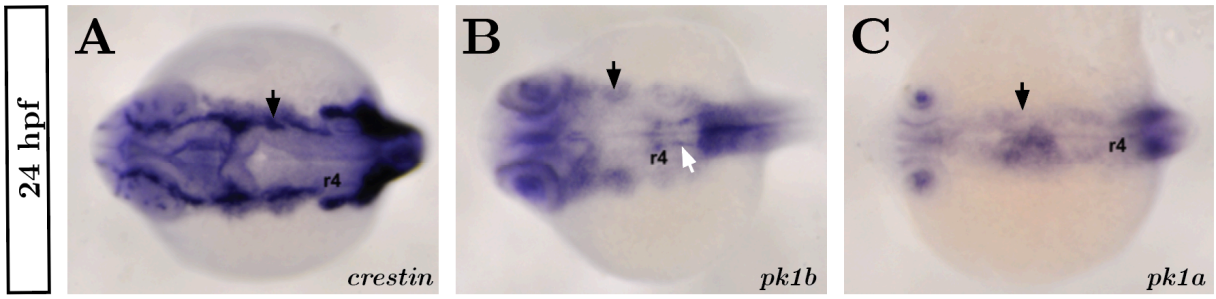

Figure 2.1: Zebrafish *pk1b* and *pk1a* are expressed in domains that partially overlap with expression of the pan-neural crest marker *crestin*

(A-C) In situ hybridizations for the pan-neural crest marker *crestin* (A), *prickle1b* (B) and *prickle1a* (C), dorsal views at 24 hpf, show that both *pk1b* and *pk1a* are expressed in tissue lateral to the neural tube consistent with expression in the pharyngeal arches. Low levels of expression are also seen on the neuroepithelium. Solid black arrows indicate gene expression in the cranial NCCs stream leading to pharyngeal arch 1 (PA1), solid white arrow indicates *pk1b* expression in the FBMNs, r4 is indicated.

To investigate the functions of *pk1b* and *pk1a* in developing cranial NCCs, we have utilized zebrafish embryos mutant for each gene. We previously described the *pk1b* $^{fh122/\ fh122}$ mutant, which is characterized by a complete block to collective cell migration of FBMNs through the hindbrain (Mapp et al., 2011). Importantly, Pk1b-morpholino (MO) knockdown precisely phenocopies the *pk1b* $^{fh122/\ fh122}$ mutant FBMN defect, implying that this C-terminal point mutation (Fig. 2.2A) is a strong hypomorph (Mapp et al., 2011). To allow analysis of Pk1a function, we used the CRISPR/Cas system to generate a novel

mutant, *pk1a*$^{ch105/ch105}$. The *ch105* allele is a predicted null, with a premature stop codon at amino acid 24, truncating the protein close to its N-terminus (Appendix A1.1). In contrast to previous reports of specimens in which *pk1a* function was disrupted using morpholino knockdown (Carreira-Barbosa et al., 2003; Veeman et al., 2003), *pk1a*$^{ch105/ch105}$ mutant embryos do not show obvious gastrulation defects, except when combined with the knockdown of Pk1b. Although homozygous *pk1a*$^{ch105/ch105}$ mutant embryos do not survive at Mendelian ratios, they can nevertheless occasionally be raised to fertile adulthood. Further details about the generation of the *pk1a*$^{ch105/ch105}$ mutant can be found in Appendix A.

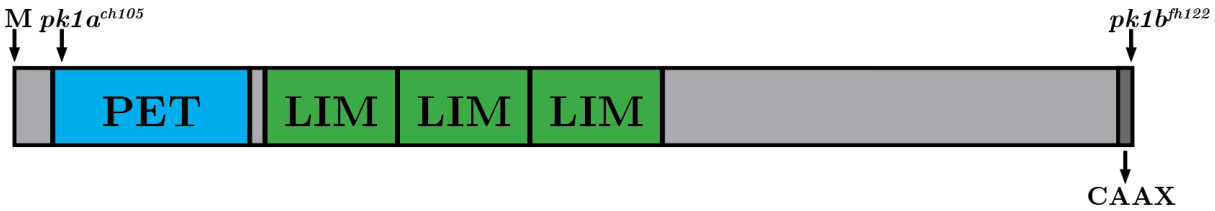

Fig. 2.2.: The protein domain structure of Prickle1b and Prickle1a.

Arrows indicate lesions in *pk1a*^{ch105} and *pk1b*^{fh122} mutants. The first codon, and the C-terminal CAAX domain are also indicated.

To investigate cranial NCC behaviors in the *pk1* mutants, we made use of the *Tg(sox10:EGFP)* line (Carney et al., 2006), which expresses GFP in all NCCs beginning at approximately 12 hpf. In the cranial region, streams of NCCs derive from specific anteroposterior (AP) regions of the developing midbrain and hindbrain and migrate out

to populate the pharyngeal arches and frontonasal process (Lumsden et al., 1991; Schilling and Kimmel, 1994). In wild-type *Tg*(*sox10*:*EGFP*) specimens counterstained with the nuclear marker DAPI at 18 hpf, streams of cranial NCCs were detected migrating ventrolaterally into the developing pharyngeal arches (PAs) as well as into the fronto-nasal process (Fig. 2.3A). By contrast, in both the *pk1b*$^{fh122/fh122}$ and *pk1a*$^{ch105/ch105}$ single homozygous mutants, fewer NCCs were present in the pharyngeal arches. Further, in *pk1*-mutants, NCCs were found in groups of closely-apposed cells located at the dorsal-most aspect of the midbrain and anterior hindbrain, showing a markedly different organization to the more dispersed, individual NCCs found in wild-type specimens (compare Fig. 2.3B, C with 2.3A).

To investigate the disposition of cranial NCCs in more detail, we imaged the cranial region of wild-type and *pk1* mutant embryos in dorsal view at 24 hpf. As our expression analyses indicated both *pk1* paralogs are expressed in neural crest adjacent to the anterior hindbrain and midbrain at 24 hpf (Fig. 2.3B, C) our analyses focused on this axial level. In wild-type specimens, although the majority of dorsal NCCs are individual, we also observed a few small groups of closely-apposed NCCs, or 'clusters' of cells (Fig. 2.3D). Both individual and closely-apposed wild-type NCCs displayed highly protrusive morphologies with filopodia and lamellipodia (Fig. 2.3D'-D''). By contrast, both *pk1b*$^{fh122/fh122}$ and *pk1a*$^{ch105/ch105}$ mutants showed both a higher frequency of and larger NCC

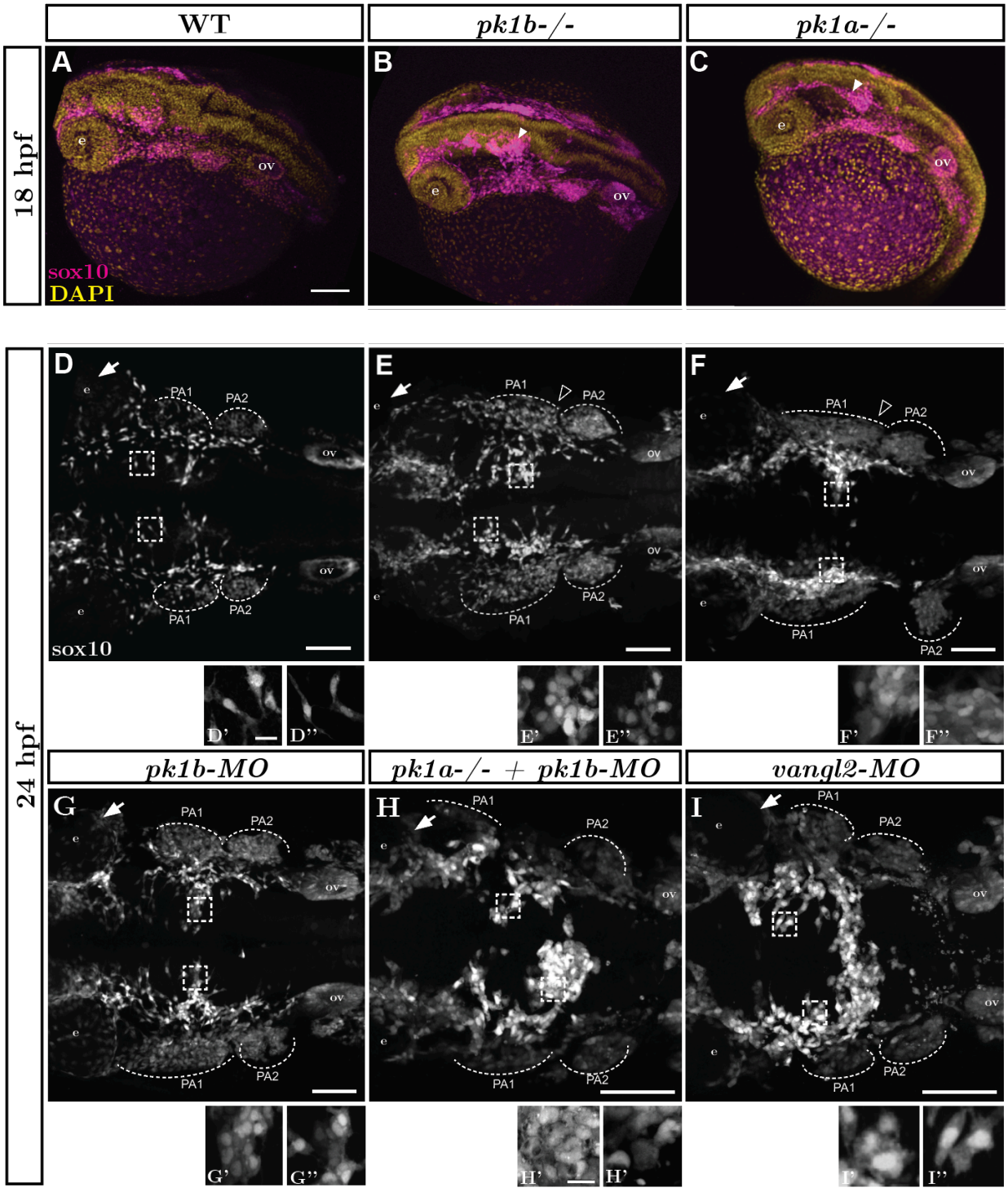

Fig. 2.3: Disruption of *pk1b or pk1a* function causes neural crest cells to cluster and disruption of *vangl2* or both *pk1b* and *pk1a* function causes more severe neural crest defects

Fig. 2.3 continued: Maximal projections of confocal images from fixed *Tg(sox10:EGFP)* embryos at 18 hpf (A-C) and 24 hpf (D-I). In comparison to wild-type (WT) (A, D), the GFP-expressing NCCs form distinct clusters located dorsally in *pk1b* $^{fh122/\ fh122}$ (B, E), *pk1a*$^{ch105/ch105}$ (C, F), *pk1b*-morphant (G), *pk1a*$^{ch105/ch105}$ + *pk1b*-morphant (H), and *vangl2*-morphant (I) embryos. (A-C) Dorsolateral views of 18 hpf embryos, counterstained with DAPI, show the 3D formation of NCC streams migrating ventrolaterally, the *pk1b* $^{fh122/\ fh122}$ (B) and *pk1a*$^{ch105/ch105}$ (C) mutant embryos exhibit dorsal clusters of NCCs along the AP axis, as indicated by solid white arrowheads; ov = otic vesicle, e = eye, scale bar = 100µm. (D-I) Maximal projection images of representative, flat-mounted deyolked embryos at 24 hpf in dorsal view show NCC clusters on the dorsal aspect of the neural tube; boxed insets at high magnification show NCC morphology. The scale (bar=100µm) is identical for all specimens shown except for *pk1a*$^{ch105/ch105}$ + *pk1b*-morphant, and *vangl2*-morphant embryos, which showed a shortened AP body axis and a wider mediolateral body axis due to convergence defects. As compared to WT embryos (n=13 embryos) (D), *pk1b* $^{fh122/\ fh122}$ (n=12 embryos) (E) and *pk1a*$^{ch105/ch105}$ (n=9 embryos) (F) mutant embryos exhibit the maintenance of dorsal NCC clusters. *pk1b*-morphant (n=18 embryos) (G) embryos phenocopy the *pk1b* $^{fh122/\ fh122}$ mutant embryos (E). The *pk1a*$^{ch105/ch105}$ + *pk1b*-morphant (n=8 embryos) (H), and *vangl2*-morphant (n=7 embryos) (I) show a more severe phenotype of dorsal NCC clustering across the midline. (D'-I'') High magnification insets from associated micrographs show that in contrast to WT NCCs (D', D'') where NCCs exhibit bipolar, protrusive morphologies, *pk1b* $^{fh122/\ fh122}$ (E', E'') *pk1a*$^{ch105/ch105}$ (F', F''), *pk1b*-morphant (G', G''), *pk1a*$^{ch105/ch105}$ + *pk1b*-morphant (H', H''), and *vangl2*-morphant (I', I'') NCCs show less protrusive, more rounded morphologies that exhibit close contacts with neighboring NCCs. The scale bar (10µm) is identical for each inset. *PA1*=pharyngeal arch 1, *PA2*=pharyngeal arch 2, *PA3*=pharyngeal arch 3, *ov*=otic vesicle.

---

clusters lying dorsally at midbrain and hindbrain levels, consistent with our observations at the 18 hpf stage, with the cells displaying rounded, non-protrusive morphologies (Fig.

2.3E'-E'', F'-F''). We confirmed that morpholino knockdown of Pk1b, using our previously described reagents (Mapp et al., 2011), fully phenocopied the *pk1b*$^{fh122/fh122}$ mutant (Fig. 2.3G-G'').

To assay embryos deficient in both Pk1b and Pk1a, we imaged *pk1a*$^{ch105/ch105}$ embryos injected with morpholinos targeted against Pk1b, and found a more severe phenotype, with larger dorsal NCC clusters than in the single homozygous mutants alone, as well as gross morphological defects consistent with disruptions in convergent extension (Fig. 2.3H-H''). We then compared this phenotype of embryos deficient in both Pk1b and Pk1a to the phenotype caused by knockdown of another core PCP molecule, Vangl2, which is also known to be important in convergent extension (Ferrante et al., 2009; Jessen et al., 2002). We found that knockdown of Vangl2 also caused a severe dorsal NCC clustering phenotype, with NCCs meeting across the dorsal midline of the neural tube at approximately the level of r3 (Fig. 2.3N-N''), as well as gross morphological defects. These results are consistent with previous reports that Vangl2 is required for proper convergence of neuroepithelial cells towards the midline during neurulation (Ciruna et al., 2006; Tawk et al., 2007). As the resultant altered neural keel morphology makes it difficult to ascribe NCC phenotypes to deficits in NCCs themselves versus earlier defects in neurulation, we elected not to study *vangl2* morphants or embryos deficient for both *pk1* paralogs in any additional detail. However, the lack of convergence defects both in single homozygous

pk1b $^{fh122/\ fh122}$ and *pk1a*$^{ch105/ch105}$ mutants, as well as in double-heterozygous embryos lacking one copy each of *pk1b* and *pk1a*, provided us a unique opportunity to study the roles of the Pk1 paralogs specifically in the developing neural crest.

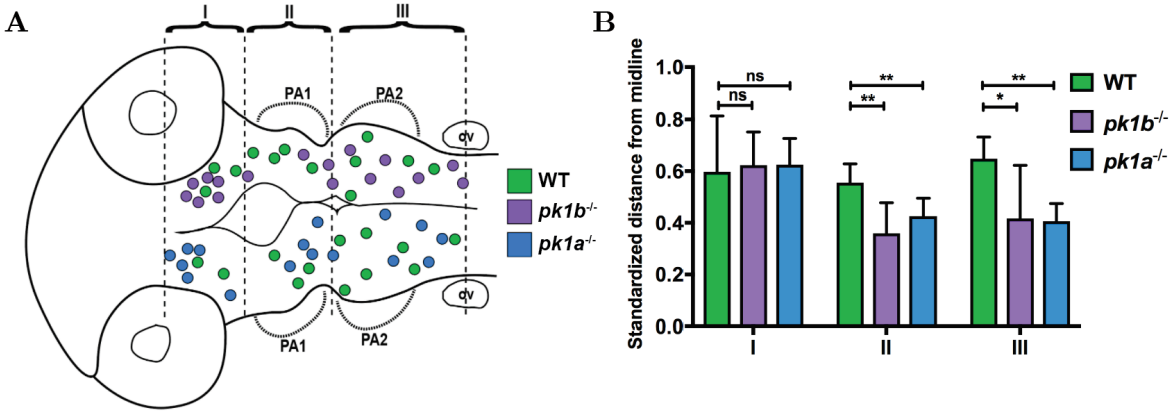

Fig. 2.4: Pk1-deficient clusters show aberrant spatial biases

(A, B) The spatial distribution of clusters across embryos shows that both *pk1b* $^{fh122/\ fh122}$ and *pk1a*$^{ch105/ch105}$ clusters show anterior and medial biases. (O) The centroids of cell clusters, defined as two or more cells in contact with one another. across multiple *pk1b* $^{fh122/\ fh122}$ specimens (n=5 embryos) are plotted above the midline and those of *pk1a*$^{ch105/ch105}$ specimens (n=5 embryos) are plotted below the midline, with WT clusters on both sides for comparison (green filled circles, n=5 embryos). There is a bias for both *pk1b* $^{fh122/\ fh122}$ and *pk1a*$^{ch105/ch105}$ clusters in R1, as well as a tendency to misalign such that the cluster cannot be ascribed to distinct streams for either PA1 or PA2. (P) Normalized distances of centroids of clusters from the midline show that in both RII and RIII there is a tendency for *pk1b* $^{fh122/\ fh122}$ and *pk1a*$^{ch105/ch105}$ NCCs to be located medially as compared to WT NCCs. The bias was found to be statistically significant for regions II and III using a two-way ANOVA test (*, $p<0.05$, **, $p<0.01$) for WT as compared to both mutant conditions. There was no statistically significant difference between WT and either mutant condition in Region I ($p>0.05$).

To investigate the unusual NCC clusters in *pk1* mutants in more detail, we mapped their spatial localization. For this analysis, we defined 'clusters' as groups of three or more cells in close apposition. We allocated the clusters to three regions, corresponding to different axial positions as indicated in Fig. 2.4A: Region I corresponds to anterior midbrain-derived NCCs that contribute to the fronto-nasal process; region II corresponds to posterior midbrain and rhombomere 1, 2 and 3 (r1-r3)-derived NCCs from the anterior hindbrain that contribute to pharyngeal arch (PA)1; region III corresponds to central hindbrain (r3-r5)-derived NCCs that migrate anterior of the otic vesicle to contribute to PA2. Interestingly, despite a widespread distribution of dorsally-located NCC clusters along the AP axis in both mutant conditions, a slight spatial bias was detectable, with clusters most frequently located towards the anterior. Moreover, NCC clusters that spanned the space between the origins of two separate streams of migratory NCCs occurred more frequently in the *pk1* mutants than in wild-type specimens (Fig. 2.4A).

To query whether there was a mediolateral bias in cluster location, we measured the distances between the centroids of clusters and the midline, and expressed the distances as a ratio of the longest possible distance between any NCC and the midline at that specific AP position. This analysis confirmed that for NCCs migrating towards PA 1 and 2 there is a statistically significant bias for cell clusters to be located closer to the midline

in both *pk1b* $^{fh122/\ fh122}$ and *pk1a*$^{ch105/ch105}$ mutant conditions as compared to wild-type. However, no such bias was found for the midbrain-derived cells migrating towards the fronto-nasal process (Fig. 2.4B). The medial bias of Pk1-deficient NCCs in clusters indicates that Pk1-deficient cells do not migrate laterally, unlike wild-type cells, and suggests that these Pk1-deficient NCCs may instead remain pre-migratory.

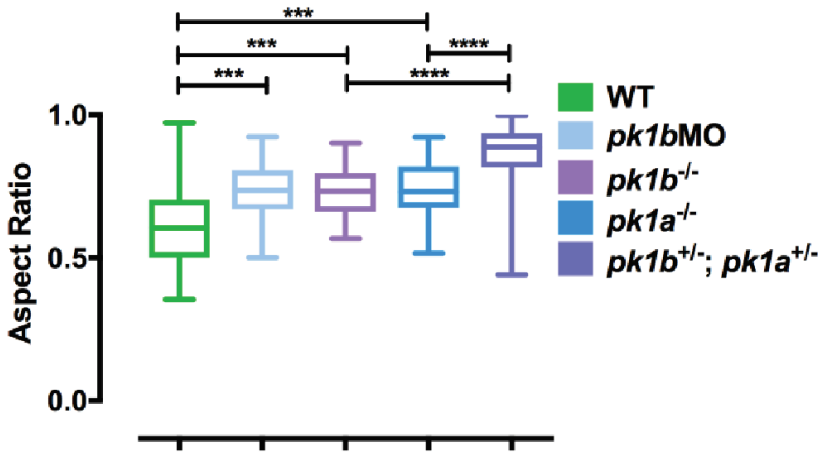

Fig. 2.5: Disruption of *pk1b* or *pk1a* function causes cells to adopt rounded morphologies

Measurements of aspect ratio (the ratio of width/length of NCCs) for WT (n=34 cells), *pk1b*-morphant (n=48 cells), *pk1b* $^{fh122/\ fh122}$ (n=40 cells), *pk1a*$^{ch105/ch105}$ (n=30 cells), and double-heterozygous *pk1a*$^{ch105/+}$; *pk1b*$^{fh122/+}$ (n=94 cells) specimens were performed by measuring the width and length ratio of NCCs either in *Tg(sox10:mRFP)* embryos, which label the membranes of all NCCs, or in *Tg(sox10:EGFP)* embryos co-injected with RNA encoding mRFP. WT NCCs had lower aspect ratios in comparison to each Pk1-deficient condition. Statistical significance was calculated in each pairwise case using unpaired t-tests (***, $p<0.001$; ****, $p<0.0001$). Double-heterozygous *pk1a*$^{ch105/+}$; *pk1b*$^{fh122/+}$ embryos showed a significantly higher aspect ratio than either *pk1b* $^{fh122/\ fh122}$ or *pk1a*$^{ch105/ch105}$ alone ($p<0.0001$ in both cases).

We qualitatively observed that wild-type NCCs were more elongated and protrusive than Pk1-deficient NCCs, which were more rounded and less protrusive. To confirm the differences in cell shape, we measured the aspect (width:length) ratios of NCCs in wild-type and mutant conditions. Wild-type NCCs showed more elongated shapes with a mean aspect ratio of 0.61. In contrast, *pk1b*-MO, *pk1b* $^{fh122/\ fh122}$, and *pk1a*$^{ch105/ch105}$ NCCs exhibited significantly higher mean aspect ratios of 0.73, 0.73, and 0.74, respectively, ($p<0.001$ for each). Interestingly, *pk1a*$^{ch105/+}$; *pk1b*$^{fh122/+}$ double-heterozygous embryos exhibited a higher mean aspect ratio, of 0.86, than either wild-type or single homozygous mutant NCCs ($p<0.0001$) (Fig. 2.5). The unusually rounded morphology of Pk1-deficient NCCs indicates that Pk1 may play a role in the acquisition of elongated, mesenchymal morphology.

In summary, we conclude that the core PCP proteins Pk1b and Pk1a are necessary for pre-migratory NCCs to acquire the elongated morphologies associated with directed migration.

2.4.2 Loss of *pk1b* or *pk1a* function disrupts ventrolateral migration of cranial neural crest cells

Based on our observations of Pk1-deficient NCC clusters at the dorsal aspect of the cranial neural tube, we hypothesized that in Pk1-deficient embryos, NCCs fail to migrate ventrolaterally into streams. We addressed this using time-lapse confocal imaging of *Tg(sox10:EGFP)* embryos over a two-hour period, from 16 hpf to 18 hpf, of active NCC migration in the cranial region. For this analysis, we imaged the region corresponding to the PA1 stream of NCCs, deriving from the midbrain and r1-r2 (indicated by the dashed box in Fig. 2.6A) in dorsal view. At 16 hpf the neural keel has not yet formed a midline, which occurs through alignment of neuroepithelial cell end feet by 18 hpf (Jimenez et al., 2016; Tawk et al., 2007). At approximately 16 hpf, cranial neural crest cells from the dorsal neural keel complete EMT and actively migrate laterally to the edges of the neural keel, and then ventrally towards the pharyngeal region. As shown for the embryo imaged in Supplemental Movie 1 and analyzed in Fig. 2.6B, wild-type NCCs form dynamic, transient contacts with neighboring NCCs and move laterally towards the edge of the neuroepithelium (line in Supplemental Movie 1, and dashed line in Fig. 2.6B) between 16 and 18 hpf. To assay the overall movement of these NCCs, we plotted displacement trajectories using the first and last position of individual cells after correcting for drift and embryo growth. We found that 89% of wild-type NCCs (n=59 cells, 3 embryos,

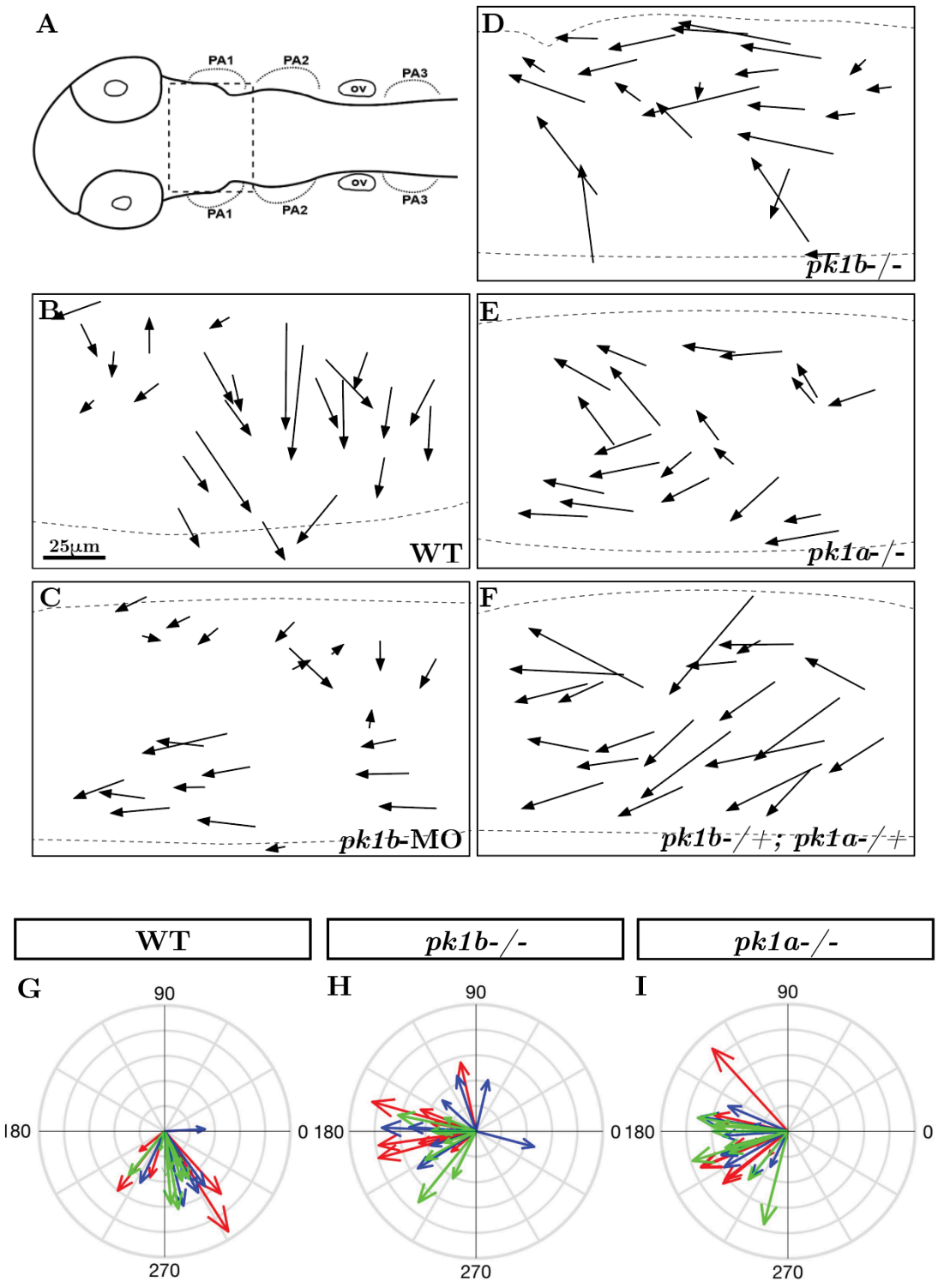

Fig. 2.6: Loss of function of either *pk1b* or *pk1a* causes aberrant motility in pre-migratory cranial neural crest cells

Fig. 2.6 continued: (A) Schematic dorsal view of a 16 hpf embryo with optic cup, pharyngeal arches (PA), and otic vesicle (ov) indicated; dashed box indicates region that was time-lapse imaged. (B-F) Displacement tracks of motile NCCs at NCCs in dorsal view, anterior to left, from 16-18 hpf. The x and y components of the displacement tracks were drift-corrected relative to bright-field images of the embryos to account for growth and movement of the embryo. In contrast to WT embryos (B) where the net displacement of NCCs is lateral towards the first stream of NCCs, the net displacement of NCCs in *pk1b*-morphant (C), *pk1b*$^{fh122/fh122}$ (D) and *pk1a*$^{ch105/ch105}$ (E) mutant embryos is in the anterior direction. NCCs in double-heterozygous *pk1a*$^{ch105/+}$; *pk1b*$^{fh122/+}$ specimens (F) also move in net anterior directions. Scale bar = 25 µm. (G-I) To show inter-embryo variation in displacement trajectories, 10 displacement trajectories for 3 embryos each were plotted at the origin, with both left and right sides of the embryo in the case of WT (G) embryos transposed on to one side for clarity. Trajectories from different embryos are colored in red, blue, and green. (G) WT NCCs move in the lateral direction as is expected for the first stage of normal ventrolateral NCC migration. (H, I) *pk1b*$^{fh122/fh122}$ and *pk1a*$^{ch105/ch105}$ mutant NCCs display a bias for anterior directionalities.

---

representative embryo shown in Supplemental Movie 1 and Fig. 2.6B) showed net lateral movement over the two-hour time period.

Because loss of Pk1b or Pk1a function caused aberrant NCC cluster formation, we postulated that it would also result in a loss of overall NCC motility. Unexpectedly, we found that *pk1b*-morphant cells did not lose motility. Rather 72% of *pk1b*-MO NCCs

(n=47 cells, 3 embryos) showed net movement in the anterior direction, with NCCs typically retaining contacts with neighboring cells as they moved in a cluster (Supplemental Movie 2, Fig. 2.6C). A similar anterior bias of NCC motility was noted in *pk1b* $^{fh122/\ fh122}$ embryos (Fig. 2.6D), with 77% of NCCs showing net movement in the anterior direction (n=65 cells, 3 embryos). In both *pk1b*-MO and *pk1b* $^{fh122/\ fh122}$ specimens, clusters of NCCs showed less dynamic and protrusive behaviors than wild-type NCCs (Supplemental Movies 2, 3, Fig. 2.6C, D). *pk1a*$^{ch105/ch105}$ embryos exhibited a similar phenotype (Supplemental Movie 4, Fig. 2.6E), with 75% of NCCs showing net movement in the anterior direction (n=47 cells, 3 embryos). We also assayed double-heterozygous *pk1a*$^{ch105/+}$; *pk1b*$^{fh122/+}$ embryos which—unlike *pk1a*$^{ch105/ch105}$ +*pk1b*-MO embryos—do not show gross morphological defects. We found that 86% of *pk1a*$^{ch105/+}$; *pk1b*$^{fh122/+}$ NCCs (n=38 cells, 3 embryos) also moved in net anterior directions (Supplemental Movie 5, Fig. 2.6F), a higher proportion than in either Pk1b-deficient or Pk1a-deficient embryos. We conclude that Pk1-deficient specimens do not demonstrate a loss of NCC motility, but instead an altered anterior directionality. We further conclude that the Pk1 paralogs function partially redundantly such that double-heterozygous embryos show a more severe phenotype than either single homozygous mutant despite the same number of alleles being disrupted, likely because of the dosage sensitivity of the combined action of the genes. There is precedent for PCP genes acting in a highly dosage-specific manner—notably in members of the Vangl family in mouse embryos (Torban et al., 2008)—such that a genetic

interaction between two homologs manifests as a more severe phenotype in a double-heterozygous embryo than a single homozygous mutant for either homolog.

To highlight the degree of inter-embryo variation in NCC motility, we plotted the displacement trajectories of 10 NCCs from three individual embryos of each of the wild-type, *pk1b* $^{fh122/\ fh122}$, and *pk1a*$^{ch105/ch105}$ conditions, with NCCs from different embryos allocated a different color (Fig. 2.6G-I). This analysis reaffirmed that wild-type NCCs move in lateral directions. Further, in mutant conditions the trend for anterior motility was highly consistent. We conclude that both Pk1b and Pk1a are required for lateral NCC migration. When two *pk1* alleles are disrupted (i.e. homozygous mutation of one *pk1* paralog, or disruption of a single copy of both *pk1* paralogs), cranial NCCs form clusters that do not migrate laterally but instead preferentially move towards the anterior.

2.4.3 Loss of Pk1 function disrupts NCC polarity

The finding that Pk1-deficient NCCs preferentially move in an anterior direction led us to postulate that the dorsally-located pre-migratory NCCs adopt aberrant polarities, rather than losing polarity entirely as might be expected in a PCP-deficient condition. Previously, it has been reported that PCP signals control the position of the intracellular microtubule organizing center (MTOC), and that cells polarize MTOCs in the direction of motility (Sepich et al., 2011). To assay the polarity of NCCs at the dorsal aspect of the

neural tube, in both wild-type and Pk1-deficient conditions, we measured the angle of the MTOC relative to the primary body axis (Fig. 2.7B).

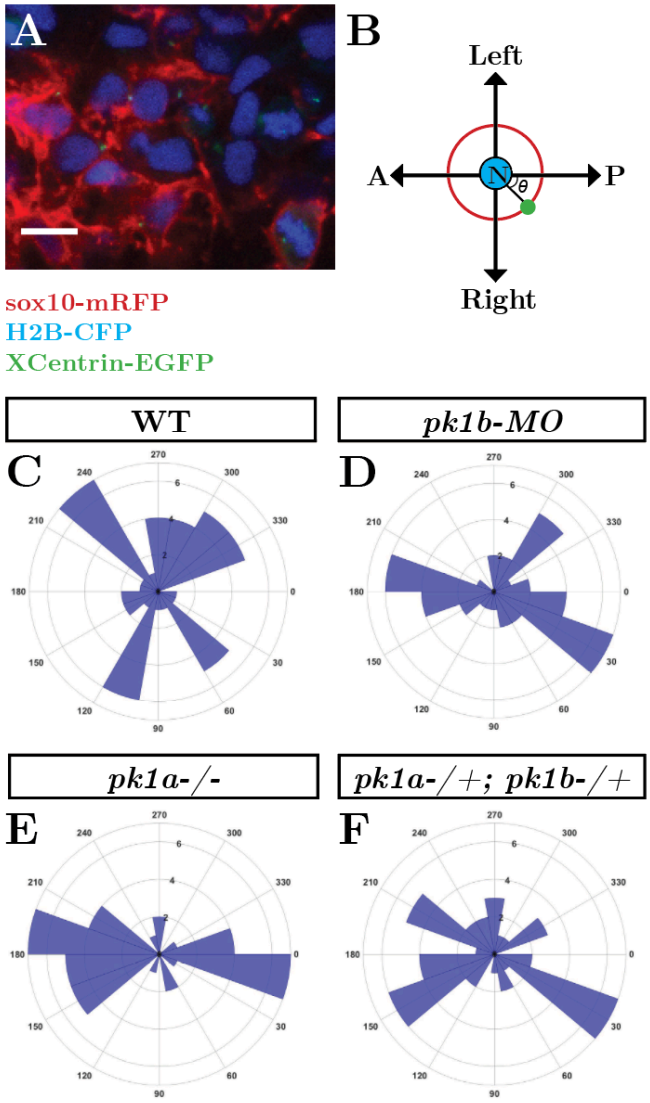

Fig. 2.7: Disruption of *pk1b* and *pk1a* causes aberrant polarity but disruption of in double-heterozygous neural crest cells causes loss of polarity in pre-migratory neural crest cells

To assay the polarity of NCCs, MTOCs in NCCs were labeled by injecting either XCentrin-EGFP RNA in one-cell stage *Tg(sox10:mRFP)* or Cherry-XCentrin RNA in one-cell stage *Tg(sox10:EGFP)* embryos that

Fig. 2.7 continued: were also injected with H2B-CFP to label nuclei. Fixed, deyolked, flat-mounted 24 hpf embryos were imaged in dorsal view (A). The angle ϑ of the MTOC relative to the nucleus and the AP body axis (B) was measured for each cell and quantified using Fiji. (C-F) Polar histograms generated using MATLAB show the polarity of assayed NCCs. In all cases, the Watson-Williams F-test was used to measure statistical significance between conditions as well as with a randomly-distributed polar histogram. In WT embryos, NCCs (n=48 cells, 5 embryos) were polarized along the mediolateral axis consistent with the lateral directionality of WT NCCs (C), with WT cells showing a significant difference from a random distribution (***, $p<0.001$). However, in *pk1b*-morphant specimens (n=42 cells, 3 embryos) (D) and $pk1a^{ch105/ch105}$ specimens (n=40 cells, 3 embryos) (E) NCCs were polarized along the AP axis, consistent with an anterior bias for directionality of *pk1*-deficient NCCs. As compared to WT NCCs, both *pk1b*-morphant and $pk1a^{ch105/ch105}$ NCCs were significantly altered and showed a significant difference from random distributions (***, $p<0.001$ for each case). However, double-heterozygous $pk1a^{ch105/+}$; $pk1b^{fh122/+}$ NCCs showed more randomized polarities than NCCs in either *pk1b*-morphant or $pk1a^{ch105}$ conditions alone (F), with no statistically significant difference for $pk1a^{ch105/+}$; $pk1b^{fh122/+}$ NCCs as compared to a random distribution ($p>0.5$), indicating that disrupting one copy each of the *pk1a* and *pk1b* genes is sufficient to randomize NCC polarity.

In accord with previous findings, we found that wild-type NCCs at 24 hpf on either side of the midline polarized laterally in the direction of normal migration (Fig. 2.7C). In contrast, *pk1b*-morphant (Fig. 2.7D, $p<0.001$) and $pk1a^{ch105/ch105}$ (Fig. 2.7E, $p<0.001$) NCCs on either side of the midline polarized along the AP axis. However, NCCs in double-heterozygous $pk1a^{ch105/+}$; $pk1b^{fh122/+}$ embryos displayed a randomized polarity (Fig. 2.7F,

p>0.5), despite our previous finding that these NCCs moved as clusters in anterior directions similar to the single *pk1* mutants (Fig. 2.6F). These findings suggest that whereas Pk1b-deficient, and Pk1a-deficient NCCs polarize to correspond to the aberrant direction of migration, in double-heterozygous NCCs, MTOC position is decoupled from the direction of migration, indicating a loss of polarity. We conclude that while both Pk1b and Pk1a are required to establish normal NCC polarity, the absence of either alone is insufficient to cause a complete loss of polarity. However, the double-heterozygous condition is sufficient for loss of polarity, indicating that the two Pk1 paralogs function redundantly and again likely reflecting the importance of gene dosage. Importantly, the altered polarity of Pk1-deficient NCCs occurs in conjunction with aberrant morphologies and increased clustering.

2.4.4 Loss of Pk1 function causes dorsal NCC clusters to form and be maintained in pre-migratory NCCs

Having observed dorsally clustered NCCs in embryos lacking either Pk1b or Pk1a function, we investigated at what stage of NCC development the clusters formed and probed their characteristics in more detail. We hypothesized that the clustering defect arose at stages prior to the migration of cranial NCCs in well-defined streams, and that

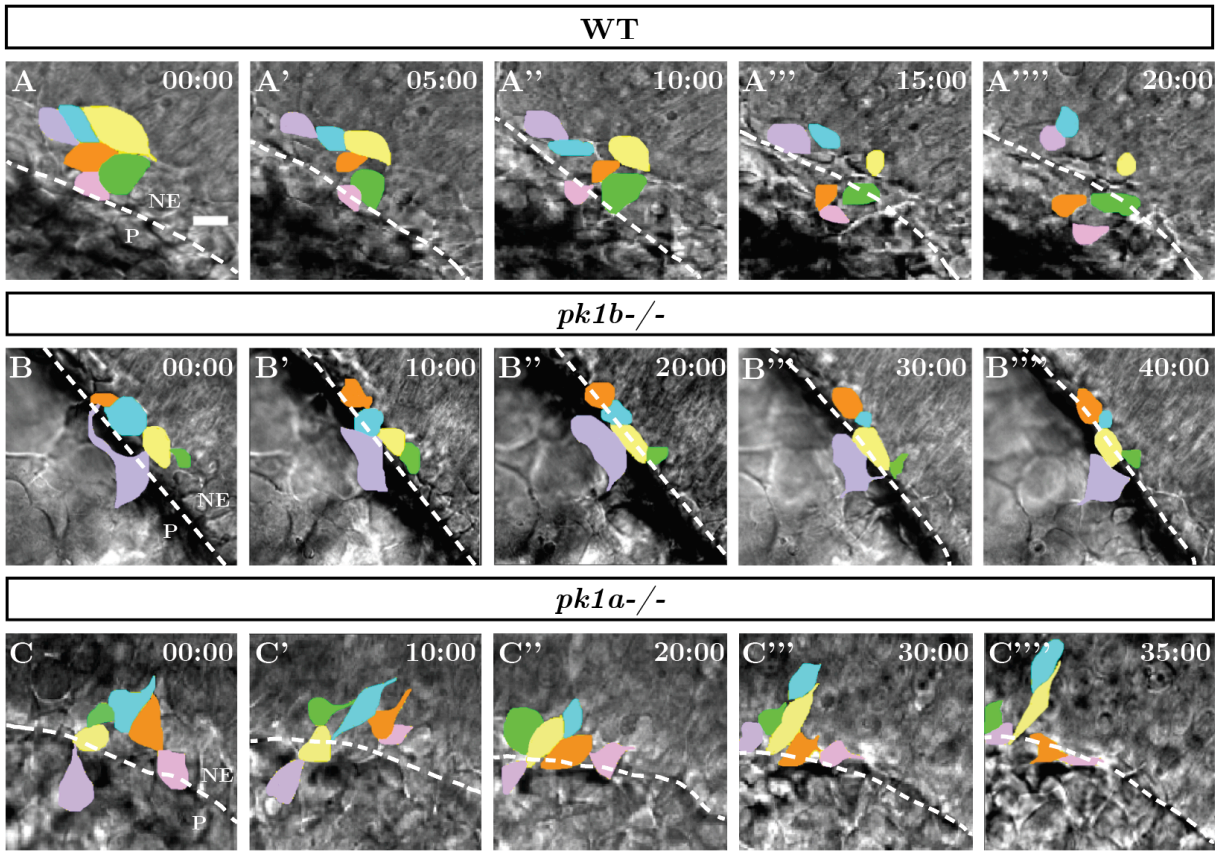

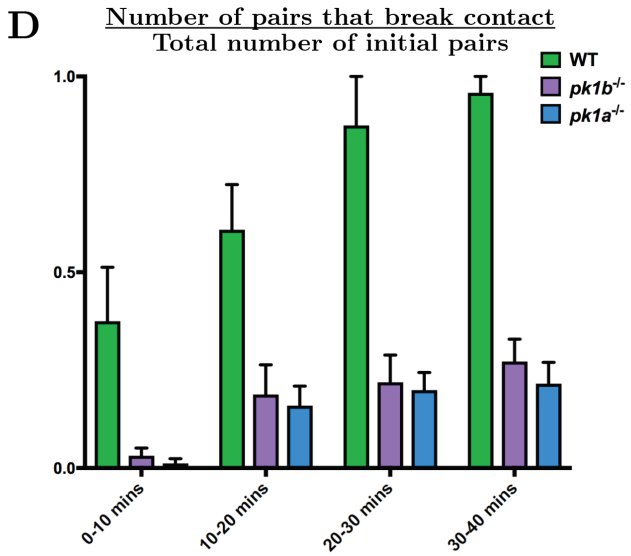

Fig. 2.8: Loss of Pk1 function causes dorsal neural crest cells to be cluster early on in neural crest development at 12 hpf

Fig. 2.8 continued: Confocal time-lapse imaging of dorsally-mounted *Tg(sox10:EGFP)* embryos was started at 12 hpf when the neural keel is still developing, with both EGFP and DIC (brightfield) images collected every 5 minutes. (A-C) Reorganization of EGFP+ NCCs (pseudocolored) in clusters of NCCs at t=0 to t=40 mins; dotted line indicates border of the neuroepithelium, located at top right in all panels. P=periphery. NE=neuroepithelium. Scale bar=10 µm. (A) In WT embryos, many of the NCCs in contact at t=0 break contact by 20 minutes, with almost all contacts breaking by 30 mins and 40 mins. (B, C) In *pk1b* $^{fh122/\ fh122}$ and *pk1a*$^{ch105/ch105}$ specimens NCC clusters largely remained in contact for 40 mins. (D) To quantify breakage of contacts between NCCs over the time intervals 0-10 min, 10-20 min, 20-30 min and 30-40 min, a ratiometric measure of 'pair breakage' within a cluster was used (Methods). In WT embryos, 57% of pairs of cells broke contacts within 10-20 minutes (n=43 pairs, 3 embryos), with the majority of pairs losing contact by 20-30 minutes. In contrast, pairs of NCCs in both *pk1b* $^{fh122/\ fh122}$ (n=61 pairs, 3 embryos) and *pk1a*$^{ch105/ch105}$ embryos (n=58 pairs, 3 embryos) did not break over extended periods of time, with only ~25% of pairs in *pk1b* $^{fh122/\ fh122}$ clusters breaking contact and ~20% of pairs in *pk1a*$^{ch105/ch105}$ clusters breaking contact by 30-40 minutes.

---

wild-type cells, even early in neural crest development, are able to resolve contacts with neighboring NCCs at faster rates than Pk1-deficient cells. To test these hypotheses, we performed time-lapse imaging of *Tg*(*sox10:EGFP*) embryos beginning at 12 hpf and extending for at least 4 hours. We noted that even as early as 12 hpf, some NCCs are present ventrolaterally, a finding which is consistent with previous reports of an early population of NCCs originating from the non-neural ectoderm adjacent to the neural keel

(Jimenez et al., 2016; Schilling and Kimmel, 1994), and one that explains why even in conditions causing severe neural crest defects, some cells are observed at ventrolateral positions in the presumptive pharyngeal arches (Fig. 2.3E-I). Importantly, we found that in wild-type embryos, NCCs in contact with one another at dorsal-most positions tended to move rapidly away from one another, with most cell contacts resolving within 20-30 mins (Fig. 2.8A-A''', with NCCs in a given group of cells pseudocolored to indicate pairs in contact). However, in both *pk1b* $^{fh122/\ fh122}$ (Fig. 2.8B-B''') and *pk1a*$^{ch105/ch105}$ (Fig. 2.8C-C''') embryos, NCCs in clusters frequently failed to break contacts, despite moving relative to other cells in the cluster.

To quantify the breakage of cell contacts, we measured the total number of pairs of NCCs in contact with one another in any given cluster. Here, we defined clusters as two or more cells in contact with one another. We then binned pairs of cells that broke contacts with one another in ten-minute time intervals relative to the total number of pairs at the beginning of observation of a given cluster (new contacts formed that were not present at time t=0 were not counted in the analysis). We found that in wild-type embryos, 57% of cell pairs broke contacts between 10 and 20 minutes (n=43 pairs, 3 embryos), with 88% of cell pairs breaking contact by 30 minutes (Fig. 2.8D). In contrast, pairs of NCCs in both *pk1b* $^{fh122/\ fh122}$ (n=61 pairs, 3 embryos) and *pk1a*$^{ch105/ch105}$ embryos (n=58 pairs, 3 embryos) typically did not break contact over extended periods of time, with only 22%

and 15% of cell pairs breaking contact in *pk1b* $^{fh122/\ fh122}$ and *pk1a*$^{ch105/ch105}$ embryos, respectively, by 30 minutes. Since Pk1-deficient NCC clusters formed well before dorsally-located NCCs begin migration, we conclude that the Pk1 paralogs are required as early as 12 hpf.

Next, we hypothesized that NCCs in *pk1*-mutants were present in larger cell clusters at 12 hpf than NCCs in wild-type embryos. To investigate the configuration of NCCs at 12 hpf, we counted the number of cells in any given configuration (as single cells, or in clusters of two or more cells). We found that 44% of NCCs in wild-type specimens were present as single cells, 28% in pairs, 15% in clusters of three cells, 10% in clusters of 4 cells, and 3% in clusters of 5 cells (n=37 cells, 3 embryos, Fig. 2.9A). By contrast, only 6% of NCCs in *pk1b* $^{fh122/\ fh122}$ specimens (n=53 cells, 3 embryos) and 9% of NCCs in *pk1a*$^{ch105/ch105}$ specimens (n=46 cells, 3 embryos) were present as individual NCCs, with far greater percentages of NCCs in clusters of two or more cells, consistent with our hypothesis (Fig. 2.9A). Notably, in Pk1-deficient specimens, clusters consisting of as many as 8 cells were observed.

We further hypothesized that since *pk1*-mutant NCCs were present in higher-order clusters than wild-type NCCs, *pk1*-mutant clusters were also likely to be maintained for extended time periods relative to wild-type cells, leading in turn to the defects we observed

at later stages. To test this hypothesis, we quantified the clusters of NCCs that maintained contact over non-overlapping time intervals of 20 minutes (see Chapter 5). This analysis showed that in wild-type embryos 53% of NCCs were largely individual (n=80 cells, 3 embryos), with transient contacts lasting less than 20 minutes. In contrast, only 5% of NCCs in *pk1b*$^{fh122/fh122}$ embryos (n=99 cells, 3 embryos) and 6% of NCCs in *pk1a*$^{ch105/ch105}$ embryos (n=148 cells, 3 embryos) remained as individuals in the same time frame (Fig. 2.9B). Wild-type embryos did include some NCCs that maintained contact with other NCCs for at least 20 minutes. 26% of these wild-type cells were pairs of cells, 13% were in clusters of 3 cells and 9% in clusters of 4 cells. In contrast, both *pk1b*$^{fh122/fh122}$ and *pk1a*$^{ch105/ch105}$ embryos maintained appreciable percentages of clusters as large as 8 cells, with most clusters comprising 3 cells (21% in *pk1b*$^{fh122/fh122}$ and 28% in *pk1a*$^{ch105/ch105}$ embryos, Fig. 2.9B) or 4 cells (28% in *pk1b*$^{fh122/fh122}$ and 24% in *pk1a*$^{ch105/ch105}$ embryos). Together, these data indicate that while NCCs establish contact with other NCCs in clusters as early as 12 hpf in both wild-type and Pk1-deficient specimens, Pk1-deficient embryos form and maintain larger NCC clusters than wild-type embryos.

We then postulated that since Pk1-deficient NCCs in clusters tended to exhibit high levels of motility—albeit in the anterior direction as opposed to the wild-type lateral direction—

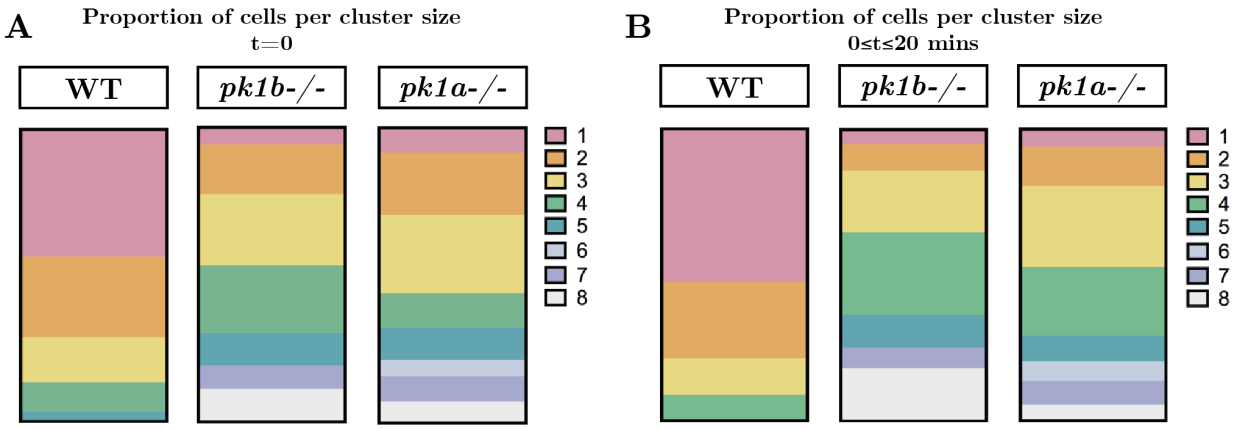

Fig. 2.9: Loss of Pk1 function shows significantly higher proportions of higher-order clusters that are maintained as clusters at 12 hpf than WT cells

(A) To measure the relative proportions of individual cells and clusters of varying sizes, the number of cells at 12 hpf in *Tg(sox10:EGFP)* embryos was measured. In WT embryos (n=37 cells, 3 embryos), 43.87% of NCCs were found as individuals, 27.56% were in pairs, 15.30% in clusters of 3 cells, 10.20% in clusters of 4 cells, and 3.06% in clusters of 5 cells. In $pk1b^{fh122-/-}$ specimens (n=53 cells, 3 embryos), 5.88% of NCCs were found as individuals, and 16.99% as pairs. Most NCCs were found in cluster sizes of 3 (24.18%) or 4 (22.87%), with clusters consisting of as many as 8 cells. In $pk1a^{ch105-/-}$ specimens (n=46 cells, 3 embryos), 8.59% of NCCs were found as individuals, and 21.09% as pairs. Most NCCs were found as pairs or in cluster sizes of 3 cells (26.56%), with appreciable percentages of cluster sizes of 4 (11.71%) and 5 (10.93%) and with clusters consisting of as many as 8 cells. (B) As another measure of the relative proportions of individual cells and clusters of varying sizes, the number of cells that persisted in a given configuration (from an individual cell to cells in increasing sizes of clusters) was measured over non-overlapping 20-minute time windows. In WT embryos (n=80 cells, 3 embryos), 52.5% of NCCs remain individual over 20 minutes, whereas 26.25% were in pairs, 12.5% in clusters of 3 cells, and 8.75% in clusters of 4 cells. In $pk1b^{fh122-/-}$ embryos (n=99 cells, 3 embryos), 5.05% of NCCs were found as individual cells over the 20-minute time window. Most NCCs were found in cluster sizes of 3 (21.2%) or 4 (28.3%), with NCCs found in clusters

Fig. 2.9 continued: consisting of as many as 8 cells. In *pk1a*$^{ch105-/-}$ embryos (n=148 cells, 3 embryos), 6.1% of NCCs were individual, with most NCCs found in cluster sizes of 3 (27.7%) or 4 (23.6%) and clusters consisting of as many as 8 cells.

---

that the persistence (a measure of the degree of directional movement calculated as the ratio of the total distance traversed by a cell relative to its displacement) of NCC motility would be dependent on the number of cells in the cluster. We found that wild-type NCCs, in any configuration, showed a high level of persistence over a 20-minute time period. By contrast, in *pk1* mutants, individual NCCs and pairs of NCCs showed lower levels of persistence than their corresponding wild-type configurations (Fig. 2.10). However, consistent with our hypothesis, in either *pk1* mutant, clusters of three or more NCCs showed high levels of persistence similar to those of wild-type NCCs, albeit in an anterior direction. We conclude that Pk1-deficient NCCs in clusters of three or more cells demonstrate a high level of targeted movement in an aberrant (anterior) direction, whereas individual cells or pairs of cells display a low level of targeted movement in any direction. In both cases, Pk1-deficient NCCs fail to migrate ventrolaterally.

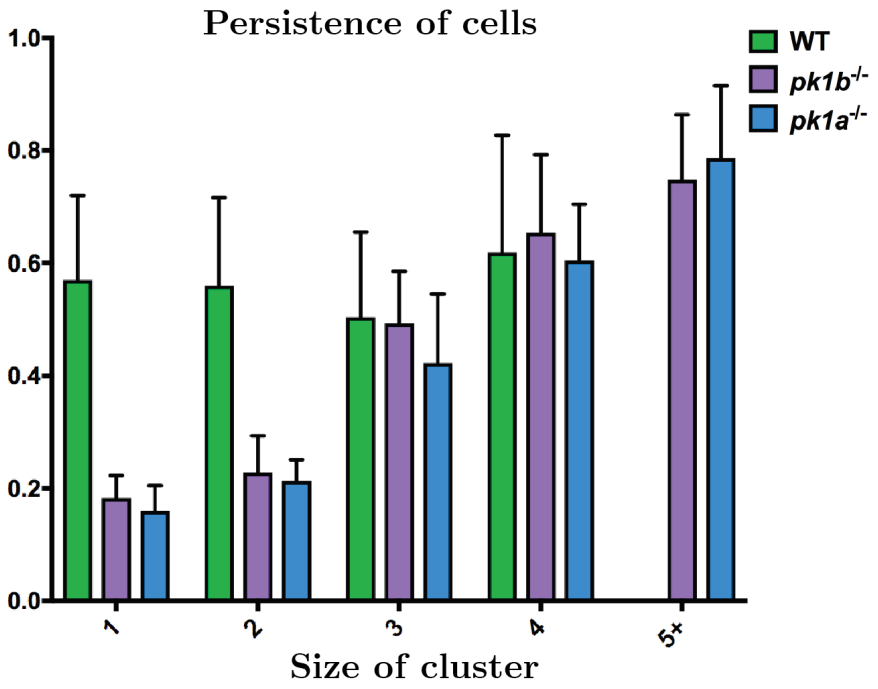

Fig. 2.10: The persistence of Pk1-deficient neural crest cells varies with the size of the cluster

To assay how persistence—a measure of the total length of a trajectory of a cell as a ratio of the displacement of the cell with a value of 1.0 indicating a targeted route from starting point to end point—varied as a function of cluster size, the persistence of individual cells and clusters of sizes 2 or more was measured for each condition. Persistence is agnostic to the 'correct' direction of the cells, and is a measure of the targeted directionality NCCs, independent of their trajectories. In WT embryos (n=42 cells, 3 embryos), the persistence of individual NCCs or clusters of 2, 3 or 4 was similar. In both *pk1b* $^{fh122/\ fh122}$ (n=49 cells, 3 embryos) and *pk1a*$^{ch105/ch105}$ embryos (n=64 cells, 3 embryos), the persistence of individual cells and cells in pairs was lower than the persistence of clusters consisting of 3 or more NCCs, or of WT NCCs. Clusters of 3 or more NCCs in both *pk1*-mutants showed high levels of persistence, with statistically insignificant ($p>0.5$) differences in persistence as compared to WT cells. Both *pk1*-mutants showed small increases in persistence as the size of the cluster increased, with no statistically significant difference between clusters of 5 or more cells.

2.5 DISCUSSION

In this study, we have used *in vivo* imaging to establish the role of zebrafish Prickle1 in the developing cranial neural crest before and during its migration. Specifically, we have uncovered equivalent roles for the two zebrafish *pk1* paralogs during directional migration of the NCCs. We find that Pk1 function is required for ventrolateral migration of the cranial crest, consistent with the previously-established roles for other core PCP molecules in contact inhibition of locomotion (CIL) of both *Xenopus laevis* and zebrafish NCCs (Carmona-Fontaine et al., 2008; De Calisto et al., 2005; Matthews et al., 2008; Theveneau et al., 2010; Theveneau et al., 2013).

A key observation that led us to investigate the roles of Prickle1b and Prickle1a as early as 12 hpf is the clustering of NCCs in Pk1-deficient specimens. Whereas in unmanipulated specimens, clear streams of NCCs corresponding to specific AP locations are present, Pk1-deficient clusters are often observed at AP locations that span two presumptive streams. In Pk1-mutants, even at 48 hpf, a large number of NCCs remain clustered dorsally, located near the frontonasal process (data not shown), although the viability of single-mutant embryos suggests that these defects are corrected, or of minimal functional significance, at subsequent stages. Szabo et al. (2016) have shown that the collective migration of *Xenopus* NCCs depends upon their initial confinement by the extracellular matrix molecule Versican, which also functions as a guidance cue, allowing NCCs to migrate

collectively in streams and respect exclusionary boundaries between streams. Other reports have shown other guidance cues, including VEGF (McLennan et al., 2015b; McLennan et al., 2010) and Sdf1 (Kasemeier-Kulesa et al., 2010; Olesnicky Killian et al., 2009; Saito et al., 2012; Theveneau et al., 2013), to be important for cranial NCC migration (reviewed in Kulesa et al., 2010). However, our data suggest that even though the conditions of *in vivo* confinement of NCCs are fulfilled and cells move collectively in Pk1-deficient embryos, they do so in aberrant directions and across boundaries between streams at dorsal locations.

The aberrant movement of pre-migratory Pk1-deficient NCCs correlates with aberrant polarities along the AP axis. Previous work has shown that in zebrafish, PCP proteins polarize neuroepithelial cells along the AP axis during neurulation, with GFP-tagged *Drosophila* Prickle protein localizing specifically on the anterior side of these cells (Ciruna et al., 2006). However, our data also indicate that polarity can be de-coupled from anterior movement in NCCs, as double-heterozygous specimens lack any clear polarity to their NCCs, yet continue to show anteriorly-directed migration of clustered NCCs. Future investigation of how the dynamics of Pk1b and Pk1a localization correlate with polarization of NCCs and their progenitors, will be important to dissect the dynamic role(s) of Prickle1. Such an approach would also clarify whether polarity causes the direction of movement, or merely correlates with it.

While previous work has implicated Frizzled and Disheveled in NCC migration, our work implicates Pk1 in the process of NCC migration as well. This suggests that the entire core PCP suite may be required during migration, which it has been assumed to do since the earliest reports (Carmona-Fontaine et al., 2008; Matthews et al., 2008; Mayor and Carmona-Fontaine, 2010; Mayor and Theveneau, 2014; Theveneau et al., 2010). However, it is formally possible that Pk1 functions alone as early as 12 hpf, to set up the asymmetries of other core PCP proteins, similar to how the *Drosophila* Prickle and Spiny legs isoforms differentially amplify the asymmetries of core PCP proteins (Gubb et al., 1999; Merkel et al., 2014; Sharp and Axelrod, 2016; reviewed in Strutt and Strutt, 2009), as well as establish the polarity of a microtubule network that determines the direction of tissue polarity in *Drosophila* (Olofsson et al., 2014). Approaches to visualize endogenous levels of zebrafish Pk1 proteins, as well as the other core PCP proteins and previously-implicated downstream molecules, would help to clarify regulatory interactions in the core PCP module during different stages of NCC development.

An important implication of the roles of Prickle1 molecules in normal neural crest development lies in the nature of the clustering phenotype coupled with the specific temporal sequence in which we find the phenotype. At 12 hpf, the neural keel has not yet developed in the cranial region, rather there is a thickening neural plate with lateral cells that border the non-neural ectoderm being the only population fated to be neural crest

(Jimenez et al., 2016; Schilling and Kimmel, 1994). Thus, in Pk1-deficient embryos defects are present well before the wave of migration that begins in earnest from the dorsal aspect of the neural tube at later stages. In neural crest development, following induction and specification, neural crest cells undergo an epithelial-to-mesenchymal transition (EMT) before they can begin migration. Scarpa et al. (2015) showed that when E-Cadherin is ectopically expressed in zebrafish embryos, NCCs cluster at the dorsal aspect, although they move at roughly the same speeds as wild-type cells in the stereotypic ventrolateral pathway. The authors concluded that an E-Cad-to-N-Cad switch is necessary for the completion of EMT and the commencement of migration. Since the clustering and motility phenotypes observed in Pk1-deficient specimens share a great deal of similarity with this reported phenotype, it is possible that the defects we see as early as 12 hpf are due to a role for the Pk1 orthologs in EMT. Other important indications of such a defect lie in the observations that Pk1-deficient NCCs show rounded morphologies with fewer protrusions than wild-type cells, and that they exhibit a high degree of preservation of contacts, observed both at the dorsal aspect at 12 hpf and later, at 16 hpf. This finding indicates key links between morphology and adhesion that relate to the process of EMT, and it is to this that we will now turn.

Overall, this chapter has shown that zebrafish Pk1 is required during cranial neural crest migration. My findings, taken together with previously-published work, allow me to

conclude that Prickle is acting like other PCP molecules as a key source of regulation to allow the proper migration of the cranial neural crest.

CHAPTER 3

THE PRICKLE1 PROTEINS REGULATE EMT IN *DANIO RERIO* CRANIAL NEURAL CREST

3.1 ABSTRACT

In Chapter 2, I detailed how Prickle1b and Prickle1a are required for normal cranial neural crest migration in streams targeted towards the pharyngeal arches, and demonstrated the specificity of the phenotype using a variety of measures in control versus Pk1-deficient specimens: directionality of movement, polarity as assayed by MTOC position, the degree of cell clustering as early as 12 hpf, the degree of breakage of contacts between cells at these early stages, and how the persistence of cell migration varies by the size of the cluster. Although each of these measures pertain to the requirement of Pk1b and Pk1a in normal ventrolateral migration of cranial neural crest cells, in this chapter, I will demonstrate that the phenotypes observed are, in large part, due to the role of Pk1b and Pk1a in the stage of neural crest development that precedes migration: EMT.

This chapter details how, using a mosaic LifeAct-GFP transient transgenesis strategy, wild-type neural crest cells can be seen to undergo EMT through a series of morphological transitions. First, elongated cells within the dorsal neuroepithelium detach from the apical surface. Following apical detachment, NCCs round up and make small protrusions before making bleb-based protrusions. Progressively, over short periods of time under 30 minutes, wild-type cells undergoing EMT adopt more protrusive, highly-filopodial, and highly-lamellipodial morphologies characteristic of mesenchymal cells, in which state they are seen to migrate in earnest towards their targets. In contrast, I show that in Pk1-deficient

embryos, pre-migratory NCCs are blocked from proceeding beyond the bleb-based transitional morphology and are largely unable to pass rapidly to a more mesenchymal morphology. Although a small proportion of NCCs do indeed transition to the mesenchymal morphology, these Pk1-deficient 'escaper' migratory cells also show defects as compared to wild-type cells. Despite a high preponderance of filopodia and lamellipodia, Pk1-deficient migratory cells are unable to separate from the neighbors over long periods of time, indicative of a defect consistent with contact-inhibition of locomotion.

The process of EMT is known to involve dynamic shifts in levels of adhesion molecules, particularly E-Cadherin (E-Cad) and N-Cadherin (N-Cad). However, whether the defects in PCP-deficient conditions correlate with defects in Cadherin levels has not been investigated. Here I show that Pk1-deficient pre-migratory and migratory cells have aberrant levels of E-Cadherin and N-Cadherin. Using immunohistochemistry, I demonstrate that E-Cad levels are high in wild-type pre-migratory NCCs and are correspondingly decreased in wild-type migratory NCCs, as expected based on previous findings (Scarpa et al., 2015; Taneyhill and Schiffmacher, 2017). By contrast, the results I present in this chapter, show that in Pk1b-deficient specimens, E-Cad levels in both pre-migratory and migratory NCCs are elevated with respect to their wild-type counterparts, although I also find a decrease in levels in migratory as compared to pre-migratory NCCs. I further demonstrate that N-Cad levels in wild-type NCCs show the reverse trend as

compared to E-Cad: pre-migratory NCCs show lower levels than migratory NCCs. In Pk1b-deficient specimens, N-Cad levels remain unchanged in pre-migratory NCCs, but are decreased in migratory NCCs.

Taken together, the results presented in this chapter demonstrate that the zebrafish Pk1b and Pk1a orthologs have roles prior to active NCC migration, and that they are required for NCCs to move from a bleb-based morphology to an actively-protrusive mesenchymal one during EMT. Further, because the absence of Pk1b shows a role in regulating E-Cad levels in pre-migratory and migratory NCCs, and in regulating N-Cad in migratory NCCs, the Pk1 molecules—perhaps in tandem with PCP signaling at large—are required to regulate E-Cad and N-Cad in the sequential stages of EMT and migration.

3.2 CONTRIBUTIONS

This chapter greatly benefitted from the work of individuals other than myself. Acknowledgements for reagents, transgenic lines, and techniques are present in Chapter 5. The author and Christina Huang used a transient transgenesis approach using LifeAct-GFP to mosaically label and image NCCs in wild-type, *pk1b*-morphant, *pk1b*-mutant specimens, and *pk1a*-mutant specimens (Figs. 3.1 and 3.2, Supplemental movies 6-9). Noor Singh conducted the immunohistochemistry for E-Cad and N-Cad, and quantified and normalized expression levels. The author and Noor Singh used statistical methods and a

normalization methodology with the help of Anastasia Beiriger. (Figs. 3.3 and 3.4). This chapter is adapted from a manuscript currently under revision, coauthored with Christina Huang, Victoria Prince, Manuel Rocha and Noor Singh.

3.3 INTRODUCTION

Whereas in Chapter 2, I dealt with the migration of cranial neural crest cells, in this chapter, I will be discussing and showing results pertaining to the process of epithelial-to-mesenchymal transition (EMT) that precedes migration. My analysis of EMT follows as a direct result of the clustering and motility analyses conducted in the previous chapter. Here I will provide an overview of EMT as it has been described in the literature, in a chronological fashion, with an emphasis on a deeper understanding of EMT from a variety of different models and cell types in more recent studies.

The largest body of literature pertaining to EMT has to do with cell adhesion; dynamic changes in adhesion have provided definitions for cells in either an "epithelial" morphology, or a "mesenchymal" morphology. In a variety of vertebrate models including zebrafish, during EMT, NCCs reduce their previously high levels of E-Cadherin, up-regulate N-Cadherin, and become highly-protrusive, migratory mesenchymal cells (Acloque et al., 2009; Hay, 2005; Scarpa et al., 2015; Wheelock et al., 2008). During EMT, NCCs have also been reported to show changes in the expression levels of other Cadherin molecules,

such as Cadherin-6, Cadherin-7, and Cadherin-11 (Acloque et al., 2009; Berndt et al., 2008; Clay and Halloran, 2014; reviewed in Taneyhill and Schiffmacher, 2017). In tandem, NCCs alter the expression of polarity molecules central to their high directionality: critically, in both *Xenopus laevis* and zebrafish embryos, NCCs lose apico-basal polarity, and activate non-canonical Wnt/PCP signaling molecules (Berndt et al., 2008; reviewed in Gallik et al., 2017; Lee et al., 2006; Mayor and Theveneau, 2014; Sauka-Spengler and Bronner-Fraser, 2008; Thiery and Sleeman, 2006; Thompson and Williams, 2008). These dynamic molecular changes are tightly associated with the changes in cell morphology and behavior that accompany the onset of NCC migration.

In recent studies, the classical understanding of the process of EMT that precedes a variety of cell migration, wound healing, and metastasis processes, has come under greater scrutiny. Classical studies have treated the EMT transition as a binary state change from a tightly-packed, highly-adhesive epithelial morphology to a highly-protrusive, migratory mesenchymal one. By contrast, more recent studies from different cell types across multiple model organisms have revealed a range of transient cell states that span the 'spectrum' or 'continuum' from epithelial to mesenchymal morphologies (reviewed in Campbell and Casanova, 2016; Nieto et al., 2016).

For instance, metastatic carcinoma cells that show hybrid characteristics during the process of EMT have been described as occupying an intermediate 'metastable' state, owing to their transitory morphology (reviewed in Lee et al., 2006; Savagner, 2010). Similarly, zebrafish cranial NCCs have also been reported to adopt transitional morphologies during EMT, which fall between the fully neuroepithelial morphology and the migratory mesenchymal morphology (Berndt et al., 2008; Clay and Halloran, 2014). First, presumptive NCCs in the neuroepithelium detach from their apical surfaces. These pre-migratory NCCs at the dorsal aspect of the neural tube change morphologically from elongated, tightly-packed cells to loose, rounded cells, capable of bleb-based protrusions. Subsequently, NCCs adopt highly mesenchymal, filopodia- and lamellipodia-based morphologies capable of migration in streams (Berndt et al., 2008; Clay and Halloran, 2014). Since 'EMT' has often been used interchangeably with the term 'delamination', an appreciation for the particular state changes that need to occur during the EMT has been lacking, causing difficulty in ascribing particular phenotypes to specific phases of neural crest development.

In this chapter, I demonstrate that the defects in cell 'clustering' that we found in Chapter 2 can be attributed to the stage in neural crest development that precedes migration: EMT. One important consideration that can be carried over from the results of Chapter 2, however, is that not only do NCCs fail to migrate ventrolaterally, they instead adopt

anteroposterior motility, and critically, the clustering defect observed is seen as early as 12 hpf, well before the neural keel has fully formed and thus well before the cells arising from the dorsal aspect of the neural tube migrate toward the periphery, indicating that Pk1b and Pk1a play a role earlier than this later wave of migration. Unlike wild-type pre-migratory NCCs that rapidly transition from a neuroepithelial morphology, through a transient blebbing state, to a mesenchymal morphology, we find that dorsal pre-migratory NCCs in Pk1-deficient specimens maintain blebbing behaviors over extended periods. Further, Pk1-deficient NCCs that successfully transition to the mesenchymal state fail to separate from neighboring NCCs, consistent with defects in CIL. Finally, we find that Pk1b regulates E-Cadherin both in pre-migratory and migratory NCCs, and N-Cadherin in migratory cells. The findings show that the core PCP Pk1 molecules are required in the process of EMT that precedes and is required for the successful migration of the cranial neural crest.

3.4 RESULTS

3.4.1 Pk1 regulates the transition from bleb-based to mesenchymal morphologies in EMT, in addition to regulating the breakage of cell contacts during migration.

We have shown that Pk1-deficient cranial NCCs cluster aberrantly at the dorsal surface of the neuroepithelium as early as 12 hpf, a stage that precedes the vast majority of ventrolateral migration of NCCs (Jimenez et al., 2016; Schilling and Kimmel, 1994). These findings led us to hypothesize that NCC defects in Pk1-deficient embryos might result from a previously undocumented role for PCP in regulating the morphological changes that NCCs must undergo before they migrate: during the epithelial-to-mesenchymal transition (EMT). The process of EMT occurs continuously at early stages, as waves of pre-migratory NCCs emerge from the neuroepithelium and prepare to migrate from more medial, dorsal positions to lateral, ventral positions. To test our hypothesis, we performed a detailed investigation of the morphological states of pre-migratory and migratory NCCs, comparing wild-type with Pk1-deficient embryos.

To observe NCC morphological transitions, we used a transient-transgenesis approach to drive expression of a LifeAct-GFP transgene from *sox10* regulatory sequences, allowing visualization of the actin-rich protrusions of both pre-migratory and migratory NCCs in dorsal views at 16 hpf. We defined pre-migratory NCCs as *sox10*-positive cells localized at the dorsal aspect of the neural tube, which in a dorsal view have not crossed the basal edge of the neuroepithelium, and migratory NCCs as *sox10*-positive cells that have moved laterally past the edge of the neuroepithelium to actively migrate ventrally.

In wild-type specimens, pre-migratory NCCs undergo a series of morphological transitions following the detachment of neuroepithelial precursor cells from the apical midline (Supplemental Movies 6-9), consistent with previous reports (Berndt et al., 2008; Clay and Halloran, 2014). Following apical detachment (Supplemental Movie 6), NCCs adopt rounded morphologies, making short, transient protrusions (Fig. 3.1A, Supplemental Movie 7), and forming blebs (Fig. 3.1A', A'', Supplemental Movie 8), which have previously been described as rounded, actin-rich extensions created through membrane invagination (Goudarzi et al., 2017). Subsequently, wild-type NCCs transition rapidly to the migratory state, which involves highly-protrusive, mesenchymal morphologies with multiple, long, dynamic protrusions, including filopodia and lamellipodia (Fig. 3.1A''', A'''', Supplemental Movie 9).

Unlike wild-type NCCs, which transition from a bleb-based morphology to mesenchymal morphology over the span of 20 minutes (Fig. 3.1A-A''''), *pk1b*-morphant (Fig. 3.1B-B''''), *pk1b* $^{fh122/\ fh122}$ (Fig. 3.1C-C''''), and *pk1a*$^{ch105/ch105}$ (Fig. 3.1D-D'''') NCCs typically maintained blebbing behaviors over the entire time span. In fact, quantifications of the cell behaviors showed that whereas 89% of wild-type NCCs transitioned from pre-migratory to migratory states over a 20-minute time interval, only 16% of *pk1b*-MO, 6% of *pk1b* $^{fh122/\ fh122}$, and 17% of *pk1a*$^{ch105/ch105}$ cells made the same transition, with the vast majority of cells instead remaining in a persistently-blebbing state over a 20-minute time

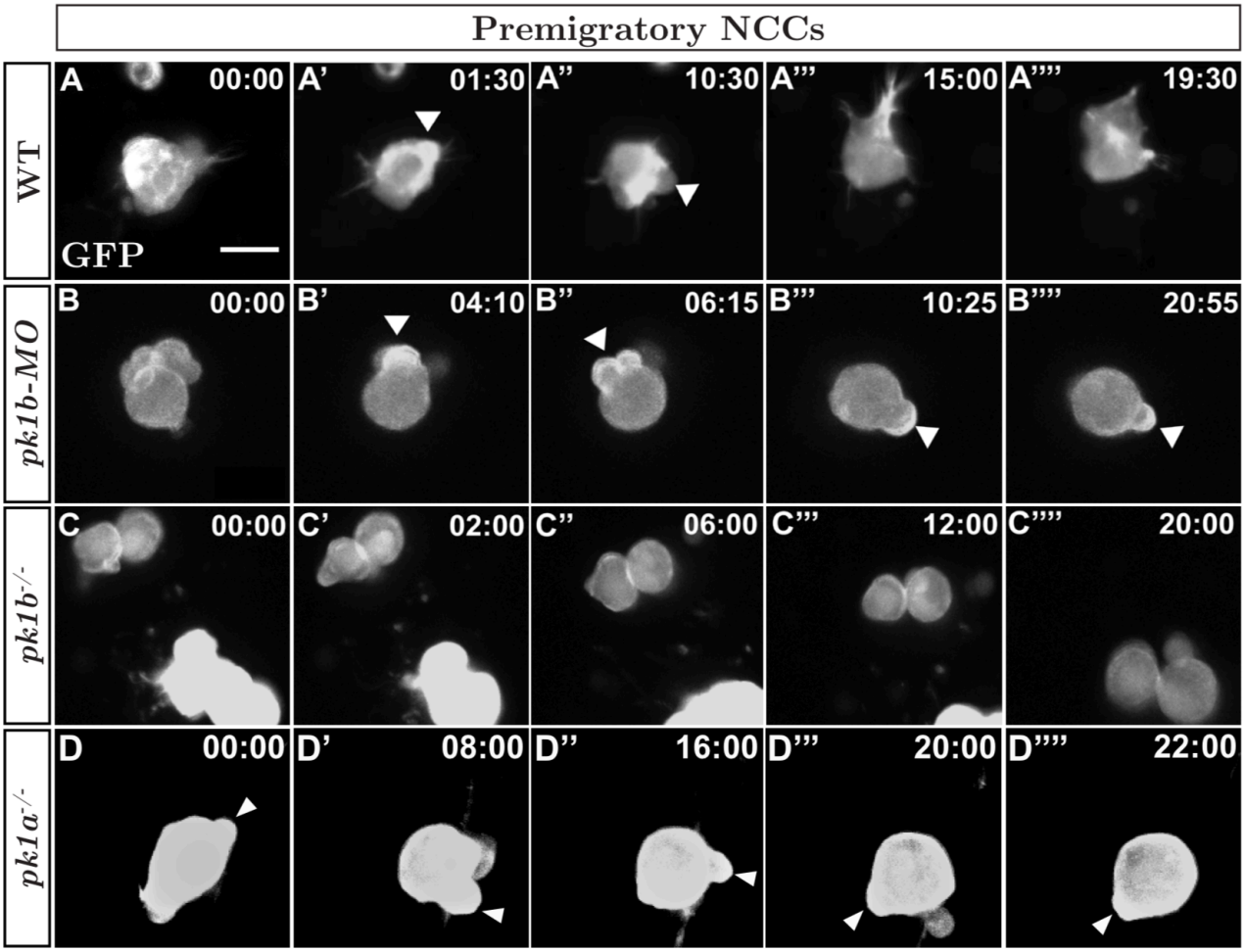

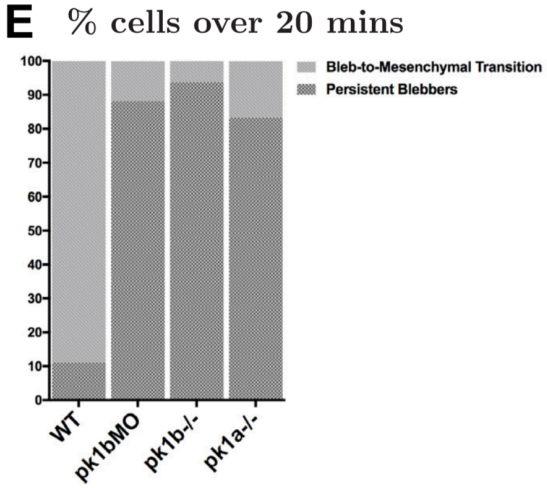

Fig. 3.1: Pk1-deficient pre-migratory neural crest cells show defects in a transitory state during EMT

Fig. 3.1 continued: To query the role of Pk1 molecules in the morphological transitions of EMT, as well as during active migration, NCCs were labeled in a mosaic fashion by injecting DNA encoding LifeAct-GFP under the control of a *sox10* promoter into one-cell stage embryos. (A-H) Confocal time-lapsing imaging of LifeAct-GFP positive cells for at least 20 minutes in 16 hpf embryos revealed F-actin rich protrusions and distinct morphologies of NCCs. Scale bar=10 µm. (A-D'''') Frames from confocal time-lapses of pre-migratory NCCs. (A-A'''') WT NCCs display short protrusions even before displaying rounded bleb-based protrusions. WT NCCs adopt this bleb-based morphology before transitioning to morphologies with longer filopodial protrusions, with NCCs moving through these transitional morphologies in EMT over the time span of approximately 20 minutes. (B-B'''', C-C'''', D-D''''). Over the same time frame as WT NCCs, *pk1b*-morphant, *pk1b* $^{fh122/\ fh122}$, and *pk1a*$^{ch105/ch105}$ NCCs show bleb-based protrusions that are actively maintained, on occasion changing the location of the bleb along the edges of a NCC (B'-B''). White arrowheads indicate bleb-based protrusions. (E) Bar graph showing the percentage of pre-migratory NCCs that successfully transitioned from a bleb-based to a highly-protrusive mesenchymal-like morphology relative to those that remained in the persistently-blebbing state over the time span of 20 minutes. 89% of WT NCCs (n=18 cells, 8 embryos) transitioned successfully; 84% of *pk1b*-morphant NCCs (n=17 cells, 8 embryos), 94% of *pk1b* $^{fh122/\ fh122}$ NCCs (n=32, 8 embryos), and 83% of *pk1a*$^{ch105/ch105}$ NCCs (n=12 cells, 5 embryos) remained in the persistently-blebbing state.

---

interval (Fig. 3.1E). These results indicate that the defects observed in *pk1*-deficient specimens reflect a failure of NCCs to complete EMT; the NCCs instead remain stuck in the transitional blebbing state. Thus, Pk1 molecules play a central role in the regulation of key changes in NCC morphology and behavior during EMT.

Although most Pk1-deficient NCCs fail to complete EMT in 20 minutes, we nevertheless found that some NCCs are present migrating ventrolaterally in Pk1-deficient embryos (Fig. 2.3B-C). These cells likely include the population of NCCs previously reported to lie lateral to the neuroepithelium as early at 12 hpf (Jimenez et al., 2016). This subset of NCCs localizes lateral to the basal edge of the neuroepithelium without migrating there from the dorsal aspect of the neuroepithelium. While our data are consistent with the presence of an early lateral population of *Tg(sox10:EGFP)* cells, we also find that a subset of Pk1-deficient NCCs arising from more dorsal locations (Supplemental Movies 2-4) 'escape' the neuroepithelium to successfully migrate ventrolaterally into the pharynx.

To observe the behaviors of migratory NCCs, we again imaged NCCs expressing LifeAct-GFP in live embryos. Our data showed that while migrating wild-type NCCs made contacts with neighboring labeled cells, the contacts were transitory and dynamic: over a 30-minute time frame NCCs broke contacts and created new contacts, even with the same cell (Fig. 3.2A-A''''). In contrast, in *pk1b*-MO (Fig. 3.2B-B''''), $pk1b^{fh122/fh122}$ (Fig. 3.2C-C''''), and $pk1a^{ch105/ch105}$ (Fig. 3.2D-D'''') embryos, we found that despite 'escaper' migratory NCCs adopting highly-protrusive mesenchymal morphologies, they were unable to separate from neighboring NCCs over extended time periods. This indicated that the

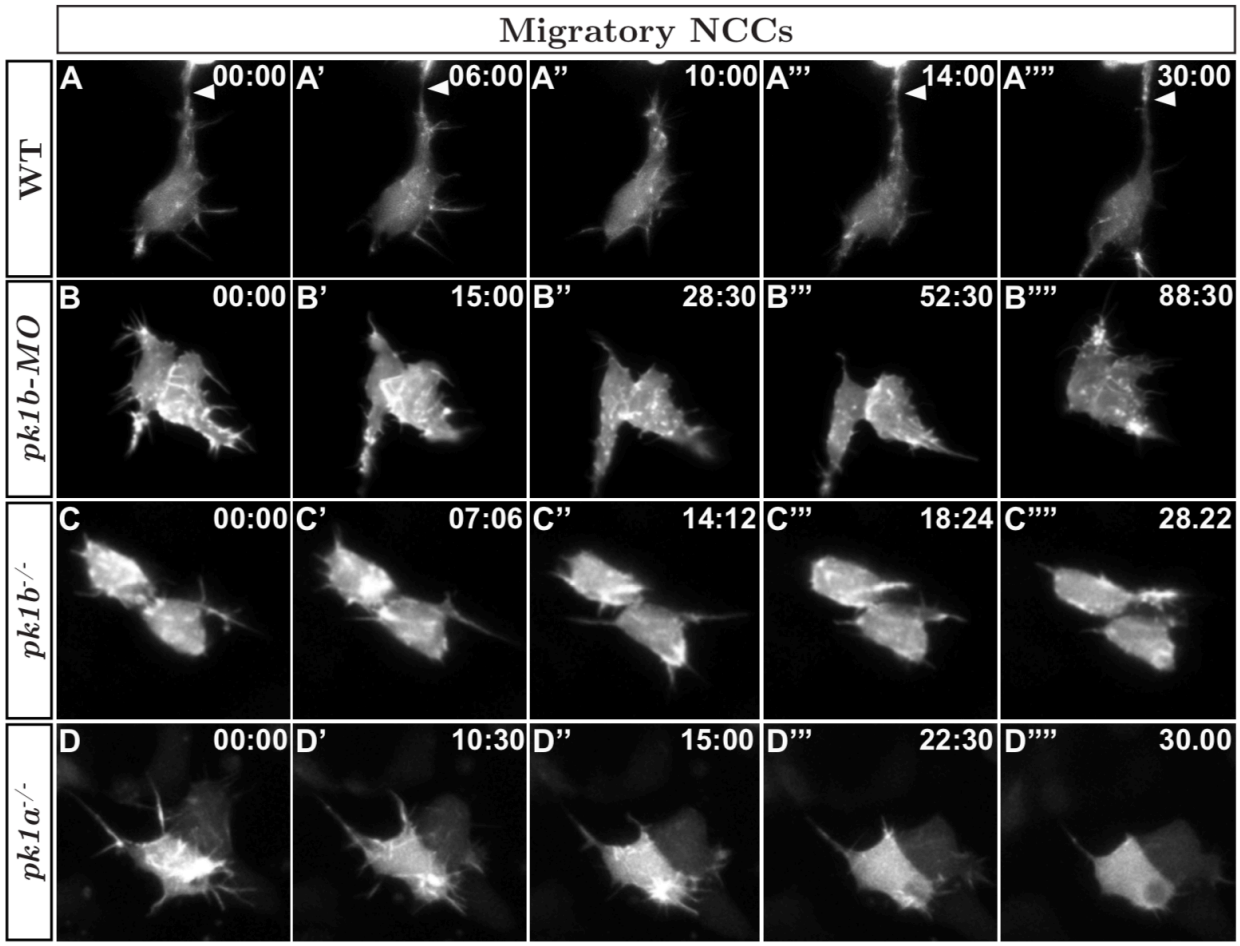

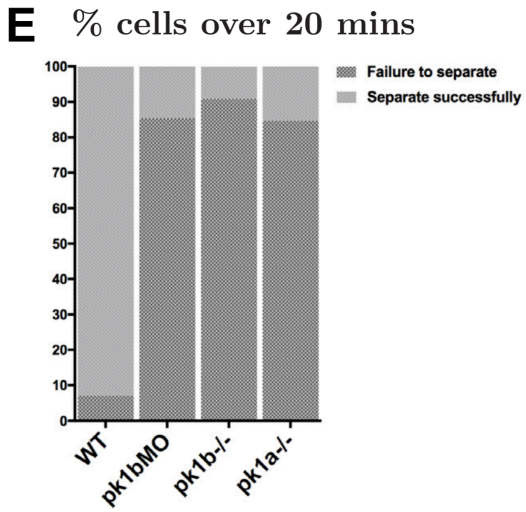

Fig. 3.2: Pk1-deficient migratory neural crest cells show defects in separating from neighboring cells

Fig. 3.2 continued: (A-D) Confocal time-lapsing imaging for at least 20 minutes of LifeAct-GFP positive NCCs in the mandibular stream actively migrating towards the first pharyngeal arch in 16 hpf embryos. Scale bar=10 µm. (A-A'''') Actively-migrating WT cells that are highly filopodial make transient contacts with neighboring cells, often making, breaking and re-establishing a contact in the form of a thick actin-rich protrusion with the same neighboring cell over a time span of at least 20 minutes. White arrowheads indicate a protrusion contacting a neighboring NCC. (B-B'''', C-C'''', D-D'''') *pk1b*-morphant, *pk1b* $^{fh122/fh122}$, and *pk1a*$^{ch105/ch105}$ migratory NCCs are highly protrusive but display an inability to separate from neighboring NCCs and maintain contact, often over extended time periods. (E) Bar graph showing the percentage of migratory NCCs that established and severed contact with a neighboring NCC relative to NCCs that failed to sever contact with a neighboring NCC over the time span of 20 minutes. 93% of WT NCCs (n=28, 6 embryos) established and severed contacts with neighboring NCCs; 85% of *pk1b*-morphant NCCs (n=41 cells, 10 embryos), 91% of *pk1b* $^{fh122/fh122}$ NCCs (n=22 cells, 7 embryos), and 85% of *pk1a*$^{ch105/ch105}$ NCCs (n=13 cells, 4 embryos) failed to separate and sever contact with neighboring NCCs.

---

clustering phenotype in Pk1-deficient embryos is not entirely exclusive to dorsal, pre-migratory NCCs. Quantifications of the cell behaviors showed that whereas 93% of labeled migratory NCCs in wild-type specimens established and severed contacts with neighboring cells over a period of 20 minutes, only 15% of migratory NCCs in *pk1b*-morphant embryos, 9% in *pk1b* $^{fh122/fh122}$ embryos, and 15% in *pk1a*$^{ch105/ch105}$ embryos severed contacts, with the majority of paired NCCs instead retaining their contacts over this time frame and beyond (Fig. 3.2E).

In summary, whereas wild-type NCCs show dynamic, transitory contacts with neighboring NCCs during their migration, Pk1-deficient NCCs instead show prolonged contact with neighboring NCCs, even during active migration. These findings for Pk1 molecules are consistent with the previously-established role for core PCP molecules in contact inhibition of locomotion of zebrafish NCCs (Carmona-Fontaine et al., 2008; Matthews et al., 2008). Together, our data show that the core PCP Pk1 molecules are required both during EMT, and in the migration of cranial neural crest.

3.4.2 Pk1b regulates E-Cad and N-Cad in NCCs

Our results indicate that cranial NCCs require Pk1 proteins for a key transition during EMT and for normal migration ventrolaterally towards the pharyngeal region. Interestingly, recent work has established that a crucial Cadherin switch must occur during EMT in order for CIL to be activated in the zebrafish NCCs. Scarpa et al. (2015) showed that zebrafish E-Cad (Cdh1) is highly expressed in epithelial NCC progenitors and subsequently downregulated in N-Cad (Cdh2)-expressing mesenchymal NCCs, and that over-expression of E-Cad is sufficient to block normal NCC migration. Therefore, we postulated that the inability of Pk1-deficient NCCs to transition from a blebbing to a mesenchymal state could be due to inappropriate levels of E-Cad and N-Cad.

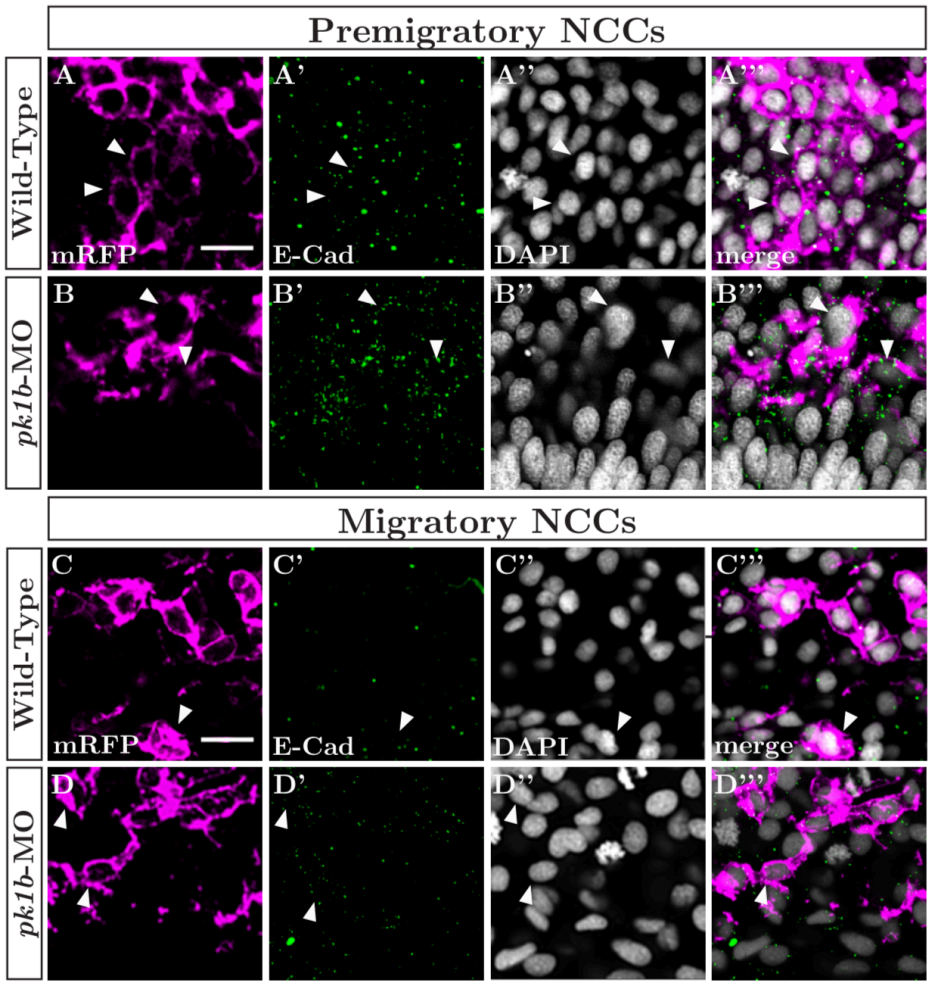

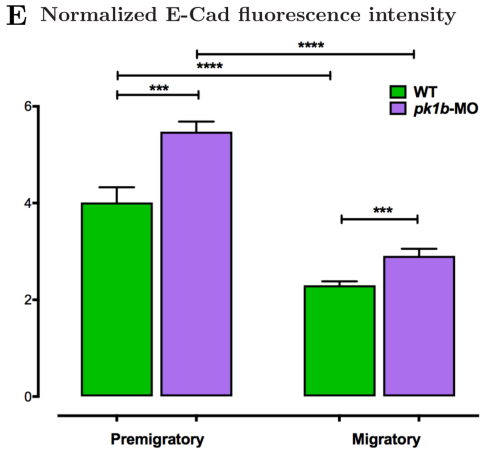

Fig. 3.3: Pk1b-deficient neural crest cells demonstrate elevated levels of E-Cad in both pre-migratory and migratory cells

Fig. 3.3 continued: To investigate the effect of Pk1b-knockdown on the levels of E-Cad (Cdh1), immunostaining was used both for pre-migratory and migratory NCCs. (A-D''') *Tg(sox10:mRFP)* (A-D), were immunostained for E-Cad (Cdh1) (A'-D'), and counterstained with DAPI to mark nuclei (A''-D'''). Scale bar=10 µm. White arrowheads indicate levels of E-Cad in NCCs with labeled membranes and nuclei. Merged channels are also shown (A'''-D'''). (A-A''') In pre-migratory NCCs, E-Cad is present at high levels in wild-type specimens (A'), with puncta localizing largely on the membrane (A'''). (B-B''') In *pk1b*-morphant specimens, E-Cad levels are elevated (B') with more puncta localizing on the membrane (B''') as compared to WT (compare A' and B'). (C-C''') In migratory NCCs, E-Cad is present at reduced levels (C', C''') as compared to pre-migratory NCCs (compare C' and A'). (D-D'''). In *pk1b*-morphant specimens, E-Cad levels are elevated (D') with more puncta localizing on the membrane (D''') as compared to WT (compare C' and D'). (E) To quantify the levels of E-Cad in different conditions, fluorescence pixel intensity was measured. Each cell was normalized by subtracting background pixel intensity and dividing the remainder by the area of the cell. High levels of E-Cad were found in pre-migratory wild-type cells (n=92 cells, 4 embryos). E-Cad levels in *pk1b*-deficient NCCs (n=73 cells, 4 embryos) were significantly elevated as compared to wild-type NCCs (***, p=0.0002). E-Cad levels in migratory wild-type cells (n=100 cells, 4 embryos), were significantly reduced as compared to levels in pre-migratory wild-type cells (****, p<0.0001), however *pk1b*-morphant migratory NCCs (n=65, 4 embryos) showed significantly higher levels of E-Cad as compared to wild-type migratory NCCs (***, p=0.0006).

As E-Cad over-expression causes a phenotype that shares properties with our *pk1*-deficient phenotypes we hypothesized that E-Cad levels would be elevated in the absence of Pk1b function. By performing immunohistochemistry, we found that E-Cad puncta are present

in both pre-migratory and migratory wild-type NCC membranes. Further, quantification of normalized fluorescence intensity revealed that E-Cad levels are higher in wild-type pre-migratory NCCs than in wild-type migratory NCCs (compare Fig. 7A-A''' and Fig. 7C-C''', $p<0.0001$), consistent with the previously reported down-regulation of E-Cad during EMT. Morpholino knockdown of Pk1b function resulted in elevated levels of E-Cad in both pre-migratory and migratory NCCs (Fig. 7B-B''', 7D-D'''). Quantification of normalized fluorescence intensity revealed a statistically significant increase in E-Cad levels in Pk1b-deficient specimens as compared to wild-type specimens in both pre-migratory and migratory NCCs (Fig. 7E, $p<0.001$ in both cases). Intriguingly, Pk1b-deficient migratory NCCs also show significantly lower levels of E-Cad than Pk1b-deficient pre-migratory NCCs ($p<0.0001$), suggesting that Pk1b-deficient 'escaper' cells require decreased E-Cad levels. Thus, the failure of Pk1b-deficient NCCs to complete EMT may be a consequence of inappropriate E-Cad levels.

Since up-regulation of N-Cad is normally required in migratory NCCs (Carmona-Fontaine et al., 2008; Theveneau et al., 2010; Theveneau et al., 2013), we further hypothesized that N-Cad levels might be reduced in the absence of Pk1b function. By performing immunohistochemistry, we found that N-Cad is also present on both pre-migratory and migratory NCC membranes in wild-type specimens. Unlike E-Cad, N-Cad levels were elevated in wild-type migratory NCCs as compared to wild-type pre-migratory NCCs

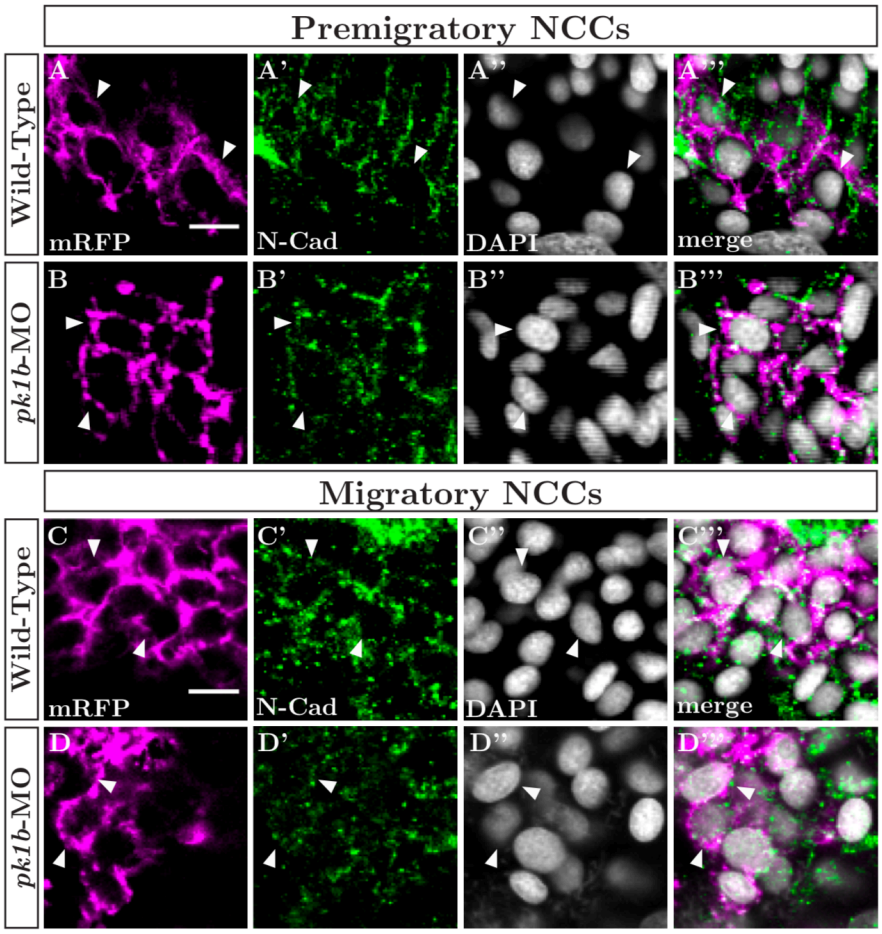

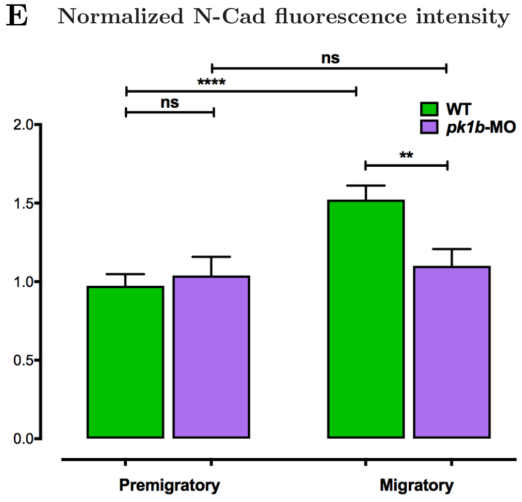

Fig. 3.4: Pk1b-deficient neural crest cells demonstrate decreased levels of N-Cad in migratory, but not pre-migratory cells.

Fig. 3.4 continued: To investigate the effect of Pk1b-knockdown on the levels of N-Cad (Cdh2), immunostaining was used both for pre-migratory and migratory NCCs. *Tg(sox10:mRFP)* embryos to mark NCC membranes (A-D) were immunostained for N-Cad (Cdh2) (A'-D'), and counterstained with DAPI to mark nuclei (A''-D''). Scale bar=10 µm. White arrowheads indicate levels of N-Cad in NCCs with labeled membranes and nuclei. Merged channels are also shown (A'''-D'''). (A-A''') In pre-migratory NCCs, N-Cad (A') is highly localized at the membrane in WT specimens (A'''). (B-B''') In *pk1b*-morphant specimens, N-Cad levels (B') showed no discernable difference in localization on the membrane (B''') as compared to WT (compare B' and A'). (C-C''') In migratory NCCs, N-Cad is present at increased levels (C', C''') as compared to pre-migratory NCCs (compare C' and A'). (I-I''') However, in *pk1b*-morphant specimens, N-Cad levels in migratory NCCs are decreased (D') with less N-Cad localization on the membrane (D''') as compared to WT (compare D' and C'). (E) To quantify the levels of N-Cad in different conditions, fluorescence pixel intensity was measured and normalized in the same manner as with E-Cad. N-Cad was present on the membrane in pre-migratory wild-type NCCs (n=164 cells, 5 embryos). N-Cad levels in *pk1b*-morphant NCCs (n=204 cells, 4 embryos) showed no difference to wild-type NCCs ($p>0.05$). N-Cad levels in migratory WT cells (n=192 cells, 5 embryos), were significantly elevated as compared to levels in pre-migratory wild-type NCCs (****, $p<0.0001$), however *pk1b*-morphant migratory NCCs (n=189, 4 embryos) showed significantly lower levels of N-Cad as compared to WT migratory NCCs (**, $p=0.0027$). N-Cad levels in WT pre-migratory, *pk1b*-morphant pre-migratory, and *pk1b*-morphant NCCs showed no significant difference from each other ($p>0.05$ for each combination).

(compare Fig. 7F-F'''and Fig. 7H-H''', $p<0.0001$), consistent with previous reports. Pk1b-deficient embryos showed no discernable change in N-Cad levels in pre-migratory NCCs

relative to unmanipulated controls (Fig. 7G-G'''', $p>0.5$). However, Pk1b-deficient migratory NCCs showed reduced levels of N-Cad at the membrane relative to wild-type specimens (Fig. 7I-I'''), consistent with our hypothesis. Quantification of normalized pixel intensity confirmed a statistically significant reduction in N-Cad levels in *pk1b*-MO specimens, as compared to wild-type specimens, in migratory ($p<0.01$), but not pre-migratory, NCCs (Fig. 7J).

In summary, in Pk1b-deficient specimens, E-Cad levels in both pre-migratory and migratory NCCs are elevated relative to unmanipulated wild-type controls. However, the Pk1b-deficient embryos do still show a downregulation of E-Cad in migratory relative to pre-migratory NCCs. Further, in Pk1b-deficient embryos, N-Cad levels are unaffected in pre-migratory NCCs, but are reduced in migratory NCCs relative to wild-type controls. Thus, Pk1b function is required for appropriate regulation of E-Cad and N-Cad levels at multiple stages during zebrafish neural crest development. We conclude that the important role played by Pk1 proteins in promoting EMT and enabling active migration of cranial neural crest cells, is at least in part mediated though the ability to regulate levels of E-Cad and N-Cad.

3.5 DISCUSSION

In Chapter 2, I showed results from *in vivo* imaging to establish the role of zebrafish Prickle1 in the developing cranial neural crest before and during its migration. In this chapter, I demonstrate equivalent roles for the two zebrafish *pk1* paralogs during both EMT and directional migration of the NCCs. I find that Pk1 function is required for ventrolateral migration of the cranial crest, consistent with the previously-established roles for other core PCP molecules in contact inhibition of locomotion (CIL) of both *Xenopus laevis* and zebrafish NCCs (Carmona-Fontaine et al., 2008; De Calisto et al., 2005; Matthews et al., 2008; Theveneau et al., 2010; Theveneau et al., 2013).

However, by investigating the complex morphological transitions that precede migration, I have also uncovered a broader role for Prickle1 before migration commences. I show that NCCs transition from neuroepithelial cells to a transient, blebbing, motile state before adopting a mesenchymal morphology capable of ventrolateral migration. These findings are consistent with previous descriptions of EMT as a series of progressive state changes rather than a binary switch (reviewed in Campbell and Casanova, 2016; Nieto et al., 2016), as well as with previous descriptions of NCC behaviors in zebrafish (Berndt et al., 2008). Critically, pre-migratory NCCs in embryos deficient in either Pk1b or Pk1a display a failure to transition from blebbing to mesenchymal morphologies.

I conclude that Prickle1 function is necessary for this key transition from blebbing, motile to mesenchymal, migratory states during NCC EMT. To my knowledge, this is the first report of a function for Prickle1—or indeed any PCP molecule — in controlling the epithelial-to-mesenchymal transition that is necessary for neural crest cells to migrate.

Previous work in other systems has shown that in some contexts, bleb-based cells are capable of migration. For instance, some modes of amoeboid migration (reviewed in Lammermann and Sixt, 2009) and zebrafish primordial germ cells (PGCs), which migrate through the developing embryo (Goudarzi et al., 2017), use blebs as the predominant type of protrusion. Here we demonstrate that although blebbing NCCs are motile, they are not capable of directed migration towards their proper targets unless they transition to mesenchymal states. Consistent with this, Scarpa et al. (2015) have demonstrated that even when EMT is blocked using ectopic E-Cadherin expression, zebrafish NCCs remain motile at speeds equivalent to those of actively-migrating cells, yet they are incapable of directed migration. I propose the bleb-based morphology of NCCs is 'metastable', a transient state in EMT (reviewed in Lee et al., 2006), and that Prickle1 regulates the transition from this metastable state to the stable, mesenchymal state. Again, this is consistent with recent understanding that EMT is a multi-state process (reviewed in Campbell and Casanova, 2016; Nieto et al., 2016). Importantly, these findings also suggest

that NCCs may use the same polarity proteins in sequential stages of neural crest development to control both EMT and CIL behaviors.

These findings suggest that the link between core PCP Pk1 molecules and EMT behavior may lie at the level of the Cadherins, possibly in the form of a feedback loop. Scarpa et al. (2015) showed that the *Xenopus* E-Cad/N-Cad switch is required for CIL; cell contacts subsequently trigger non-canonical Wnt/PCP signaling (Carmona-Fontaine et al., 2008; Theveneau et al., 2013). Although down-regulation of E-Cad has long been considered a hallmark of the end of EMT and the beginning of NCC migration, E-Cad is nevertheless not only present, but also required, in migrating cranial NCCs of *Xenopus*, chick, and mouse (reviewed in Cousin, 2017). Consistent with findings in other species, these findings show that in unmanipulated zebrafish embryos E-Cad is indeed detectable in migrating NCCs at low levels. Notably, E-Cad levels are elevated in Pk1-deficient specimens, both in pre-migratory and migratory NCCs, and N-Cad levels are reduced in migratory NCCs. I suggest that the previously-proposed activation of PCP signaling in response to decreased levels of E-Cad and increased levels of N-Cad may be part of a broader feedback loop, such that Pk1 (a core PCP molecule) is in turn necessary to regulate both E-Cad levels and N-Cad. Consistent with this model, the analysis shown indicates that disruption of two of the four available alleles of zebrafish *pk1* (by mutation of either *pk1b* or *pk1a,* or in double-heterozygous specimens) is sufficient to disrupt the typical reduction of E-

Cad levels, leading to NCCs becoming trapped in the transitional blebbing morphology rather than completing EMT. According to this model, once EMT is completed, Pk1 is necessary for increase of N-Cad levels, and the continued reduction of E-Cad, such that cells make only transient contacts with neighbors, and migrate in streams, consistent with CIL behavior (Carmona-Fontaine et al., 2008; Theveneau et al., 2010; Theveneau et al., 2013).

A key observation that led us to investigate EMT in more detail is the clustering of NCCs in Pk1-deficient specimens shown in Chapter 2. As detailed in the Discussion for Chapter 2, the ECM molecule Versican or other guidance cues like VEGF or Sd1 may be acting on Pk1-deficient NCCs while they are still in the process of EMT (Kasemeier-Kulesa et al., 2010; McLennan et al., 2015b; McLennan et al., 2010; Olesnicky Killian et al., 2009; Saito et al., 2012; Szabo and Mayor, 2016; Szabo et al., 2016; Theveneau et al., 2013). However, in conjunction with data from Chapter 2, an alternative interpretation is that Pk1-deficient embryos move in aberrant directions and across boundaries between streams at dorsal locations because NCCs in metastable states of EMT are unable to respond to normal guidance cues.

As discussed earlier, the aberrant movement of pre-migratory Pk1-deficient NCCs correlates with aberrant polarities along the AP axis. A recent study found that in both

in vivo mouse mammary gland epithelia and *in vitro* 3D mammary gland cultured cells, EMT was accompanied by a change in polarity, and that polarity reversal promoted the scattering of mesenchymal cells (Burute et al., 2017). Moreover, previous work has shown that in zebrafish, PCP proteins polarize neuroepithelial cells along the AP axis during neurulation, with GFP-tagged *Drosophila* Prickle protein localizing specifically on the anterior side of these cells (Ciruna et al., 2006). Together with these previous studies, our findings suggest that when key transitions during EMT are blocked, NCCs move in aberrant directions because of a failure to switch from a neuroepithelial-like polarity to a mesenchymal polarity. Future work querying the endogenous localization of Prickle1 will help to answer if anterior localization of Prickle1 is indeed required before EMT, and a polarity reversal in localization during EMT, or the polarity reversal is not reflected in a switch in localization of a PCP molecule, but of another protein—perhaps a small GTPase (Clay and Halloran, 2013; Matthews et al., 2008).

As stated earlier, previous work has implicated Frizzled and Disheveled in NCC migration. However, our work implicates Pk1 both in NCC EMT as well as in subsequent NCC migration. This suggests that the entire core PCP suite may be required during EMT. It is probable that the core PCP factors act in concert at the same developmental stages when we have established Pk1 functions, especially given the previously-elucidated role of PCP-signaling in CIL. However, it is also formally possible that Pk1 functions at an earlier

stage, to set up the asymmetries of other core PCP proteins, similar to how the *Drosophila* Prickle and Spiny legs isoforms differentially amplify the asymmetries of core PCP proteins (Gubb et al., 1999; Merkel et al., 2014; Sharp and Axelrod, 2016; reviewed in Strutt and Strutt, 2009), as well as establish the polarity of a microtubule network that determines the direction of tissue polarity in *Drosophila* (Olofsson et al., 2014). Approaches to visualize endogenous levels of zebrafish Pk1 proteins, as well as other core PCP proteins coupled with detailed temporal analysis during EMT processes, as well as in conjunction with a dynamic read-out for vesicle trafficking (as a proxy for dynamic microtubule polarity) instead of merely the position of the MTOC, would provide greater resolution in to the question of which proteins act first, and how.

I will address the methods and results pertaining specifically to the CRISPR/Cas-generated *pk1a*^{ch105} mutant in more detail in Appendix A, however a discussion as to how this pertains to the results in this chapter is relevant here. A central function of vertebrate PCP molecules is the regulation of embryonic convergence movements that are necessary for both gastrulation and neurulation to proceed normally. The absence of convergence defects in either of the *pk1b* $^{fh122/\ fh122}$ and *pk1a*$^{ch105/ch105}$ mutants likely reflects functional redundancy between these paralogous genes. Consistent with this model we have found that Pk1b-knockdown in *pk1a*$^{ch105/ch105}$ mutants does indeed cause morphological defects similar to those resulting from loss of function of other core PCP molecules, such as Vangl2

(Ciruna et al., 2006; Jessen et al., 2002; Veeman et al., 2003). The functional redundancy of the *pk1* paralogs has proven to be a significant advantage of the zebrafish model in this study, as it has allowed the nuanced roles of the Pk1 molecules in NCC development, including during EMT, to be teased apart from their earlier roles in convergence. In contrast to the results we present here, previous reports (Carreira-Barbosa et al., 2003; Ciruna et al., 2006; Veeman et al., 2003) have suggested that Pk1a function is necessary for convergence movements. While it is formally possible that our $pk1a^{ch105/ch105}$ mutant does not represent a genetic null, we consider this unlikely given the N-terminal location of the genetic lesion. Rather, we note that the previous analyses of Pk1a-function relied exclusively on morpholino knockdown, and some aspects of the phenotypes could thus reflect off-target effects of the reagent. Alternatively, the discrepancy between the morpholino knockdown and the $pk1a^{ch105/ch105}$ mutant phenotype may be a consequence of genetic compensation, as recently described for other zebrafish mutants (Rossi et al., 2015). Importantly, by generating the $pk1a^{ch105/ch105}$ mutation, we have generated a useful new tool that will enable detailed investigations of the range of functions of zebrafish Pk1 proteins.

Overall, our study has revealed that zebrafish Pk1 is required during cranial neural crest EMT and migration. Together with previously-published work, our findings reveal broad functions for the core PCP molecule Prickle1 in neural crest development. We conclude

that PCP molecules act as a key source of regulation and feedback for the complex cellular dynamics, including EMT processes, that function to allow proper development of the cranial neural crest.

CHAPTER 4

DISCUSSION

4.1 CONCLUSIONS

I will briefly summarize the conclusions from the work in Chapter 2 and Chapter 3, and in doing so will additionally sketch out a model that provides a mechanism for the action of Pk1b and Pk1a in the cranial neural crest.

Through my investigation of the roles of zebrafish Prickle1 through time-lapse imaging and mutant analysis, I have shown that Prickle1 is required for the ventrolateral migration of cranial NCCs and for pre-migratory cells to adopt polarities along the mediolateral axis. The inability of Pk1-deficient cells to polarize along the mediolateral axis as in wild-type cells, and instead to polarize along the antero-posterior axis correlates with the directionality of movement as Pk1-deficient cells move in net anterior directions. This aberrant motility of Pk1-deficient NCCs seems to correlate with a tendency of NCCs to cluster in groups of 3 or more cells at dorsal levels in the neural tube, such that cells in clusters of 3 or more cells show significantly higher levels of persistence in the aberrant direction than Pk1-deficient individual cells or cells in pairs. Further, the *majority* of Pk1-deficient cells are present in clusters of 3 to 8 cells and are maintained as such for far longer than wild-type cells, the *majority* of which are present and maintained as individual cells. Critically, though Pk1-deficient clusters move persistently in an aberrant direction, they show similar levels of persistence to wild-type cells moving in lateral directions. From this set of data, I conclude that Pk1b and Pk1a are required for NCCs to separate from

neighboring cells relatively quickly, to polarize cells along the mediolateral axis, and to ensure that cells make only transient contacts with one another and migrate ventrolaterally. However, while Pk1b and Pk1a are required to polarize cells along the mediolateral axis, a complete absence of polarity does not correlate with an absence of motility, since trans-heterozygous NCCs adopt randomized polarities but still move in anterior directions. Thus, it seems that the default state for cells in the absence of the core PCP Prickle1 molecules is *not* a complete loss of directionality—as previous models have postulated for the PCP molecules Dsh and Fzd7 and presumed to be true for other core PCP molecules (Carmona-Fontaine et al., 2008; Theveneau et al., 2010; Theveneau and Mayor, 2011a, b, 2012)—but an *anterior* directionality. From this I further conclude that Pk1b and Pk1a are required for normal polarization and migration of NCCs, but they are *not* required for NCCs to acquire the capacity for *motility*. This is in sharp contrast to the previous wisdom on the role of PCP during migration (Carmona-Fontaine et al., 2008; Theveneau et al., 2010), but crucially, while earlier studies inferred a lack of polarity *solely* from the inability of two colliding NCCs to reorient away from each other, I assay polarity through orientation of the MTOC. Since the polarity through orientation of the MTOC is known to correlate with the directionality of movement, it is striking that in trans-heterozygous embryos, NCCs adopt net anterior directionalities even though their polarity through the orientation of the MTOC is not biased in any direction. From this I conclude that a lack of polarity *does not* necessarily mean a lack of directionality.

My analysis of the clusters formed in Prickle1-deficient conditions demonstrates that Prickle1 is required for NCCs to separate from each other as early as 12 hpf before cells begin migrating ventrolaterally. However, Prickle1 is not required *solely* for NCCs to separate from one another. Instead, Pk1b and Pk1a are required in at least two separate

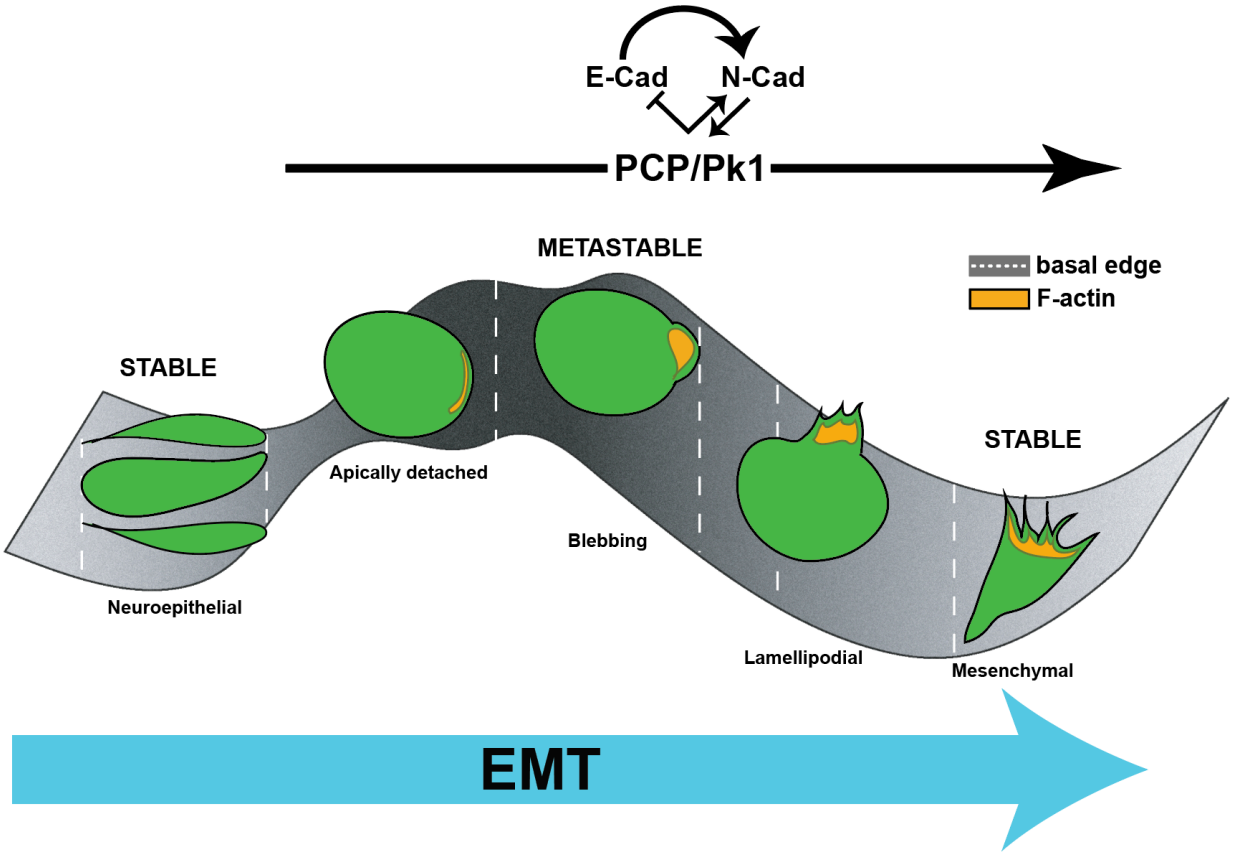

Fig. 4.1: A proposed model for Prickle1/PCP action in both EMT and migration of cranial neural crest cells in zebrafish. Through EMT, as is described in detail in Chapter 3, cranial neural crest cells go through a series of morphological transitions that can be described as belonging along a free energy spectrum, where both neuroepithelial and mesenchymal morphologies are "stable" and NCCs can remain in those morphologies in the normal state over extended periods of time, but transitional morphologies along the free energy "spectrum," represent higher-energy and thus less stable, or "meta-stable" morphologies. As

Fig. 4.1 continued: my results show, Prickle1 is required in EMT for cranial NCCs to move from the blebbing state to the filopodial- and lamellipodial-based mesenchymal state and in migration—this could possibly speak to a role for the entire PCP module through neural crest development. Further, as an E-Cad-to-N-Cad switch has been shown to be required for the completion of EMT, the model proposes that Pk1 and/or the entire PCP module is directly or indirectly responsible for the inhibition of E-Cadherin in pre-migratory and migratory cells and promotion of N-Cadherin in migratory cells required for that switch.

---

processes during neural crest development. The first role for Prickle1 molecules is in EMT, for NCCs to transition from the blebbing morphology to an actively protrusive mesenchymal morphology, and thus to ensure cells move from a transitory "metastable" state to a "stable" mesenchymal state to complete EMT. As discussed in Chapter 1, the concept of 'metastable' is defined based on literature in carcinoma cells with hybrid characteristics of both 'epithelial' and 'mesenchymal' (Lee et al., 2006). The second role for Prickle1 molecules is during migration, to ensure that neighboring NCCs separate from each other even when they have adopted highly mesenchymal morphologies. Further, Prickle1, directly or indirectly, is required to inhibit E-Cadherin in pre-migratory and migratory cells as well as to promote N-Cadherin in migratory cells. Since E-Cad levels have been shown to be reduced just as N-Cadherin levels are elevated in a previously-proposed E-Cad-to-N-Cad "switch", I conclude that Prickle1 is required for that switch by inhibiting E-Cadherin levels in pre-migratory cells and it continues to be important for

NCC migratory behavior by promoting N-Cadherin in migratory cells. I conclude that Prickle1b and Prickle1a act as early as 12 hpf in EMT and migration. Thus, I propose a model whereby both Pk1b and Pk1a proteins and/or the entire core PCP module have roles in EMT and migration over a window of at least 12 hours (12 hpf to 24 hpf) through a mechanism of sustained regulation of E-Cadherin and N-Cadherin (Fig. 4.1), which is likely only one form of regulation by PCP molecules.

4.2 LIMITATIONS & FUTURE DIRECTIONS

Although difficulties remain in testing aspects of the model as presented above, the model poses a number of intriguing questions for research on cranial NCCs in zebrafish. I will not attempt an exhaustive list, but will summarize the main limitations of the methodologies used, and will address questions left unanswered for future work.

4.2.1 Neural crest cell-intrinsic activity

First, while *pk1b* and *pk1a* are expressed in pharyngeal domains similar to the pan-neural crest marker *crestin*, they are both expressed in pharyngeal domains at low levels and it is far from clear whether either or both play roles by acting *within* NCCs and/or in surrounding tissues. Either answer remains a formal possibility. Further, it is possible that one paralog functions in a different tissue/cell type than the other. In other contexts, different PCP molecules have been found to behave in different cell types. For instance,

in the tangential migration of facial branchiomotor neurons (FBMNs), detailed analysis of mutants, genetic chimeras, and high-resolution imaging of the localization of PCP molecules, has indicated (although some contradictions in the literature persist) that different PCP molecules act to influence FBMN migration within neurons, in neuroepithelial cells, and/or in the floor plate of the neural tube (Davey et al., 2016; Mapp et al., 2011; Mapp et al., 2010; Pan et al., 2014; Sittaramane et al., 2013).

Pk1b and/or Pk1a could act within NCCs as Dsh and Fzd7 have been *inferred* to act in migrating NCCs on the basis of imaging fluorescently-tagged fusion proteins (Carmona-Fontaine et al., 2008). That one can only make an inference based on localization of the fusion proteins, instead of using it as a read-out, is because the correlation of localization does not imply the causation of sole function in the region where localization has been assayed (the published study does not detail whether the fusion proteins also localize elsewhere *in vivo*). Fluorescently-tagged Dsh localizes at the point of contact between two colliding NCCs and thus is thought to act at least predominantly within NCCs. However, a formal test of whether a given PCP molecule is required within NCCs would require analysis of phenotypes in two conditions: 1, NCCs are deficient in one or another PCP molecule but the rest of the embryo is genetically wild-type; 2, NCCs are genetically wild-type for one or another PCP molecule but the rest of the embryo, or a subset of tissues (such as the mesoderm, for instance) is deficient for any given PCP molecule. Such

experiments have been done in *Drosophila* using genetic mosaic analysis (Strutt and Strutt, 2015; Zallen, 2007). In zebrafish embryos, this has generally been attempted by generating chimeric embryos using transplantation of cells from donor embryos of one genetic background into host embryos of another. Regardless, my approach of using *pk1a* or *pk1b* homozygous mutant embryos or embryos injected with morpholinos targeted against *pk1b* at the 1-cell stage precludes an answer to the question of where the two proteins play their roles. Transplantation experiments to generate chimeras as outlined above, or a CRISPR/Cas conditional approach that causes *pk1b* or *pk1a* mutations only in specific cell-types or tissues, would be useful to address this question.

4.2.2 PCP and cell autonomy

Furthermore, my investigation does not address the question (related, but not identical, to the question above) as to whether Pk1b or Pk1a are acting cell-autonomously or non-cell-autonomously. It is possible, and perhaps even likely, that NCCs communicate the polarity and directionality conferred by Pk1b and Pk1a to each other in the same manner as *Drosophila* epithelial cells in a sheet. Such behavior has been described as both cell-autonomous and non-cell-autonomous (Davey and Moens, 2017; Peng and Axelrod, 2012): in *Drosophila*, although cells propagate PCP information across a sheet non-cell-autonomously, proximal and distal complexes of PCP molecules act repulsively within a single cell thus acting cell-autonomously. The PCP module has been interpreted in the

field to act similarly in vertebrates: altering Vangl or Fzd expression mosaically in either *Xenopus* or chick epithelia affects the polarity of adjacent wild-type cells—since the specific molecular interactions and asymmetric localization of PCP molecules have been shown to be largely conserved, it is inferred that PCP molecules behave similarly in vertebrates as they do in *Drosophila* (Butler and Wallingford, 2015; Davey and Moens, 2017; Mitchell et al., 2009; Sienknecht et al., 2011).

My experimental design has prevented me from answering the question of cell-autonomy directly, however the clustering phenotype in Pk1-deficient specimens raises an intriguing possibility: could PCP-deficient NCCs in clusters behave more like *Drosophila* epithelial cells than their wild-type counterparts? This is suggested by the maintenance of higher-order clusters as well as the concerted directionality of Pk1-deficient clusters, but *not* individual cells, in the anterior direction. If so, this would suggest that in the wild-type condition, PCP molecules in NCCs undergoing EMT act in a *different* way than they do in migrating NCCs which also make contacts with each other, however transiently, while maintaining a high persistence in the ventrolateral direction. Assaying the localization of Pk proteins both in wild-type specimens and in specimens deficient in one PCP molecule, to observe the changes in localization of the others, could address this question.

4.2.3 The localization of PCP proteins

Work in *Drosophila* and vertebrates has demonstrated that the core PCP module functions with the asymmetric localization of Frizzled, Disheveled, Vangl, Diego, and Prickle (Davey and Moens, 2017; Jones and Chen, 2007; Lawrence et al., 2002; Weston and Thiery, 2015; Zallen, 2007). Thus, where PCP has been implicated it has been necessary to assay the "orientation" of the PCP proteins' asymmetric localization. Fluorescently-tagged PCP proteins have been previously used in vertebrate systems to assay localization: Dvl1, Vangl1, and Pk2 in *Xenopus* ciliated epithelia (Butler and Wallingford, 2015); Vangl2 and Fzd3 in neuroepithelial progenitor cells in zebrafish (Ciruna et al., 2006; Davey et al., 2016; Roszko et al., 2009) and *Xenopus* (Ossipova et al., 2015); Vangl2 and Dsh in converging mesoderm cells in zebrafish (Heisenberg et al., 2000; Jessen et al., 2002; Yin et al., 2008), *Xenopus* (Darken et al., 2002; Djiane et al., 2000; Goto and Keller, 2002; Tada and Smith, 2000; Wallingford and Harland, 2001; Wallingford et al., 2000), and mouse (Criley, 1969; Kibar et al., 2001; Murdoch et al., 2001), and of course, Fzd7 and Dsh in neural crest in zebrafish (Matthews et al., 2008) and *Xenopus* (Carmona-Fontaine et al., 2008; De Calisto et al., 2005; Matthews et al., 2008). However, where attempts have been made to assay the localization of Prickle, all groups have only used a fusion protein consisting of Drosophila Prickle tagged with GFP both in zebrafish (Ciruna et al., 2006; Veeman et al., 2003; Yin et al., 2008) and *Xenopus*

(Ossipova et al., 2015; Takeuchi et al., 2003). I believe this is a flawed approach for two reasons: first, which of the many vertebrate homologs of *Drosophila* Prickle the fusion protein is acting as is unclear; second, since *Drosophila* Prickle has an isoform, Sple, which acts antagonistically to Prickle, it is possible that the vertebrate homologs act similarly, in which case the localization of *Drosophila*-Prickle could, at best, show one homolog's localization or the antagonistic reverse localization of another. A CRISPR/Cas "knock-in" approach to tag endogenous Prickle1b and Prickle1a with a fluorescent tag could be used in future work. Regardless, assaying the localization of the zebrafish-specific proteins is the only way to observe the dynamics of the Prickle1 and other core PCP molecules.

4.2.4 Rescuing neural crest defects

One key test of my model—whether NCC phenotypes in Pk1-deficient specimens, such as the dorsal clustering phenotype and/or the persistent blebbing state can be 'rescued'—has not been attempted. Since it has been widely reported that the overexpression of PCP molecules gives the same phenotype as specimens deficient in PCP molecules, and thus that the precise level of each PCP molecules is integral to its function (Lin and Gubb, 2009; Mapp et al., 2011; Zhu and Owen, 2013), I reasoned global overexpression by injecting *pk1b* or *pk1a* mRNA would be unlikely to rescue Pk1-deficient phenotypes. However, $pk1b^{fh122}$ mutants show a phenotype that blocks migration of FBMNs, and this phenotype has previously been rescued using a construct that expresses Pk1b specifically

in FBMNs using a FBMN-specific minimal promoter (Mapp et al., 2011). A similar construct targeted to express Pk1b and/or Pk1a specifically in NCCs using the *-4.9sox10* promoter could be used to attempt rescue of the NCC phenotype and give additional information about cell-autonomy.

Further, my results show that Pk1b functions to decrease levels of E-Cadherin, directly or indirectly, in both pre-migratory NCCs undergoing EMT and migratory NCCs. Thus, our model predicts that a depletion of E-Cadherin levels would at least partially rescue NCC defects in Pk1-deficient specimens. However, I have not attempted this experiment because *half-baked*/E-Cad mutant embryos are lethal at epiboly stages (Kane et al., 2005) and do not survive to the stages I have assayed. A transplantation approach to transplant blastula-stage E-Cad mutant cells into the domain of the gastrula fated to produce the neural crest is formally possible, though as with a similar approach attempted with N-Cadherin in the Prince lab (Wanner and Prince, 2013) and by others (Stockinger et al., 2011), it is likely that E-Cadherin-deficient cells would fail to integrate with wild-type neural tissue.

4.2.5 PCP function in EMT

In this dissertation, I show that the Prickle1 molecules are necessary for NCCs to transition from a transitory blebbing morphology, while pre-migratory, to a fully

mesenchymal migratory morphology during EMT. This is the first time any PCP molecules have been implicated in an EMT process in any system, and as such there are a number of intriguing implications of these results.

The first implication of my results is the need to reconceive previous work in light of the increasing knowledge about the morphological states NCCs pass through in a "spectrum" from epithelial cells to mesenchymal cells. In classical neural crest literature, many genes have been ascribed roles in NCC migration alone based on the inability of cells deficient in the gene of interest to migrate ventrolaterally. However, as my results show, the retention of NCCs at the dorsal surface of the neural tube is paired with a block in moving through EMT transitions, and thus, these genes could be reinvestigated to establish whether they in fact act in both EMT and migration.

One caveat at the outset, however, is in how I have defined "pre-migratory" NCCs throughout this dissertation: cells that, in a dorsal view, are located in dorsal-most slices along the z-axis and in medial positions because they have not migrated past the basal edge of the neural tube. Although they remain at the dorsal-most aspect of the neural keel/tube, Pk1-deficient clusters are highly motile in the anterior direction, but I have not conclusively shown precisely where the cells in clusters are located relative to the neuroepithelium. Since the NCCs' high motility seems inherently incompatible with the

cells being embedded within the neuroepithelium, I suggest that these motile cells likely lie immediately dorsal to the developing neural tube, in a domain that has previously been referred to as the "staging area". My findings suggest that cells perform blebbing behaviors in the staging area, and only become fully mesenchymal as they leave this domain and migrate ventrolaterally. Reaching the staging area is presumably dependent on prior apical detachment, the first element of the EMT process, which has been documented by Clay and Halloran (2014) using mosaic labeling with mCherry-UtrCH, and by Jimenez et al. (2016), using the NCC-progenitor marker *Tg(snail1:GFP)*. Similarly, I have observed apical detachment behavior in LifeAct-GFP-expressing NCCs, with no discernable differences between wild-type and *pk1*-deficient specimens. Future high resolution imaging analysis in multiple views, using a variety of markers for NCCs and their progenitors, will be necessary to more fully describe the precise locations of zebrafish NCCs at all stages of development.

My investigations of the roles of Pk1b and Pk1a show that they are required in EMT and migration, and that in Pk1-deficient specimens, NCCs cluster at the dorsal neural tube and move in anterior directions. The clustering phenotype was an important factor in querying whether Pk1 molecules have a role in EMT as early as 12 hpf. However, although Pk1b-deficient clustered pre-migratory cells show elevated levels of E-Cadherin, adopt rounded, bleb-based morphologies and can thus be thought of as having some epithelial

characteristics, this does not necessarily mean that the tendency of NCCs to cluster in the Pk1-deficient condition is *solely* due to a role for Pk1b and Pk1a in EMT. As stated above, since these clustered cells are motile, the absence of Pk1 molecules is not sufficient to render NCCs immobile. Interestingly, other cell types that undergo EMT have been shown to require a 'polarity reversal' such that centrosomes changed their position during EMT (Burute et al., 2017). Critically, this depends on the control of microtubule network assembly and disassembly as well as F-actin. Through the processes of neural crest development, NCCs require the dynamics of F-actin localization and microtubule networks to be tightly-controlled (Berndt et al., 2008; Clay and Halloran, 2013; Moore et al., 2013). Thus, it is possible that Pk1b and Pk1a act in pre-migratory neuroepithelial cells to cause 'polarity reversal' and allow for the completion of EMT and commencement of migration. Since Fzd7 and Dsh have been shown to be required for the dynamic regulation of F-actin (Banerjee et al., 2011; Clay and Halloran, 2010; Matthews et al., 2008), it is possible that PCP regulates F-actin, and thus polarity in neuroepithelial cells and is also responsible for changing F-actin localization dynamics so neuroepithelial cells can undergo and complete EMT. Such a model could formally be tested using our transient transgenesis strategy to mosaically-label cells with LifeAct-GFP, but in my experience, there is no effective way to ensure consistent dosage of LifeAct-GFP in embryos, or to control the number of copies integrated, making it hard to precisely quantify the 'peaks' of F-actin localization. Further, LifeAct-GFP has been shown to cause artefacts in other

systems (Courtemanche et al., 2016). An approach where the F-actin biosensor is present in all NCCs (achieved by establishing a stable transgenic line) would be preferable, as opposed to a mosaically-labelled population, to observe the dynamics of neighbor cells—despite known artefacts, this would have the advantage of having a consistent copy-number of LifeAct-GFP integrated in the genome, something that is difficult to achieve using transient transgenesis.

The mosaic approach I have detailed in this thesis could also be used to assay the localization dynamics of E-Cadherin or N-Cadherin in pre-migratory and migratory NCCs, along with an approach to simultaneously label endogenous Pk1b or Pk1a protein. However, again, because the efficiency of the mosaic approach is hard to standardize, a pan-neural crest F-actin biosensor would be preferable. Such an approach would be able to address where and how E-Cad and/or N-Cad are present in the specific metastable morphology I have demonstrated NCCs adopt during EMT, as well as in the pre-bleb and early-mesenchymal states. Coupled with an approach to assay the endogenous localization of Pk1b and Pk1a in wild-type and Pk1-deficient specimens, the model could be taken another step further: Does the localization of E-Cad or N-Cad, as the model would predict, depend on Pk1b and Pk1a localization asymmetrically at a particular 'side' of NCCs? If so, which sides do specific PCP proteins, and associated RhoGTPases, E-Cad, N-Cad localize to?

The mechanistic links between Prickle1b and Prickle1a, or any other PCP molecules, with E-Cad, N-Cad and/or other Cadherins could be assayed using a candidate-based approach. Several molecules have been implicated in *Xenopus* and zebrafish as downstream of PCP signaling: for instance, the PTK7/Ror2 co-receptor complex in neural crest (Podleschny et al., 2015; Shnitsar and Borchers, 2008), a suite of RhoGTPases including RhoA and ROCK (Matthews et al., 2008; Mayor and Theveneau, 2014; Theveneau and Mayor, 2011a), the formin-homology domain protein Daam1 and the actin-binding protein Shroom3 (Habas et al., 2001; Nishimura and Takeichi, 2008). Using embryos deficient in Pk1b/Pk1a/another core PCP molecule, three forms of analysis could be performed. First, since the effect on all molecules implicated except Rac1 seems to be that of PCP positively regulating these proteins, a rescue of the phenotypes due to PCP-deficiency could be attempted by over-expression of any of these molecules in zebrafish embryos, and the subsequent effect on E-Cad and N-Cad localization compared to wild-type and PCP-deficient specimens. Second, endogenous localization of any of these molecules could be assayed in PCP-deficient embryos, and the change as compared to WT embryos investigated. Third, analysis in mutant embryos deficient for both a PCP molecule and one of these downstream components could be used to investigate possible genetic interactions. In $pk1a^{ch105/ch105}$+*pk1b*-MO and $pk1b^{fh122/+}$;$pk1a^{ch105/+}$ trans-heterozygotes, an exacerbation of the phenotype could indicate that the PCP molecules

and the candidate molecule are functioning in the same molecular pathway. Would such specimens abrogate the successful completion of EMT completely, for instance?

It is important to note, however, that it is not only molecules previously implicated as downstream of PCP molecules that would be useful candidates to investigate mechanistic links. My data shows that Prickle1b and Prickle1a are involved in the presumptive neural crest as early as 12 hpf. Thus, the molecules Snai1b and FoxD3, which are termed 'neural crest specifier' molecules, but have been found to have roles in EMT as well (Jimenez et al., 2016; Stewart et al., 2006), could well be implicated. Indeed, Manuel Rocha in our lab has found some preliminary results that show a change in expression levels of *snai1b*—as assayed by in situ hybridization—in Pk1-deficient specimens as compared to WT specimens. Since Snai1b directly affects E-Cadherin levels (Jimenez et al., 2016; Simoes-Costa and Bronner, 2015), it is possible that Prickle1b acts on E-Cad through Snai1b. Such a link would elucidate how Prickle1 molecules act mechanistically earlier in neural crest development, implicating more molecules in the pathways and feedback loops that Prickle1 molecules are likely involved in to affect zebrafish neural crest EMT and migration.

In sum, there are many implications of a role for PCP signaling within EMT given that this investigation is the first to report such a role, and they primarily entail a

reconceptualization of EMT as consisting of particular transitions rather than a binary state switch. As detailed in Chapter 1, a role for PCP molecules in maintaining a cell morphology or adopting another is not unprecedented (Adler, 2002; Carreira-Barbosa et al., 2003; Ciruna et al., 2006; Clarke, 2009; Davey and Moens, 2017; Djiane et al., 2000; Gallik et al., 2017; Goto and Keller, 2002; Jones and Chen, 2007; Zallen, 2007). This would additionally require a rethinking of the GRNs acting during specific phases of neural crest development (induction, specification, EMT, migration) that have been proposed based on decades of work in neural crest (Simoes-Costa and Bronner, 2015; Simoes-Costa et al., 2014), potentially showing that molecules are involved in more 'phases' than previously thought. My study provides an entry-point to a more nuanced and complex understanding of EMT, and the role(s) of PCP signaling within it.

CHAPTER 5

MATERIALS & METHODS

5.1 Acknowledgments

I am grateful to numerous colleagues for sharing genetic tools and reagents that made this study possible. The *Tg(-4.9sox10:EGFP)ba2* fish line was provided by Tom Schilling with permission from Rob Kelsh and the *Tg(-7.2sox10:mRFP)vu234* fish line was provided by Bruce Appel. The *-4.9sox10:*LifeAct-GFP construct was provided by Michael Granato, the Cherry-XCentrin and EGFP-XCentrin plasmids by Diane Sepich, the *pk1a* probe by Diane Slusarski, and the Vangl2 morpholino reagent by Anand Chandrasekhar. I thank Sarah Wanner and Crystal Love for general technical guidance, Rachel Warga for advice on Cadherin antibody staining, Gokhan Dalgin for advice on CRISPR/Cas9 mutagenesis and for sharing reagents, and Anita Ng and Noor Singh for expert fish care. I have been supported by the George A. Hines Scholarship fund, and work for this thesis was funded in part by the Chicago Biomedical Consortium with support from the Searle Funds at The Chicago Community Trust, and by the National Center for Advancing Translational Sciences of the National Institutes of Health through Grant Number UL1 TR000430. This work also benefitted from the resources of the ZFIN database (zfin.org).

5.2 Zebrafish husbandry

Zebrafish (*Danio rerio*) were maintained using standard procedures and used in accord with IACUC-approved protocols. Embryos were maintained in E3 solution (in mM: 5.0 NaCl, 0.17 KCl, 0.33 CaCl, 0.33 $MgSO_4$) at 24^{o}C-28.5^{o}C and staged as described (Kimmel

et al., 1995). Embryos were obtained from crosses of adult fish stocks of mutants and/or transgenics. Specimens analyzed at stages later than 24 hours post-fertilization (hpf) were treated with 0.2 mM 1-phenyl 2-thiourea (PTU; Sigma) from 24 hpf onwards to inhibit melanin synthesis. Transgenic zebrafish lines *Tg(-4.9sox10:EGFP)*^{ba2} (hereafter *Tg(sox10:EGFP)* (Carney et al., 2006) and *Tg(-7.2sox10:mRFP)*^{vu234} (hereafter *Tg(sox10:mRFP)*) (Kirby and Hutson, 2010) and the mutant line *pk1b*^{fh122} (Mapp et al., 2011) have been previously described.

5.3 In situ hybridization

Detection of *pk1b* (Rohrschneider et al., 2007), *pk1a* (Carreira-Barbosa et al., 2003; Veeman et al., 2003), and *crestin* (Solomon et al., 2003), by in situ hybridization was carried out as previously described (Prince et al., 1998) using NBT/BCIP as the enzyme substrate. Embryos were cleared in 70% dimethylformamide overnight at 4°C, washed twice with 100% Methanol for 30 minutes at room temperature, and then mounted in 80% glycerol in PBS+0.1%Tween-20. Images were acquired using a Nikon D5000 digital camera mounted on a Leica MZFLIII microscope.

5.4 Morpholino design and microinjection

Two morpholinos (MOs) designed to block *pk1b* splicing (Gene Tools, LLC) were used as previously described (Rohrschneider et al., 2007) at a standard concentration of 2 ng/nl.

The first MO was targeted to intron3-exon4, with a sequence of 5'-GGCAGTAGCGAATCTGTGTTGAAGC-3', and the second MO was targeted to exon6-intron6 with a sequence of 5'-TTAATGAAACTCACCAATATTCTCT-3'. MOs were solubilized in water (Sigma-Aldrich) for a stock concentration of 20 mg/ml. Tg(sox10:EGFP) and Tg(sox10:mRFP) embryos were microinjected with MOs at the one-cell stage. The *vangl2*-MO (5'-GTACTGCGACTCGTTATCCATGTC-3') was used as previously described (Jessen et al., 2002) at a concentration of 1 ng/nl.

5.5 Image Acquisition

For assays in fixed specimens, embryos were fixed in 4% paraformaldehyde (PFA, diluted in 1X phosphate buffered saline; PBS) overnight. Following overnight fixation, embryos were washed in 1X PBS five times for 10 minutes each. For long-term storage of embryos, embryos were washed in 30%, 60% and 100% methanol (diluted in 1X PBS) and stored in 100% methanol at -20^{o}C. If stored in 100% methanol, embryos were progressively washed in 60%, 30% methanol as well as 1X PBS + 0.1%Tween-20 before being transferred to 80% glycerol. The embryos were cleared in 80% glycerol, deyolked using fine forceps and flat-mounted in glycerol in dorsal view. Images were collected using an upright Zeiss LSM710 confocal microscope using either a Plan-Apochromat 20x/0.8 (working distance: 0.55mm) objective or a Plan Apochromat 40x/1.0 water-immersion (working distance: 2.5mm) objective. Green fluorescent proteins (GFP) and dyes (Alexa

Fluor 488) were excited by a 488nm laser. Red fluorescent proteins (mRFP, RFP) and dyes (Alexa Fluor 564) were excited by a 543nm laser. DAPI dye and cyan fluorescent protein (CFP) were excited using a 405nm laser. For a single fluorophore or a combination of fluorophores, spectral unmixing was used to define emission fluorescence range. For each sample, transmitted-light images were also collected. Images were acquired and saved as .czi files using Zen (Zeiss) software.

Live imaging was performed at room temperature by mounting 16 hpf embryos in 1% low-melt agarose (MidSci IB70051 St. Louis, Missouri) prepared in E3 medium with anesthetic (MS-222, tricaine methanesulfonate, Sigma-Aldrich; 0.20mg/mL in E3 solution). Embryos were staged before and after experimentation. A Plan-Apochromat 40X/1.0 water-immersion objective (working distance: 0.55mm) on a Zeiss LSM710 confocal microscope was used over a period of two hours with images captured at a time interval between 1 and 2 mins, with images collected with transmitted light (brightfield) acquired before and after experimentation to provide a reference for drift correction in image processing of migrating cells relative to static cells. Longer time-lapses were performed at room temperature by mounting 12 hpf embryos in 0.5% low-melt agarose and imaged in the same fashion as above with a time interval of 5 mins and transmitted light images acquired at each time point to allow drift correction.

5.6 mRNA generation and microinjection

Capped mRNA was generated using the MEGAscript SP6 or T7 Kit (Ambion). mRNAs at concentrations of Tol2 Transposase (150 ng/µl) (Kawakami and Shima, 1999), EGFP-XCentrin (105 ng/µl), Cherry-XCentrin (150 ng/µl) (Sepich et al., 2011), H2B-CFP (300 ng/µl), and mRFP (200 ng/µl) (last two generously provided by Gokhan Dalgin) (Dalgin and Prince, 2015) were kept on ice and microinjected into the yolk-cell interphase of one-cell stage embryos.

5.7 NCC aspect ratio measurements

Measurements of the width and length ratio of NCCs were performed in wild-type embryos and mutant embryos in the Tg(*sox10*:EGFP) background. Embryos were co-injected with RNA encoding mRFP, and width and length was measured using the mRFP label in sox10-positive cells.

5.8 Quantification of NCC contacts over time

To quantify breakage of contacts between NCCs over time intervals of 0-10 min, 10-20 min, 20-30 min and 30-40 min, we counted the total number of pairs of NCCs in contact within a cluster at t=0 such that a single cell could be in pairs with multiple cells in contact, and then counted the pairs that broke at each time interval. Dividing the second measure by the first, we generated a ratiometric measure of 'pair breakage' within a

cluster. To measure the relative proportions of individuals NCCs and NCC clusters of varying sizes, we measured the number of cells that persisted in a given configuration (from an individual cell to cells in increasing sizes of clusters) over non-overlapping 20-minute time windows.

5.9 Transient transgenesis

To label cranial NCCs mosaically, a DNA construct encoding I-SceI *-4.9sox10:*LifeAct-GFP (gift from Michael Granato, University of Pennsylvania) was microinjected as described (Banerjee et al., 2011) into one-cell stage Tg(*sox10*:mRFP) embryos at a concentration of 100 ng/µl together with the meganuclease I-SceI (NEB) at a concentration of 1U/µl in 1X phosphate-buffered saline. Cells were imaged in live embryos, mounted as described above, and imaged at approximately 16 hpf for at least 20 minutes using a Plan-Apochromat 40X/1.0 water-immersion objective (working distance: 0.55mm) on a Zeiss LSM710 confocal microscope. Transmitted light (brightfield) images were also collected to categorize cells as pre-migratory or migratory based on their position relative to the basal edge of the neural tube.

5.10 Immunohistochemistry

Embryos were fixed in 4% paraformaldehyde (PFA; Sigma), and immunohistochemistry was performed as previously described (Prince et al., 1998) using the following primary

antibodies: rabbit polyclonal anti-Cdh1 (E-Cadherin; 1:100; GeneTex GTX100443), rabbit polyclonal Cdh2 (N-Cadherin; 1:200; GeneTex GTX125885) and rabbit polyclonal anti-Sox10 (1:250; Genetex GTX128374). The following secondary antibodies were used: goat-anti mouse highly cross-adsorbed Alexa Fluor Plus 488 (Molecular Probes A32723), goat anti-rabbit highly cross-adsorbed Alexa Fluor 488 (Molecular Probes A11034), goat anti-rabbit cross-adsorbed Alexa Fluor 546 conjugate (Molecular Probes A11010), and anti-GFP Alexa Fluor 488 conjugate (Molecular Probes A21311). Embryos were then cleared in 80% glycerol, deyolked and flat-mounted.

5.11 Subcellular localization measurements

To quantitate subcellular localization of E-Cad, fluorescence intensity in Tg(*sox10*:mRFP) embryos immunostained with E-Cad, and counterstained with DAPI was measured at the plasma membrane with average ratios calculated and intensities normalized with respect to background levels of E-Cad. To determine subcellular localization of N-Cad, Tg(*sox10*:mRFP) embryos were stained for N-Cad and counterstained with DAPI and fluorescence intensities measured in the same manner as for E-Cad.

To determine subcellular localization of the intracellular mitrotubule organizing center (MTOC) in NCCs, either Tg(*sox10*:mRFP) embryos were injected with RNA coding for EGFP-XCentrin as described (Sepich et al., 2011) as well as RNA coding for H2B-CFP,

or Tg(*sox10*:EGFP) embryos were injected with RNA coding for Cherry-XCentrin (Sepich et al., 2011) as well as RNA coding for H2B-CFP. Injected embryos were fixed at 24 hpf. To quantitate angles of the MTOC relative to the nucleus and the AP axis, bisecting lines were drawn from the MTOC to the nucleus, the angle relative to the AP axis for each cell determined, and measurements of the angle of the MTOC with respect to the nucleus and the AP body axis performed using Fiji and analyzed using MATLAB.

5.12 Quantification and statistical analysis

Fiji (NIH) was used to process and analyze data, and Prism (GraphPad) and Microsoft Excel were used for statistical analyses. Cell counts for z-stacks of confocal images with optical sections between 2 and 4μm were performed using the Fiji cell counter plugin. Cell aspect ratio and area quantifications were performed using the Fiji Cell Magic Wand plugin. Statistical significance was determined using two-way ANOVA or the student t-test (* indicates $p<0.05$, ** indicates $p<0.01$, *** indicates $p<0.001$, **** indicates $p<0.0001$).

Polar plots for directionality trajectories were made by importing Excel-generated measurements of displacement vectors into MATLAB to allow for generation of polar plots. Polarity measurements were analyzed using Fiji; statistical measurements and polar histograms were generated using MATLAB. Statistical significance ($p<0.05$) for polar

plots was determined using the Watson-Williams F-test.

Manual tracking of migrating cells was performed using the Fiji MTrackJ plugin by following cells through multiple stacks. Persistence measurements were made using tracking data imported into Excel and using the open-source program DiPer, an open-source set of Excel macros, as previously described (Gorelik & Gautreau, 2014). Collected time-lapse data were registered using Fiji and exported as TIF images and AVI videos.

For cluster rearrangement analysis, a MATLAB script (available upon request) was used to threshold and segment cells, enabling counts on pair breaks within clusters. The data on pair breaks within clusters was then imported into Prism and tabulated. All figures were created in Illustrator and InDesign (Adobe).

APPENDIX A:
CRISPR/CAS GENERATION OF PRICKLE1A MUTANT ZEBRAFISH

A.1 Design

The CHOPCHOP website (Montague et al., 2014) was used to select genomic target sites on the zebrafish *pk1a* locus. Two gRNAs targeting exon 2 were designed and one gRNA (genomic target sequence in gRNA for *pk1a* endogenous gene is underlined in Fig. A.1.1, with PAM sequence indicated and start site in blue) was selected based on higher efficacy as determined using a T7 endonuclease I assay (Fig A.1.2).

		PAM
WT	AGGGGGTGTTAGTGATGGAGCTGGAGAATCGCGGTGGGTCCACATGGGGTCA	
***pk1a*^{ch105}**	AGGGGGTGTTAGTGATGGAGCTGGAG----------C--TGGGGTCA	

Fig. A.1: The sequence of the *pk1a* endogenous gene and the *pk1a*^{ch105} allele

The complete gRNA sequence is shown below. It was designed to contain an SP6 promoter (underlined), genomic target site (sequence in lowercase, with PAM sequence italicized, as also shown in Fig. A.1.1) and an optimized single guide (sg) RNA scaffold, modified for efficient transcription with an extended stem loop designed to improve interaction with the Cas9 protein (Chen et al., 2013) was purchased as a gBlock from Integrated DNA Technologies and used as a template for transcribing sgRNA:

5'-

AAAAATTTAGGTGACACTATAgtgatggagctggagaat*cgg*TTTAAGAGCTATGCTGGA

AACAGCATAGCAAGTTTAAATAAGGCTAGTCCGTTATCAACTTGAAAAAGTG

GCACCGAGTCGGTGCTTTTTTT-3'

sgRNA and Cas9 RNA were transcribed, purified and injected as previously described (Dalgin & Prince 2015). The sgRNA (final stock concentration: 100-200 ng/µl) and Cas9 mRNA (final stock concentration: 600 ng/µl) were transcribed using the MEGAscript SP6 Kit (Ambion), treated with TURBO DNase from the Ambion kit, extracted using an equal volume of phenol/chloroform, and precipitated using 3 volumes of 100% ethanol. RNA was resuspended in water, and 70 pg sgRNA and 500 pg Cas9 RNA were injected into one-cell stage embryos. For the T7 Endonuclease Assay I, genomic DNA was extracted from 10-15 48 hpf embryos. DNA was resuspended in 10 µl TE buffer and stored at 4^{o}C. A PCR reaction using 2 µl of genomic DNA was assembled using primers that amplified a 230 bp genomic region flanking the *pk1a* target site (forward primer 5'-GTAAGTGTGTGGCGGTA-3', reverse primer 5'-CCATACCTGCTCTGGTCTGAGT-3').

The T7 Endonuclease Assay I was performed on PCR amplicons as a measure of gRNA efficiency as previously described (Dalgin and Prince, 2015). The purpose of the T7 Endonuclease Assay I is to distinguish PCR products which have mismatched double-

stranded DNA (for instance: a Cytosine base in one strand incorrectly matched with a Tyrosine base) that result from Cas9-induced INDELs at the gRNA site: the T7Ei enzyme cleaves double-stranded DNA at the point of mismatch. If INDELs are present, the

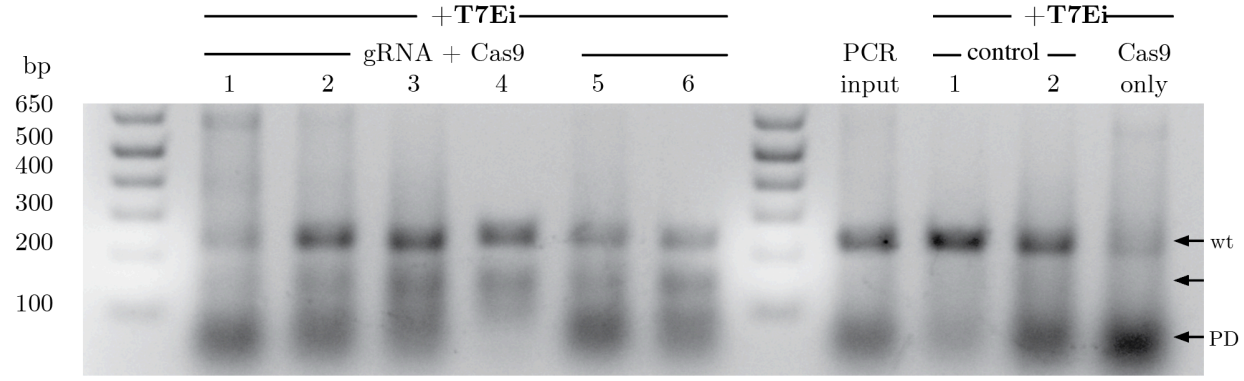

Fig. A.2: T7Ei assay on *pk1a* DNA extracted from 6 embryos injected with Cas9 and gRNA targeted to the *pk1a* endogenous gene assayed shows multiple bands due to mismatches in the endogenous gene sequence. The 1kb+ladder and size of bands is indicated on the far left. Expected size of PCR product on *pk1a* endogenous gene was 230 bp. Arrows on the far right show the location of the wild-type band, a band produced due to T7Ei cleavage, and primer dimers (PD). Lanes labeled 1 to 6 show the result of the T7Ei assay on PCR products from DNA extracted from 6 different embryos injected with the targeted gRNA and Cas9 enzyme. The controls are to the right of the second ladder: the first control is the PCR input (no T7Ei assay) for embryo 6. Controls 1 and 2 are the T7Ei assay on PCR products on DNA extracted from wild-type embryos that were not injected with either gRNA or Cas9. The lane marked Cas9 only shows the results of the T7Ei assay on PCR products from DNA extracted from an embryo where Cas9 enzyme, but not the gRNA, was injected.

resulting DNA will show more bands on a gel than the uncleaved PCR product alone (Fig. A.1.2) As shown in Fig. A.1.2, PCR products of the endogenous *pk1a* gene from the genomic DNA extracted from 6 embryos showed mismatches and multiple bands due to the T7Ei essay. Controls were as follows. 1. DNA was extracted from wild-type embryos, PCR using the same primers was conducted and the T7Ei assay was performed (control 1 and 2 on far right in Fig. A.1.2) to ensure that the results of the T7Ei assay were due to the specific targeting of the *pk1a* locus by the gRNA and Cas9. 2. Wild-type embryos were injected with Cas9 enzyme but not gRNA to ensure that targeting was specific to the *pk1a* locus. DNA was extracted, PCR performed and the T7Ei assay performed as before. 3. The PCR input for embryo 6 injected with both gRNA and Cas9, without performing the T7Ei assay, was run on the same gel to ensure that the difference seen was due to the cleavage by the T7 endonuclease.

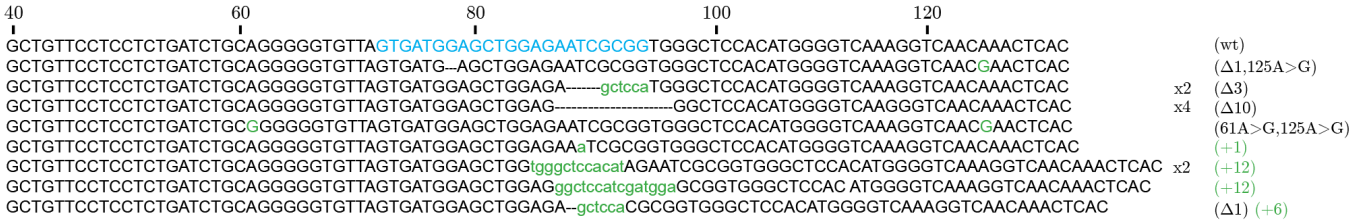

Fig. A.3: Embryos injected with Cas9 and gRNA targeted to the *pk1a* endogenous gene show an array of mutations. Mutant copies of the gene from 10 sequenced embryos shown. The top row shows the wild-type *pk1a* endogenous sequence, with gRNA targeting sequence indicated in blue. Insertions are indicated in green, deletions with hyphens. Frequency of sequences that appeared more than once is indicated on the far-right.

PCR products for each embryo was subcloned into the pGEM-T Easy vector (Promega A1360) according to manufacturer's protocols, and clones were sequenced to identify insertion/deletion mutant alleles. As the gRNA and Cas9 injected in any given embryo can cause an array of mutations in somatic cells, as expected we found an array of mutations even within a given embryo, as shown in Fig. A.1.3.

A.2 Generation of the *pk1a*^{ch105} mutant

Injected F0 specimens were raised to adulthood and outcrossed to wild-type AB embryos. Genomic DNA was extracted from 10-15 F1 offspring embryos per cross, PCR amplified as described above, and subcloned to identify INDELs. Since F1 progeny would only contain mutations at the *pk1a* locus if the gRNA+Cas9 injected in F0 embryos induced germline mutations, many F1 embryos did not show mutations, indicating that the founder F0 fish did not have germline mutations. In this manner, sequence information from F1 offspring identified two founder F0 fish with putative germline mutations. F1 offspring from these founders were then raised to adult stages, and subsequently DNA was isolated from fin clips used to genotype putative mutants as described (Jing, 2012).

Of these F1 offspring, multiple F1 fish were heterozygous for specific mutations (since not all germline cells in the two founders carried mutant copies, only some F1 fish would carry

mutations). One F1 fish was identified as heterozygous for a putative null *pk1a* genomic allele, hereafter designated *pk1a*^{ch105}. The *pk1a*^{ch105} allele has a 19 bp deletion, causing a frame shift and predicted STOP at amino acid 24 (Fig. A.2.1A), causing a truncated protein towards the beginning of the PET domain (Fig. A.2.1B). A subsequent F2 generation was raised by out-crossing the F1 mutant fish to a *Tg(sox10:EGFP)* fish. Fin clips from F2 adult fish were used to genotype and identify heterozygous *pk1a*^{ch105}

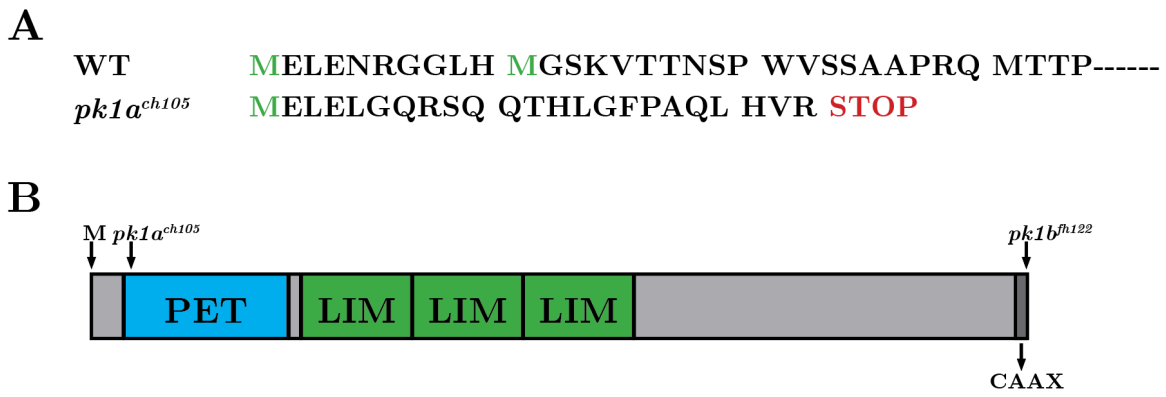

Fig. A.4: The predicted null *pk1a*^{ch105} mutant encodes a truncated protein. (A) Amino-acid sequence of Pk1a N-terminus; the *pk1a*^{ch105} mutant encodes a truncated protein with a premature STOP codon. (B) Schematic of protein domain structure for both Prickle1b and Prickle1a. Arrows indicate lesions in *pk1a*^{ch105} and *pk1b*^{fh122} mutants. The first codon, and the C-terminal CAAX domain are also indicated.

---

mutant fish using PCR with primer sequences 5'-GTAAGTGTGTGGTGGCGGTA-3' and 5'-TCAGTCGTTTAAGGCGGGTC-3'. The resulting PCR products were then run on a 4% agarose gel. Heterozygous and wild-type fish were distinguished by the presence

of two bands 19 bp apart, versus a single band. Heterozygous F2 adults were in-crossed to raise an F3 generation, which were also genotyped using fin-clipping. Although homozygous mutants did not survive to adulthood at Mendelian ratios, approximately 10% of adult F3 fish were homozygous mutants. All experimental work shown in Chapters 2 and 3 has used the F4 progeny of adult F3 homozygous *pk1a*^{ch105} mutant fish.

APPENDIX B:
A POTENTIAL ROLE FOR PRICKLE1B AND REST IN REGULATING DIFFERENTIATION OF CRANIAL NEURAL CREST

B.1 Introduction & Hypotheses:

Previous work in our lab, specifically on the tangential migration of facial branchiomotor neurons (FBMNs) from r4 to r6/r7 in the zebrafish hindbrain, has implicated Prickle1b as acting specifically within FBMNs to regulate the localization of the RE1-silencing transcription factor (Rest) (Love and Prince, 2015; Mapp et al., 2011). Prior to these studies, Rest had been well-known as a repressor of neuronal genes in both neuronal progenitors and non-neuronal cells, thus acting as a regulator of the specification of neuronal cells (reviewed in Ballas and Mandel, 2005; Qureshi and Mehler, 2009). Rest is known to bind specifically to a highly-conserved RE1 consensus sequence upstream of many neuron-specific genes and forms a repression complex with its co-receptors to silence its gene targets—when the Rest complex no longer binds to this sequence, the previously-silenced genes can be expressed allowing for the regulation of terminal differentiation of neuronal cells (Ballas et al., 2005; Love and Prince, 2015).

Importantly, in the model that was elucidated in both Mapp et al. (2011) and Love and Prince (2015): 1, Pk1b was found to localize at the FBMN nucleus, and this nuclear

localization was in turn found to be required for FBMN migration; 2, Pk1b prevents the precocious maturation of FBMNs before they successfully migrate to r6/r7 by enabling (directly or indirectly) the nuclear translocation of Rest; 3, In Pk1b-deficient specimens, FBMNs do not migrate out of r4, and further they show signs of 'precocious maturation' characteristic of neurons in r6/r7; 4, Nuclear-localized Rest can rescue the migration of FBMNs in Rest-deficient embryos, but not Pk1b-deficient embryos, indicating that Pk1b does not act solely through its role with Rest in FBMN migration. Nonetheless, the overall model indicated that Pk1b—in what is likely a PCP-independent role—regulates FBMN migration at least partly through enabling Rest to repress neuronal genes before migration is complete, thus allowing for the normal maturation of neurons when they reach r6/r7, but not before.

These findings in FBMNS, coupled with my early investigation into the role of Pk1b in NCC migration, led us to hypothesize that: A, Pk1b acts to regulate the localization of Rest in cranial NCCs, and B, that Rest is a critical effector that allows for the right timing of the differentiation of neurons in the cranial ganglia.

B.2 Results

B.2.1 Pk1b-deficient specimens show Rest-depletion in nuclei of migrating NCCs

First, I hypothesized that since Rest is present in the developing embryo in non-neural tissues as well as in neural stem cells and progenitor populations, that it would be present in migrating NCCs as well. To investigate whether Pk1b has a role in regulating the localization of Rest in NCCs, I performed immunohistochemistry using a previously-described Rest antibody (Mapp et al., 2011) (Abcam, ab21635) in both wild-type and *pk1b*-morphant embryos at 24 hpf. I found that although wild-type NCCs showed Rest localization throughout the cytoplasm, *pk1b*-morphant embryos showed a depletion of Rest specifically from the nuclei (Fig. B.1 A-B'''). Quantification of the nuclear: cytoplasmic fluorescence intensity ratio in wild-type and *pk1b*-morphant cells showed a statistically significant decrease in Rest localization in the nuclei of *pk1b*-morphant cells as compared to wild-type cells (Fig. B.1 C).

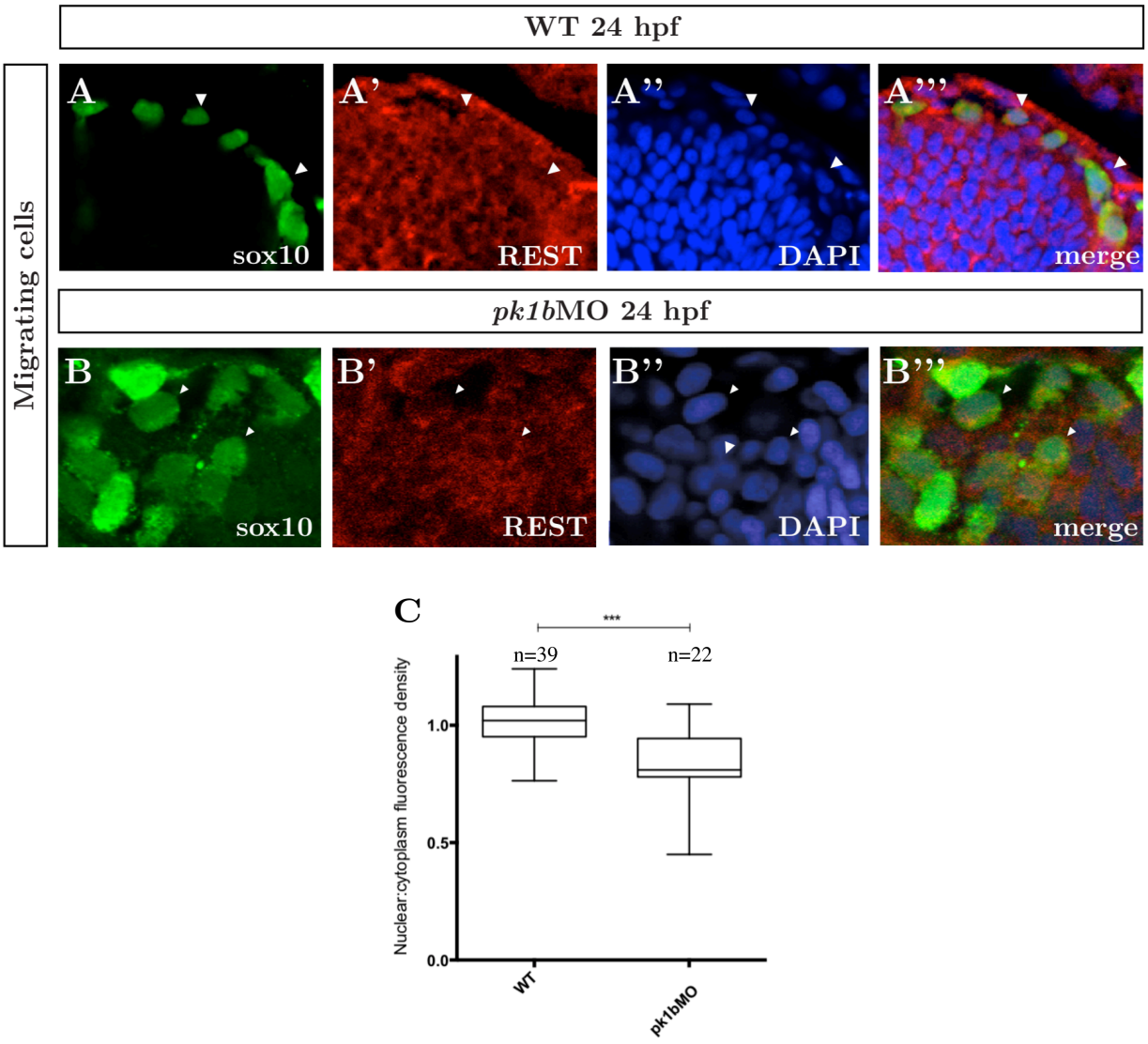

Fig. B.1: Pk1b-deficient specimens show depletion of Rest in the nuclei of migrating NCCs as compared to wild-type specimens.

To investigate the effect of Pk1b-knockdown on the localization of Rest, immunostaining was used both for wild-type and *pk1b*-morphant migratory NCCs. (A-B''') *Tg(sox10:EGFP)* (A-B), were immunostained for Rest (A'-B'), and counterstained with DAPI to mark nuclei (A''-B'''). White arrowheads indicate migrating NCCs to distinguish from adjacent neuroepithelial cells. Merged channels are also shown (A'''-B'''). (A-A''') In wild-type migrating NCCs, Rest is present throughout the cytoplasm and nucleus (A'-A'''). (B-B''') In

Fig. B.1 continued: *pk1b*-morphant specimens, Rest is depleted from nuclei (B') despite showing localization in the cytoplasm (B''') as compared to WT (compare A' and B'). (C) To quantify the degree of Rest depletion from the nucleus, fluorescence pixel intensity was measured for the whole cell as well as for the region of the nucleus marked by DAPI. The ratio of nuclear : cytoplasmic fluorescence intensity was calculated for each cell and normalized, by dividing by whole-cell pixel intensity. Rest was uniformly localized in wild-type migrating NCCs (n=39 cells, 5 embryos), but was depleted from nuclei in *pk1b*-morphant migrating NCCs.

B.2.2 Pk1b-deficient specimens show Rest-depletion in nuclei of pharyngeal arch-1 cells

Since migrating NCCs showed a depletion of Rest from the nuclei, I hypothesized that the first pharyngeal (mandibular) arch (PA-1) cells would show a similar pattern of uniform localization in wild-type specimens and nuclear-depletion in *pk1b*-morphant specimens, since PA-1 cells are not fated to become neurons. I used a similar approach of immunohistochemistry in both wild-type and *pk1b*-morphant 24 hpf specimens, and found a similar localization pattern as in migrating NCCs: wild-type cells showed uniform levels of Rest throughout the NCCs, whereas *pk1b*-morphant cells showed depletion of Rest from the nuclei (Fig. B.2).

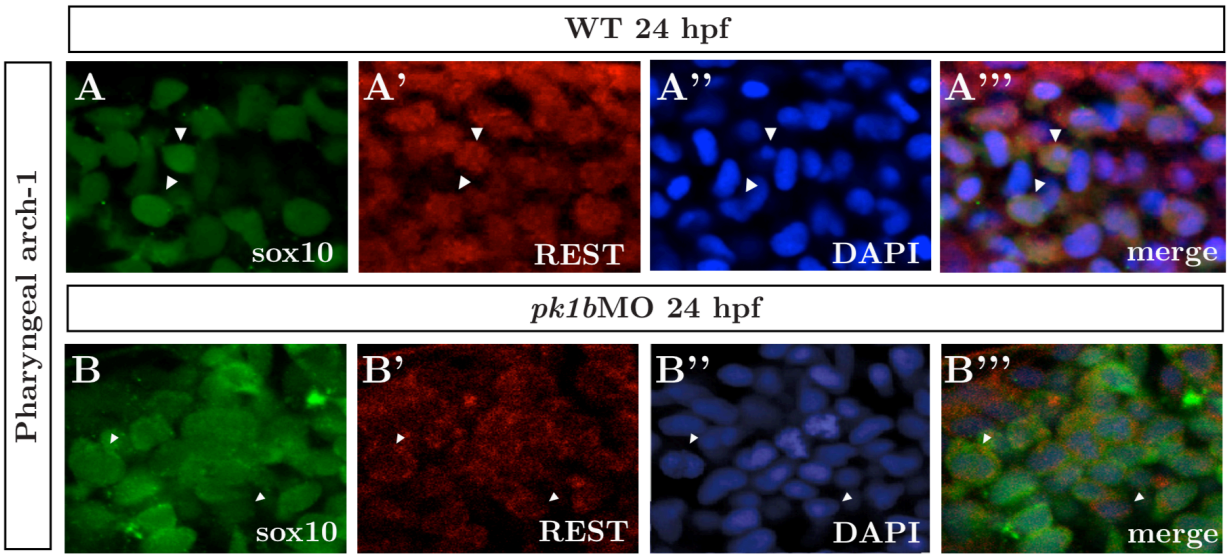

Fig. B.2: Pk1b-deficient specimens show depletion of Rest in the nuclei of PA-1 NCCs as compared to NCCs in wild-type specimens.

To investigate the effect of Pk1b-knockdown on the localization of Rest in PA-1 NCCs, immunostaining was used both for wild-type and *pk1b*-morphant specimens. (A-B''') *Tg(sox10:EGFP)* (A-B), were immunostained for Rest (A'-B'), and counterstained with DAPI to mark nuclei (A''-B'''). White arrowheads indicate migrating NCCs to distinguish from adjacent neuroepithelial cells. Merged channels are also shown (A'''-B'''). (A-A''') In wild-type migrating NCCs, Rest is present throughout the cytoplasm and nucleus (A'-A'''). (B-B''') In *pk1b*-morphant specimens, Rest is depleted from nuclei (B') despite showing localization in the cytoplasm (B''') as compared to WT (compare A' and B').

B.2.3 Rest-deficient specimens show premature neurogenesis in cranial ganglia

Based on my finding that Pk1b-deficiency causes specific depletion of Rest from the nuclei of both migratory, and thus presumably un-fated, NCCs as well as PA-1 cells that are

fated to differentiate into cartilage and bone cells, I further hypothesized that Rest plays a role in the cranial sensory ganglia in the vertebrate head that arise in part from cranial neural crest contributions and express neuronal-specific bHLH transcription factors such as Neurogenin-1 and Neurod (Andermann et al., 2002; Obholzer et al., 2008; Wilson et al., 2007). To investigate the role of Rest in the zebrafish cranial sensory ganglia, I used the *Tg[neurod:EGFP]* line (Dalgin and Prince, 2015; Obholzer et al., 2008) that marks cranial sensory placodes and ganglia, and lateral line neuromasts. Further, I utilized morpholinos targeted against Rest as previously described (Love and Prince, 2015; Mapp et al., 2011). In wild-type *Tg[neurod:EGFP]* embryos, imaging showed that the anterodorsal lateral line, anteroventral lateral line, facial placodes/ganglia, and posterior lateral line placodes, were all present in 48 hpf wild-type specimens. In Rest-deficient *Tg[neurod:EGFP]* specimens, each of these structures were also present in 48 hpf specimens, but in addition, the octavel/statoacoustic ganglia precursors were detected (Fig. B.3). While the staging of the appearance of cranial sensory ganglia and placodes needs to be better-established, particularly in the particular transgenic line being used, this preliminary result suggests that—consistent with previous reports—Rest-deficient embryos show premature maturation of neuronal populations, in this case the octavel/statoacoustic ganglia precursors.

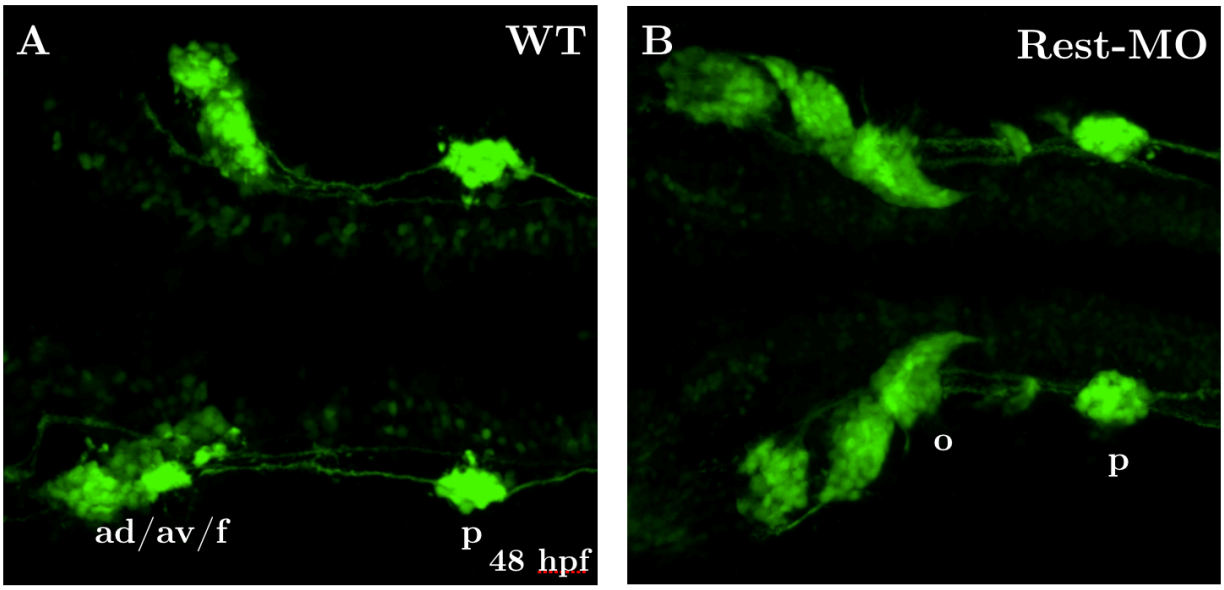

Fig. B.3 Rest-deficient specimens show premature maturation of the octavel/statoacoustic ganglia precursors

To investigate the effect of Rest-deficiency, both *Tg[neurod:EGFP]* wild-type (A) embryos and *Tg[neurod:EGFP]* embryos injected with Rest-morpholinos at the one-cell stage (B) were imaged at 48 hpf. (A) Wild-type embryos (n=4) showed well-formed posterior lateral line placode as well as anterodorsal lateral line, anteroventral lateral line and facial placodes/ganglia. (B) However, Rest-deficient embryos (n=4) showed well-formed octavel/statoacoustic ganglia precursors that were not observed in wild-type embryos. ad/av/f= anterodorsal/anteroventral lateral line/facial placodes/ganglia; p=posterior lateral line placode; o=octavel/statoacoustic ganglia precursors.

B.3 Conclusions & Discussion

This appendix provides preliminary data that indicate a role for Pk1b in regulating Rest in cranial NCCs, and thus a role for Rest in the differentiation of cell types that arise

from NCCs. Moreover, these preliminary observations suggest that as with FBMNs (Love and Prince, 2015; Mapp et al., 2011), it is possible Pk1b plays a role in regulating the localization and activity of Rest through a mechanism that is independent from the other, PCP-based, roles shown in this dissertation. While Rest is broadly expressed in the developing embryo, it does localize in migrating NCCs, and Pk1b activity is, in some way, responsible for the nuclear translocation of Rest such that in its absence, Rest is depleted from the nuclei of migrating NCCs. This role is also shown in NCCs in the mandibular arch. However, one major caveat of the experiments conducted is that they are a snapshot of 24 hpf embryos—PA1 cells may well have different patterns of Rest localization at a later stage. This indicates the importance of staging when neural crest cells differentiate into particular cell types, and establishing which markers reliably indicate those fates, including cartilage and bone, as well as neuronal cells.

That Rest-deficiency seems to lead to a premature mass of a particular type of cranial sensory ganglia is intriguing. Since the other ganglia and precursors do not seem significantly different in size between wild-type and Rest-deficient specimens, it raises the possibility that Rest-deficiency is not sufficient to increase the number of neuronal cells, only the timing of their differentiation. Regardless, more careful staging needs to be done in wild-type embryos to specify precisely where and when Rest is playing a role. Furthermore, since I did not assay the consequence of Pk1b-deficiency in

Tg[neurod:EGFP] embryos, it is unclear to what degree Pk1b may be involved in mediating Rest's role in the differentiation and formation of the cranial sensory ganglia.

SUPPLEMENTAL FILE LEGENDS

Supplemental movie files available through a shared Dropbox folder.

Supplemental Movie 1

Maximum-projection confocal movie with 4 min 30 sec interval of wild-type *Tg(sox10:EGFP)* embryo with anterior to left showing movement of NCCs at the dorsal aspect of the neuroepithelium. Solid line indicates edge of neuroepithelial as assayed using DIC imaging. Above solid line is NCCs dorsal to neuroepithelium, below is cells migrating towards periphery. Embryo imaged using upright Zeiss LSM710 confocal microscope using a Plan Apochromat 40x/1.0 water-immersion (working distance: 2.5mm) objective from roughly 16 hpf to 18 hpf. Time stamp at top left follows hh:mm format.

Supplemental Movie 2

Maximum-projection confocal movie with 5 min 0 sec interval of *pk1b*-morphant *Tg(sox10:EGFP)* embryo, with anterior to left and lateral above and below, showing movement of NCCs at the dorsal aspect of the neuroepithelium. Solid line indicates edge of neuroepithelial as assayed using DIC imaging, with NCCs dorsal to neuroepithelium at center above solid line. Time stamp at top left follows hh:mm format.

Supplemental Movie 3

Maximum-projection confocal movie with 3 min 30 sec interval of homozygous mutant *pk1b*$^{fh122/fh122}$ *Tg(sox10:EGFP)* embryo, with anterior to left and lateral above and below, showing movement of NCCs at the dorsal aspect of the neuroepithelium. Solid line indicates edge of neuroepithelial as assayed using DIC imaging, with NCCs dorsal to neuroepithelium at center between solid lines. Time stamp at top left follows hh:mm format.

Supplemental Movie 4

Maximum-projection confocal movie with 2 min 0 sec interval of homozygous mutant *pk1a*$^{ch105/ch105}$ *Tg(sox10:EGFP)* embryo, with anterior to left and lateral above and below, showing movement of NCCs at the dorsal aspect of the neuroepithelium. Solid line indicates edge of neuroepithelial as assayed using DIC imaging, with NCCs dorsal to neuroepithelium at center between solid lines. Time stamp at top left follows hh:mm format.

Supplemental Movie 5

Maximum-projection confocal movie with 2 min 30 sec interval of double-heterozygous *pk1b*$^{fh122/+}$;*pk1a*$^{ch105/+}$ *Tg(sox10:EGFP)* embryo, with anterior to left and lateral above and below, showing movement of NCCs at the dorsal aspect of the neuroepithelium. Solid

line indicates edge of neuroepithelial as assayed using DIC imaging, with NCCs dorsal to neuroepithelium at center between solid lines. Time stamp at top left follows hh:mm format.

Supplemental Movie 6

Maximum-projection confocal movie with 1 min 8 sec interval of wild-type embryo injected with *sox10:*LifeAct-GFP DNA showing apically-delaminating cell rounding up within the neuroepithelium, with the neuroepithelial midline to left and basal edge of neuroepithelium to right. Time stamp at top left in minutes, with two decimal places. Scale bar=10 µm

Supplemental Movie 7

Maximum-projection confocal movie with 33 sec interval of wild-type embryo injected with *sox10:*LifeAct-GFP DNA showing transition of NCC on the dorsal neural tube undergoing a transition from a rounded morphology to a one with small protrusions, with basal edge of neuroepithelium to right. Time stamp at top left in minutes, with two decimal places. Scale bar=10 µm.

Supplemental Movie 8

Maximum-projection confocal movie with 1 min 18 sec interval of wild-type embryo injected with *sox10:*LifeAct-GFP DNA showing blebbing cell on the dorsal neural tube, with basal edge of neuroepithelium to right. Time stamp at top left in minutes, with two decimal places. Scale bar=10 µm.

Supplemental Movie 9

Maximum-projection confocal movie with 1 min 9 sec interval of wild-type embryo injected with *sox10:*LifeAct-GFP DNA showing the transition of a NCC with small protrusions to a highly-protrusive mesenchymal NCC, with position of NCC traversing the basal edge of the neuroepithelium. Embryo imaged using upright Zeiss LSM710 confocal microscope using a Plan Apochromat 40x/1.0 water-immersion objective. Time stamp at top left in minutes with two decimal places. Scale bar=10 µm.

REFERENCES

1. Abercrombie, M., and Heaysman, J.E. (1953). Observations on the social behaviour of cells in tissue culture. I. Speed of movement of chick heart fibroblasts in relation to their mutual contacts. Exp Cell Res *5*, 111-131.

2. Abercrombie, M., and Heaysman, J.E. (1954). Observations on the social behaviour of cells in tissue culture. II. Monolayering of fibroblasts. Exp Cell Res *6*, 293-306.

3. Abercrombie, M., and Heaysman, J.E. (1976). Invasive behavior between sarcoma and fibroblast populations in cell culture. J Natl Cancer Inst *56*, 561-570.

4. Abitua, P.B., Gainous, T.B., Kaczmarczyk, A.N., Winchell, C.J., Hudson, C., Kamata, K., Nakagawa, M., Tsuda, M., Kusakabe, T.G., and Levine, M. (2015). The pre-vertebrate origins of neurogenic placodes. Nature *524*, 462-465.

5. Abitua, P.B., Wagner, E., Navarrete, I.A., and Levine, M. (2012). Identification of a rudimentary neural crest in a non-vertebrate chordate. Nature *492*, 104-107.

6. Acloque, H., Adams, M.S., Fishwick, K., Bronner-Fraser, M., and Nieto, M.A. (2009). Epithelial-mesenchymal transitions: the importance of changing cell state in development and disease. J Clin Invest *119*, 1438-1449.

7. Adams, R.H., Diella, F., Hennig, S., Helmbacher, F., Deutsch, U., and Klein, R. (2001). The cytoplasmic domain of the ligand ephrinB2 is required for vascular morphogenesis but not cranial neural crest migration. Cell *104*, 57-69.

8. Adler, P.N. (2002). Planar signaling and morphogenesis in Drosophila. Dev Cell *2*, 525-535.

9. Ahlstrom, J.D., and Erickson, C.A. (2009). The neural crest epithelial-mesenchymal transition in 4D: a 'tail' of multiple non-obligatory cellular mechanisms. Development *136*, 1801-1812.

10. Ambegaonkar, A.A., and Irvine, K.D. (2015). Coordination of planar cell polarity pathways through Spiny-legs. Elife *4*.

11. Andermann, P., Ungos, J., and Raible, D.W. (2002). Neurogenin1 defines zebrafish cranial sensory ganglia precursors. Dev Biol *251*, 45-58.

12. Axelrod, J.D. (2001). Unipolar membrane association of Dishevelled mediates Frizzled planar cell polarity signaling. Genes Dev *15*, 1182-1187.

13. Axelrod, J.D., and McNeill, H. (2002). Coupling planar cell polarity signaling to morphogenesis. ScientificWorldJournal *2*, 434-454.

14. Ayukawa, T., Akiyama, M., Mummery-Widmer, J.L., Stoeger, T., Sasaki, J., Knoblich, J.A., Senoo, H., Sasaki, T., and Yamazaki, M. (2014). Dachsous-dependent asymmetric localization of spiny-legs determines planar cell polarity orientation in Drosophila. Cell Rep *8*, 610-621.

15. Baker, C.V., and Bronner-Fraser, M. (1997). The origins of the neural crest. Part I: embryonic induction. Mech Dev *69*, 3-11.

16. Ballas, N., Grunseich, C., Lu, D.D., Speh, J.C., and Mandel, G. (2005). REST and its corepressors mediate plasticity of neuronal gene chromatin throughout neurogenesis. Cell *121*, 645-657.

17. Ballas, N., and Mandel, G. (2005). The many faces of REST oversee epigenetic programming of neuronal genes. Curr Opin Neurobiol *15*, 500-506.

18. Banerjee, S., Gordon, L., Donn, T.M., Berti, C., Moens, C.B., Burden, S.J., and Granato, M. (2011). A novel role for MuSK and non-canonical Wnt signaling during segmental neural crest cell migration. Development *138*, 3287-3296.

19. Barembaum, M., and Bronner, M.E. (2013). Identification and dissection of a key enhancer mediating cranial neural crest specific expression of transcription factor, Ets-1. Dev Biol *382*, 567-575.

20. Bastock, R., Strutt, H., and Strutt, D. (2003). Strabismus is asymmetrically localised and binds to Prickle and Dishevelled during Drosophila planar polarity patterning. Development *130*, 3007-3014.

21. Berndt, J.D., Clay, M.R., Langenberg, T., and Halloran, M.C. (2008). Rho-kinase and myosin II affect dynamic neural crest cell behaviors during epithelial to mesenchymal transition in vivo. Dev Biol *324*, 236-244.

22. Betancur, P., Bronner-Fraser, M., and Sauka-Spengler, T. (2010). Genomic code for Sox10 activation reveals a key regulatory enhancer for cranial neural crest. Proc Natl Acad Sci U S A *107*, 3570-3575.

23. Bingham, S., Higashijima, S., Okamoto, H., and Chandrasekhar, A. (2002). The Zebrafish trilobite gene is essential for tangential migration of branchiomotor neurons. Dev Biol *242*, 149-160.

24. Borovina, A., Superina, S., Voskas, D., and Ciruna, B. (2010). Vangl2 directs the posterior tilting and asymmetric localization of motile primary cilia. Nat Cell Biol *12*, 407-412.

25. Bronner, M.E., and LeDouarin, N.M. (2012). Development and evolution of the neural crest: an overview. Dev Biol *366*, 2-9.

26. Burute, M., Prioux, M., Blin, G., Truchet, S., Letort, G., Tseng, Q., Bessy, T., Lowell, S., Young, J., Filhol, O., *et al.* (2017). Polarity Reversal by Centrosome Repositioning Primes Cell Scattering during Epithelial-to-Mesenchymal Transition. Dev Cell *40*, 168-184.

27. Butler, M.T., and Wallingford, J.B. (2015). Control of vertebrate core planar cell polarity protein localization and dynamics by Prickle 2. Development *142*, 3429-3439.

28. Campbell, K., and Casanova, J. (2016). A common framework for EMT and collective cell migration. Development *143*, 4291-4300.

29. Carmona-Fontaine, C., Matthews, H.K., Kuriyama, S., Moreno, M., Dunn, G.A., Parsons, M., Stern, C.D., and Mayor, R. (2008). Contact inhibition of locomotion in vivo controls neural crest directional migration. Nature *456*, 957-961.

30. Carney, T.J., Dutton, K.A., Greenhill, E., Delfino-Machin, M., Dufourcq, P., Blader, P., and Kelsh, R.N. (2006). A direct role for Sox10 in specification of neural crest-derived sensory neurons. Development *133*, 4619-4630.

31. Carreira-Barbosa, F., Concha, M.L., Takeuchi, M., Ueno, N., Wilson, S.W., and Tada, M. (2003). Prickle 1 regulates cell movements during gastrulation and neuronal migration in zebrafish. Development *130*, 4037-4046.

32. Chalpe, A.J., Prasad, M., Henke, A.J., and Paulson, A.F. (2010). Regulation of cadherin expression in the chicken neural crest by the Wnt/beta-catenin signaling pathway. Cell Adh Migr *4*, 431-438.

33. Chen, B., Gilbert, L.A., Cimini, B.A., Schnitzbauer, J., Zhang, W., Li, G.W., Park, J., Blackburn, E.H., Weissman, J.S., Qi, L.S., *et al.* (2013). Dynamic imaging of genomic loci in living human cells by an optimized CRISPR/Cas system. Cell *155*, 1479-1491.

34. Cheung, M., Chaboissier, M.C., Mynett, A., Hirst, E., Schedl, A., and Briscoe, J. (2005). The transcriptional control of trunk neural crest induction, survival, and delamination. Dev Cell *8*, 179-192.

35. Chu, C.W., and Sokol, S.Y. (2016). Wnt proteins can direct planar cell polarity in vertebrate ectoderm. Elife *5*.

36. Ciruna, B., Jenny, A., Lee, D., Mlodzik, M., and Schier, A.F. (2006). Planar cell polarity signalling couples cell division and morphogenesis during neurulation. Nature *439*, 220-224.

37. Clarke, J. (2009). Role of polarized cell divisions in zebrafish neural tube formation. Curr Opin Neurobiol *19*, 134-138.

38. Clay, M.R., and Halloran, M.C. (2010). Control of neural crest cell behavior and migration: Insights from live imaging. Cell Adh Migr *4*, 586-594.

39. Clay, M.R., and Halloran, M.C. (2013). Rho activation is apically restricted by Arhgap1 in neural crest cells and drives epithelial-to-mesenchymal transition. Development *140*, 3198-3209.

40. Clay, M.R., and Halloran, M.C. (2014). Cadherin 6 promotes neural crest cell detachment via F-actin regulation and influences active Rho distribution during epithelial-to-mesenchymal transition. Development *141*, 2506-2515.

41. Colas, J.F., and Schoenwolf, G.C. (2001). Towards a cellular and molecular understanding of neurulation. Dev Dyn *221*, 117-145.

42. Coles, E.G., Taneyhill, L.A., and Bronner-Fraser, M. (2007). A critical role for Cadherin6B in regulating avian neural crest emigration. Dev Biol *312*, 533-544.

43. Couly, G.F., Coltey, P.M., and Le Douarin, N.M. (1993). The triple origin of skull in higher vertebrates: a study in quail-chick chimeras. Development *117*, 409-429.

44. Courtemanche, N., Pollard, T.D., and Chen, Q. (2016). Avoiding artefacts when counting polymerized actin in live cells with LifeAct fused to fluorescent proteins. Nat Cell Biol *18*, 676-683.

45. Cousin, H. (2017). Cadherins function during the collective cell migration of Xenopus Cranial Neural Crest cells: revisiting the role of E-cadherin. Mech Dev *148*, 79-88.

46. Creuzet, S., Vincent, C., and Couly, G. (2005). Neural crest derivatives in ocular and periocular structures. Int J Dev Biol *49*, 161-171.

47. Creuzet, S.E. (2009a). Neural crest contribution to forebrain development. Semin Cell Dev Biol *20*, 751-759.

48. Creuzet, S.E. (2009b). Regulation of pre-otic brain development by the cephalic neural crest. Proc Natl Acad Sci U S A *106*, 15774-15779.

49. Criley, B.B. (1969). Analysis of embryonic sources and mechanims of development of posterior levels of chick neural tubes. J Morphol *128*, 465-501.

50. Curtin, J.A., Quint, E., Tsipouri, V., Arkell, R.M., Cattanach, B., Copp, A.J., Henderson, D.J., Spurr, N., Stanier, P., Fisher, E.M., *et al.* (2003). Mutation of Celsr1 disrupts planar polarity of inner ear hair cells and causes severe neural tube defects in the mouse. Curr Biol *13*, 1129-1133.

51. Dalgin, G., and Prince, V.E. (2015). Differential levels of Neurod establish zebrafish endocrine pancreas cell fates. Dev Biol *402*, 81-97.

52. Darken, R.S., Scola, A.M., Rakeman, A.S., Das, G., Mlodzik, M., and Wilson, P.A. (2002). The planar polarity gene strabismus regulates convergent extension movements in Xenopus. EMBO J *21*, 976-985.

53. Das, G., Jenny, A., Klein, T.J., Eaton, S., and Mlodzik, M. (2004). Diego interacts with Prickle and Strabismus/Van Gogh to localize planar cell polarity complexes. Development *131*, 4467-4476.

54. Davey, C.F., Mathewson, A.W., and Moens, C.B. (2016). PCP Signaling between Migrating Neurons and their Planar-Polarized Neuroepithelial Environment Controls Filopodial Dynamics and Directional Migration. PLoS Genet *12*, e1005934.

55. Davey, C.F., and Moens, C.B. (2017). Planar cell polarity in moving cells: think globally, act locally. Development *144*, 187-200.

56. Davidson, L.A., and Keller, R.E. (1999). Neural tube closure in Xenopus laevis involves medial migration, directed protrusive activity, cell intercalation and convergent extension. Development *126*, 4547-4556.

57. Davy, A., Aubin, J., and Soriano, P. (2004). Ephrin-B1 forward and reverse signaling are required during mouse development. Genes Dev *18*, 572-583.

58. De Bellard, M.E., Ching, W., Gossler, A., and Bronner-Fraser, M. (2002). Disruption of segmental neural crest migration and ephrin expression in delta-1 null mice. Dev Biol *249*, 121-130.

59. De Calisto, J., Araya, C., Marchant, L., Riaz, C.F., and Mayor, R. (2005). Essential role of non-canonical Wnt signalling in neural crest migration. Development *132*, 2587-2597.

60. Dee, C.T., Szymoniuk, C.R., Mills, P.E., and Takahashi, T. (2013). Defective neural crest migration revealed by a Zebrafish model of Alx1-related frontonasal dysplasia. Hum Mol Genet *22*, 239-251.

61. Djiane, A., Riou, J., Umbhauer, M., Boucaut, J., and Shi, D. (2000). Role of frizzled 7 in the regulation of convergent extension movements during gastrulation in Xenopus laevis. Development *127*, 3091-3100.

62. Donoghue, P.C., Graham, A., and Kelsh, R.N. (2008). The origin and evolution of the neural crest. Bioessays *30*, 530-541.

63. Eickholt, B.J. (2008). Functional diversity and mechanisms of action of the semaphorins. Development *135*, 2689-2694.

64. Eickholt, B.J., Mackenzie, S.L., Graham, A., Walsh, F.S., and Doherty, P. (1999). Evidence for collapsin-1 functioning in the control of neural crest migration in both trunk and hindbrain regions. Development *126*, 2181-2189.

65. Erickson, C.A., and Perris, R. (1993). The role of cell-cell and cell-matrix interactions in the morphogenesis of the neural crest. Dev Biol *159*, 60-74.

66. Evans, D.J., and Noden, D.M. (2006). Spatial relations between avian craniofacial neural crest and paraxial mesoderm cells. Dev Dyn *235*, 1310-1325.

67. Farlie, P.G., Kerr, R., Thomas, P., Symes, T., Minichiello, J., Hearn, C.J., and Newgreen, D. (1999). A paraxial exclusion zone creates patterned cranial neural crest cell outgrowth adjacent to rhombomeres 3 and 5. Dev Biol *213*, 70-84.

68. Feiguin, F., Hannus, M., Mlodzik, M., and Eaton, S. (2001). The ankyrin repeat protein Diego mediates Frizzled-dependent planar polarization. Dev Cell *1*, 93-101.

69. Ferrante, M.I., Romio, L., Castro, S., Collins, J.E., Goulding, D.A., Stemple, D.L., Woolf, A.S., and Wilson, S.W. (2009). Convergent extension movements and ciliary

function are mediated by ofd1, a zebrafish orthologue of the human oral-facial-digital type 1 syndrome gene. Hum Mol Genet *18*, 289-303.

70. Friedl, P., and Gilmour, D. (2009). Collective cell migration in morphogenesis, regeneration and cancer. Nat Rev Mol Cell Biol *10*, 445-457.

71. Friedl, P., and Wolf, K. (2003). Tumour-cell invasion and migration: diversity and escape mechanisms. Nat Rev Cancer *3*, 362-374.

72. Gallik, K.L., Treffy, R.W., Nacke, L.M., Ahsan, K., Rocha, M., Green-Saxena, A., and Saxena, A. (2017). Neural crest and cancer: Divergent travelers on similar paths. Mech Dev *148*, 89-99.

73. Gammill, L.S., Gonzalez, C., and Bronner-Fraser, M. (2007). Neuropilin 2/semaphorin 3F signaling is essential for cranial neural crest migration and trigeminal ganglion condensation. Dev Neurobiol *67*, 47-56.

74. Gammill, L.S., Gonzalez, C., Gu, C., and Bronner-Fraser, M. (2006). Guidance of trunk neural crest migration requires neuropilin 2/semaphorin 3F signaling. Development *133*, 99-106.

75. Gans, C., and Northcutt, R.G. (1983). Neural crest and the origin of vertebrates: a new head. Science *220*, 268-273.

76. Gavert, N., Ben-Shmuel, A., Raveh, S., and Ben-Ze'ev, A. (2008). L1-CAM in cancerous tissues. Expert Opin Biol Ther *8*, 1749-1757.

77. Geldmacher-Voss, B., Reugels, A.M., Pauls, S., and Campos-Ortega, J.A. (2003). A 90-degree rotation of the mitotic spindle changes the orientation of mitoses of zebrafish neuroepithelial cells. Development *130*, 3767-3780.

78. Genuth, M.A., Allen, C.D.C., Mikawa, T., and Weiner, O.D. (2018). Chick cranial neural crest cells use progressive polarity refinement, not contact inhibition of locomotion, to guide their migration. Dev Biol.

79. Glasco, D.M., Sittaramane, V., Bryant, W., Fritzsch, B., Sawant, A., Paudyal, A., Stewart, M., Andre, P., Cadete Vilhais-Neto, G., Yang, Y., *et al.* (2012). The mouse Wnt/PCP protein Vangl2 is necessary for migration of facial branchiomotor neurons, and functions independently of Dishevelled. Dev Biol *369*, 211-222.

80. Goto, T., and Keller, R. (2002). The planar cell polarity gene strabismus regulates convergence and extension and neural fold closure in Xenopus. Dev Biol *247*, 165-181.

81. Goudarzi, M., Tarbashevich, K., Mildner, K., Begemann, I., Garcia, J., Paksa, A., Reichman-Fried, M., Mahabaleshwar, H., Blaser, H., Hartwig, J., *et al.* (2017). Bleb Expansion in Migrating Cells Depends on Supply of Membrane from Cell Surface Invaginations. Dev Cell *43*, 577-587 e575.

82. Green, S.A., Simoes-Costa, M., and Bronner, M.E. (2015). Evolution of vertebrates as viewed from the crest. Nature *520*, 474-482.

83. Griffith, C.M., Wiley, M.J., and Sanders, E.J. (1992). The vertebrate tail bud: three germ layers from one tissue. Anat Embryol (Berl) *185*, 101-113.

84. Gross, J.B., and Hanken, J. (2005). Cranial neural crest contributes to the bony skull vault in adult Xenopus laevis: insights from cell labeling studies. J Exp Zool B Mol Dev Evol *304*, 169-176.

85. Grunert, S., Jechlinger, M., and Beug, H. (2003). Diverse cellular and molecular mechanisms contribute to epithelial plasticity and metastasis. Nat Rev Mol Cell Biol *4*, 657-665.

86. Gubb, D., and Garcia-Bellido, A. (1982). A genetic analysis of the determination of cuticular polarity during development in Drosophila melanogaster. J Embryol Exp Morphol *68*, 37-57.

87. Gubb, D., Green, C., Huen, D., Coulson, D., Johnson, G., Tree, D., Collier, S., and Roote, J. (1999). The balance between isoforms of the prickle LIM domain protein is critical for planar polarity in Drosophila imaginal discs. Genes Dev *13*, 2315-2327.

88. Gupta, G.P., and Massague, J. (2006). Cancer metastasis: building a framework. Cell *127*, 679-695.

89. Habas, R., Kato, Y., and He, X. (2001). Wnt/Frizzled activation of Rho regulates vertebrate gastrulation and requires a novel Formin homology protein Daam1. Cell *107*, 843-854.

90. Hale, R., and Strutt, D. (2015). Conservation of Planar Polarity Pathway Function Across the Animal Kingdom. Annu Rev Genet *49*, 529-551.

91. Hall, B.K. (2000). The neural crest as a fourth germ layer and vertebrates as quadroblastic not triploblastic. Evol Dev *2*, 3-5.

92. Hall, B.K., and Hall, B.K. (2009). The neural crest and neural crest cells in vertebrate development and evolution, 2nd edn (New York: Springer).

93. Halloran, M.C., and Berndt, J.D. (2003). Current progress in neural crest cell motility and migration and future prospects for the zebrafish model system. Dev Dyn *228*, 497-513.

94. Hanken, J., and Gross, J.B. (2005). Evolution of cranial development and the role of neural crest: insights from amphibians. J Anat *207*, 437-446.

95. Hashimoto, M., Shinohara, K., Wang, J., Ikeuchi, S., Yoshiba, S., Meno, C., Nonaka, S., Takada, S., Hatta, K., Wynshaw-Boris, A.*, et al.* (2010). Planar polarization of node cells determines the rotational axis of node cilia. Nat Cell Biol *12*, 170-176.

96. Hay, E.D. (2005). The mesenchymal cell, its role in the embryo, and the remarkable signaling mechanisms that create it. Dev Dyn *233*, 706-720.

97. Heisenberg, C.P., Tada, M., Rauch, G.J., Saude, L., Concha, M.L., Geisler, R., Stemple, D.L., Smith, J.C., and Wilson, S.W. (2000). Silberblick/Wnt11 mediates convergent extension movements during zebrafish gastrulation. Nature *405*, 76-81.

98. Helms, J.A., Cordero, D., and Tapadia, M.D. (2005). New insights into craniofacial morphogenesis. Development *132*, 851-861.

99. Helms, J.A., and Schneider, R.A. (2003). Cranial skeletal biology. Nature *423*, 326-331.

100. Hörstadius, S.O. (1950). The neural crest; its properties and derivatives in the light of experimental research (London, New York,: Oxford University Press).

101. Huang, C., Kratzer, M.C., Wedlich, D., and Kashef, J. (2016a). E-cadherin is required for cranial neural crest migration in Xenopus laevis. Dev Biol *411*, 159-171.

102. Huang, M., Miller, M.L., McHenry, L.K., Zheng, T., Zhen, Q., Ilkhanizadeh, S., Conklin, B.R., Bronner, M.E., and Weiss, W.A. (2016b). Generating trunk neural crest from human pluripotent stem cells. Sci Rep *6*, 19727.

103. Hurley, I.A., Mueller, R.L., Dunn, K.A., Schmidt, E.J., Friedman, M., Ho, R.K., Prince, V.E., Yang, Z., Thomas, M.G., and Coates, M.I. (2007). A new time-scale for ray-finned fish evolution. Proc Biol Sci *274*, 489-498.

104. Jenny, A., Reynolds-Kenneally, J., Das, G., Burnett, M., and Mlodzik, M. (2005). Diego and Prickle regulate Frizzled planar cell polarity signalling by competing for Dishevelled binding. Nat Cell Biol *7*, 691-697.

105. Jessen, J.R., Topczewski, J., Bingham, S., Sepich, D.S., Marlow, F., Chandrasekhar, A., and Solnica-Krezel, L. (2002). Zebrafish trilobite identifies new roles for Strabismus in gastrulation and neuronal movements. Nat Cell Biol *4*, 610-615.

106. Jia, L., Cheng, L., and Raper, J. (2005). Slit/Robo signaling is necessary to confine early neural crest cells to the ventral migratory pathway in the trunk. Dev Biol *282*, 411-421.

107. Jimenez, L., Wang, J., Morrison, M.A., Whatcott, C., Soh, K.K., Warner, S., Bearss, D., Jette, C.A., and Stewart, R.A. (2016). Phenotypic chemical screening using a zebrafish neural crest EMT reporter identifies retinoic acid as an inhibitor of epithelial morphogenesis. Dis Model Mech *9*, 389-400.

108. Jing, L. (2012). Genotyping for Single Zebrafish (Fin Clip) or Zebrafish Embryo. Bio-protocol *2*, e182.

109. Jones, C., and Chen, P. (2007). Planar cell polarity signaling in vertebrates. Bioessays *29*, 120-132.

110. Jones, M.C. (1990). The neurocristopathies: reinterpretation based upon the mechanism of abnormal morphogenesis. Cleft Palate J *27*, 136-140.

111. Jussila, M., and Ciruna, B. (2017). Zebrafish models of non-canonical Wnt/planar cell polarity signalling: fishing for valuable insight into vertebrate polarized cell behavior. Wiley Interdiscip Rev Dev Biol *6*.

112. Kane, D.A., McFarland, K.N., and Warga, R.M. (2005). Mutations in half baked/E-cadherin block cell behaviors that are necessary for teleost epiboly. Development *132*, 1105-1116.

113. Kasemeier-Kulesa, J.C., McLennan, R., Romine, M.H., Kulesa, P.M., and Lefcort, F. (2010). CXCR4 controls ventral migration of sympathetic precursor cells. J Neurosci *30*, 13078-13088.

114. Kaufman, C.K., Mosimann, C., Fan, Z.P., Yang, S., Thomas, A.J., Ablain, J., Tan, J.L., Fogley, R.D., van Rooijen, E., Hagedorn, E.J., *et al.* (2016). A zebrafish melanoma model reveals emergence of neural crest identity during melanoma initiation. Science *351*, aad2197.

115. Kawakami, K., and Shima, A. (1999). Identification of the Tol2 transposase of the medaka fish Oryzias latipes that catalyzes excision of a nonautonomous Tol2 element in zebrafish Danio rerio. Gene *240*, 239-244.

116. Kibar, Z., Vogan, K.J., Groulx, N., Justice, M.J., Underhill, D.A., and Gros, P. (2001). Ltap, a mammalian homolog of Drosophila Strabismus/Van Gogh, is altered in the mouse neural tube mutant Loop-tail. Nat Genet *28*, 251-255.

117. Kimmel, C.B., Ballard, W.W., Kimmel, S.R., Ullmann, B., and Schilling, T.F. (1995). Stages of embryonic development of the zebrafish. Dev Dyn *203*, 253-310.

118. Kirby, M.L., and Hutson, M.R. (2010). Factors controlling cardiac neural crest cell migration. Cell Adh Migr *4*, 609-621.

119. Klingensmith, J., Nusse, R., and Perrimon, N. (1994). The Drosophila segment polarity gene dishevelled encodes a novel protein required for response to the wingless signal. Genes Dev *8*, 118-130.

120. Klymkowsky, M.W., Rossi, C.C., and Artinger, K.B. (2010). Mechanisms driving neural crest induction and migration in the zebrafish and Xenopus laevis. Cell Adh Migr *4*, 595-608.

121. Knight, R.D., and Schilling, T.F. (2006). Cranial neural crest and development of the head skeleton. Adv Exp Med Biol *589*, 120-133.

122. Kulesa, P.M., Bailey, C.M., Kasemeier-Kulesa, J.C., and McLennan, R. (2010). Cranial neural crest migration: new rules for an old road. Dev Biol *344*, 543-554.

123. Lallier, T., Leblanc, G., Artinger, K.B., and Bronner-Fraser, M. (1992). Cranial and trunk neural crest cells use different mechanisms for attachment to extracellular matrices. Development *116*, 531-541.

124. Lammermann, T., and Sixt, M. (2009). Mechanical modes of 'amoeboid' cell migration. Curr Opin Cell Biol *21*, 636-644.

125. Lawrence, P.A., Casal, J., and Struhl, G. (2002). Towards a model of the organisation of planar polarity and pattern in the Drosophila abdomen. Development *129*, 2749-2760.

126. Le Douarin, N. (1973). A biological cell labeling technique and its use in expermental embryology. Dev Biol *30*, 217-222.

127. Le Douarin, N., and Kalcheim, C. (1999). The neural crest, 2nd edn (Cambridge, UK ; New York, NY, USA: Cambridge University Press).

128. Le Douarin, N.M., Brito, J.M., and Creuzet, S. (2007). Role of the neural crest in face and brain development. Brain Res Rev *55*, 237-247.

129. Le Douarin, N.M., Couly, G., and Creuzet, S.E. (2012). The neural crest is a powerful regulator of pre-otic brain development. Dev Biol *366*, 74-82.

130. Le Douarin, N.M., Creuzet, S., Couly, G., and Dupin, E. (2004). Neural crest cell plasticity and its limits. Development *131*, 4637-4650.

131. Lee, J.M., Dedhar, S., Kalluri, R., and Thompson, E.W. (2006). The epithelial-mesenchymal transition: new insights in signaling, development, and disease. J Cell Biol *172*, 973-981.

132. Lin, Y.Y., and Gubb, D. (2009). Molecular dissection of Drosophila Prickle isoforms distinguishes their essential and overlapping roles in planar cell polarity. Dev Biol *325*, 386-399.

133. Love, C.E., and Prince, V.E. (2015). Rest represses maturation within migrating facial branchiomotor neurons. Dev Biol *401*, 220-235.

134. Lowery, L.A., and Sive, H. (2004). Strategies of vertebrate neurulation and a re-evaluation of teleost neural tube formation. Mech Dev *121*, 1189-1197.

135. Lumsden, A., Sprawson, N., and Graham, A. (1991). Segmental origin and migration of neural crest cells in the hindbrain region of the chick embryo. Development *113*, 1281-1291.

136. Maguire, L.H., Thomas, A.R., and Goldstein, A.M. (2015). Tumors of the neural crest: Common themes in development and cancer. Dev Dyn *244*, 311-322.

137. Mapp, O.M., Walsh, G.S., Moens, C.B., Tada, M., and Prince, V.E. (2011). Zebrafish Prickle1b mediates facial branchiomotor neuron migration via a farnesylation-dependent nuclear activity. Development *138*, 2121-2132.

138. Mapp, O.M., Wanner, S.J., Rohrschneider, M.R., and Prince, V.E. (2010). Prickle1b mediates interpretation of migratory cues during zebrafish facial branchiomotor neuron migration. Dev Dyn *239*, 1596-1608.

139. Matthews, H.K., Marchant, L., Carmona-Fontaine, C., Kuriyama, S., Larrain, J., Holt, M.R., Parsons, M., and Mayor, R. (2008). Directional migration of neural crest cells in vivo is regulated by Syndecan-4/Rac1 and non-canonical Wnt signaling/RhoA. Development *135*, 1771-1780.

140. May-Simera, H., and Kelley, M.W. (2012). Planar cell polarity in the inner ear. Curr Top Dev Biol *101*, 111-140.

141. Mayor, R., and Carmona-Fontaine, C. (2010). Keeping in touch with contact inhibition of locomotion. Trends Cell Biol *20*, 319-328.

142. Mayor, R., and Theveneau, E. (2014). The role of the non-canonical Wnt-planar cell polarity pathway in neural crest migration. Biochem J *457*, 19-26.

143. McGreevy, E.M., Vijayraghavan, D., Davidson, L.A., and Hildebrand, J.D. (2015). Shroom3 functions downstream of planar cell polarity to regulate myosin II distribution and cellular organization during neural tube closure. Biol Open *4*, 186-196.

144. McLennan, R., Schumacher, L.J., Morrison, J.A., Teddy, J.M., Ridenour, D.A., Box, A.C., Semerad, C.L., Li, H., McDowell, W., Kay, D.*, et al.* (2015a). Neural crest migration is driven by a few trailblazer cells with a unique molecular signature narrowly confined to the invasive front. Development *142*, 2014-2025.

145. McLennan, R., Schumacher, L.J., Morrison, J.A., Teddy, J.M., Ridenour, D.A., Box, A.C., Semerad, C.L., Li, H., McDowell, W., Kay, D.*, et al.* (2015b). VEGF signals induce trailblazer cell identity that drives neural crest migration. Dev Biol *407*, 12-25.

146. McLennan, R., Teddy, J.M., Kasemeier-Kulesa, J.C., Romine, M.H., and Kulesa, P.M. (2010). Vascular endothelial growth factor (VEGF) regulates cranial neural crest migration in vivo. Dev Biol *339*, 114-125.

147. Medina, A., Reintsch, W., and Steinbeisser, H. (2000). Xenopus frizzled 7 can act in canonical and non-canonical Wnt signaling pathways: implications on early patterning and morphogenesis. Mech Dev *92*, 227-237.

148. Mellott, D.O., and Burke, R.D. (2008). Divergent roles for Eph and ephrin in avian cranial neural crest. BMC Dev Biol *8*, 56.

149. Merkel, M., Sagner, A., Gruber, F.S., Etournay, R., Blasse, C., Myers, E., Eaton, S., and Julicher, F. (2014). The balance of prickle/spiny-legs isoforms controls the amount of coupling between core and fat PCP systems. Curr Biol *24*, 2111-2123.

150. Milet, C., and Monsoro-Burq, A.H. (2012). Neural crest induction at the neural plate border in vertebrates. Dev Biol *366*, 22-33.

151. Mitchell, B., Stubbs, J.L., Huisman, F., Taborek, P., Yu, C., and Kintner, C. (2009). The PCP pathway instructs the planar orientation of ciliated cells in the Xenopus larval skin. Curr Biol *19*, 924-929.

152. Miyayama, Y., and Fujimoto, T. (1977). Fine morphological study of neural tube formation in the teleost, Oryzias latipes. Okajimas Folia Anat Jpn *54*, 97-120.

153. Montague, T.G., Cruz, J.M., Gagnon, J.A., Church, G.M., and Valen, E. (2014). CHOPCHOP: a CRISPR/Cas9 and TALEN web tool for genome editing. Nucleic Acids Res *42*, W401-407.

154. Montcouquiol, M., and Kelley, M.W. (2003). Planar and vertical signals control cellular differentiation and patterning in the mammalian cochlea. J Neurosci *23*, 9469-9478.

155. Moore, R., Theveneau, E., Pozzi, S., Alexandre, P., Richardson, J., Merks, A., Parsons, M., Kashef, J., Linker, C., and Mayor, R. (2013). Par3 controls neural crest migration by promoting microtubule catastrophe during contact inhibition of locomotion. Development *140*, 4763-4775.

156. Morriss-Kay, G., Wood, H., and Chen, W.H. (1994). Normal neurulation in mammals. Ciba Found Symp *181*, 51-63; discussion 63-59.

157. Murdoch, J.N., Doudney, K., Paternotte, C., Copp, A.J., and Stanier, P. (2001). Severe neural tube defects in the loop-tail mouse result from mutation of Lpp1, a novel gene involved in floor plate specification. Hum Mol Genet *10*, 2593-2601.

158. Nieto, M.A., Huang, R.Y., Jackson, R.A., and Thiery, J.P. (2016). Emt: 2016. Cell *166*, 21-45.

159. Nishimura, T., Honda, H., and Takeichi, M. (2012). Planar cell polarity links axes of spatial dynamics in neural-tube closure. Cell *149*, 1084-1097.

160. Nishimura, T., and Takeichi, M. (2008). Shroom3-mediated recruitment of Rho kinases to the apical cell junctions regulates epithelial and neuroepithelial planar remodeling. Development *135*, 1493-1502.

161. Noden, D.M., and Schneider, R.A. (2006). Neural crest cells and the community of plan for craniofacial development: historical debates and current perspectives. Adv Exp Med Biol *589*, 1-23.

162. Obholzer, N., Wolfson, S., Trapani, J.G., Mo, W., Nechiporuk, A., Busch-Nentwich, E., Seiler, C., Sidi, S., Sollner, C., Duncan, R.N., *et al.* (2008). Vesicular glutamate transporter 3 is required for synaptic transmission in zebrafish hair cells. J Neurosci *28*, 2110-2118.

163. Olesnicky Killian, E.C., Birkholz, D.A., and Artinger, K.B. (2009). A role for chemokine signaling in neural crest cell migration and craniofacial development. Dev Biol *333*, 161-172.

164. Olofsson, J., Sharp, K.A., Matis, M., Cho, B., and Axelrod, J.D. (2014). Prickle/spiny-legs isoforms control the polarity of the apical microtubule network in planar cell polarity. Development *141*, 2866-2874.

165. Osborne, N.J., Begbie, J., Chilton, J.K., Schmidt, H., and Eickholt, B.J. (2005). Semaphorin/neuropilin signaling influences the positioning of migratory neural crest cells within the hindbrain region of the chick. Dev Dyn *232*, 939-949.

166. Ossipova, O., Kim, K., Lake, B.B., Itoh, K., Ioannou, A., and Sokol, S.Y. (2014). Role of Rab11 in planar cell polarity and apical constriction during vertebrate neural tube closure. Nat Commun *5*, 3734.

167. Ossipova, O., Kim, K., and Sokol, S.Y. (2015). Planar polarization of Vangl2 in the vertebrate neural plate is controlled by Wnt and Myosin II signaling. Biol Open *4*, 722-730.

168. Pan, X., Sittaramane, V., Gurung, S., and Chandrasekhar, A. (2014). Structural and temporal requirements of Wnt/PCP protein Vangl2 function for convergence and extension movements and facial branchiomotor neuron migration in zebrafish. Mech Dev *131*, 1-14.

169. Peeters, M.C., Viebahn, C., Hekking, J.W., and van Straaten, H.W. (1998). Neurulation in the rabbit embryo. Anat Embryol (Berl) *197*, 167-175.

170. Peng, Y., and Axelrod, J.D. (2012). Asymmetric protein localization in planar cell polarity: mechanisms, puzzles, and challenges. Curr Top Dev Biol *101*, 33-53.

171. Piloto, S., and Schilling, T.F. (2010). Ovo1 links Wnt signaling with N-cadherin localization during neural crest migration. Development *137*, 1981-1990.

172. Podleschny, M., Grund, A., Berger, H., Rollwitz, E., and Borchers, A. (2015). A PTK7/Ror2 Co-Receptor Complex Affects Xenopus Neural Crest Migration. PLoS One *10*, e0145169.

173. Powell, D.R., Williams, J.S., Hernandez-Lagunas, L., Salcedo, E., O'Brien, J.H., and Artinger, K.B. (2015). Cdon promotes neural crest migration by regulating N-cadherin localization. Dev Biol *407*, 289-299.

174. Prince, V.E., Moens, C.B., Kimmel, C.B., and Ho, R.K. (1998). Zebrafish hox genes: expression in the hindbrain region of wild-type and mutants of the segmentation gene, valentino. Development *125*, 393-406.

175. Qu, Y., Glasco, D.M., Zhou, L., Sawant, A., Ravni, A., Fritzsch, B., Damrau, C., Murdoch, J.N., Evans, S., Pfaff, S.L.*, et al.* (2010). Atypical cadherins Celsr1-3 differentially regulate migration of facial branchiomotor neurons in mice. J Neurosci *30*, 9392-9401.

176. Qureshi, I.A., and Mehler, M.F. (2009). Regulation of non-coding RNA networks in the nervous system--what's the REST of the story? Neurosci Lett *466*, 73-80.

177. Reichenbach, A., Schaaf, P., and Schneider, H. (1990). Primary neurulation in teleosts--evidence for epithelial genesis of central nervous tissue as in other vertebrates. J Hirnforsch *31*, 153-158.

178. Richardson, J., Gauert, A., Briones Montecinos, L., Fanlo, L., Alhashem, Z.M., Assar, R., Marti, E., Kabla, A., Hartel, S., and Linker, C. (2016). Leader Cells Define Directionality of Trunk, but Not Cranial, Neural Crest Cell Migration. Cell Rep *15*, 2076-2088.

179. Rida, P.C., and Chen, P. (2009). Line up and listen: Planar cell polarity regulation in the mammalian inner ear. Semin Cell Dev Biol *20*, 978-985.

180. Rohrschneider, M.R., Elsen, G.E., and Prince, V.E. (2007). Zebrafish Hoxb1a regulates multiple downstream genes including prickle1b. Dev Biol *309*, 358-372.

181. Rossi, A., Kontarakis, Z., Gerri, C., Nolte, H., Holper, S., Kruger, M., and Stainier, D.Y. (2015). Genetic compensation induced by deleterious mutations but not gene knockdowns. Nature *524*, 230-233.

182. Roszko, I., Sawada, A., and Solnica-Krezel, L. (2009). Regulation of convergence and extension movements during vertebrate gastrulation by the Wnt/PCP pathway. Semin Cell Dev Biol *20*, 986-997.

183. Ruf, R.G., Xu, P.X., Silvius, D., Otto, E.A., Beekmann, F., Muerb, U.T., Kumar, S., Neuhaus, T.J., Kemper, M.J., Raymond, R.M., Jr., *et al.* (2004). SIX1 mutations cause branchio-oto-renal syndrome by disruption of EYA1-SIX1-DNA complexes. Proc Natl Acad Sci U S A *101*, 8090-8095.

184. Saito, D., Takase, Y., Murai, H., and Takahashi, Y. (2012). The dorsal aorta initiates a molecular cascade that instructs sympatho-adrenal specification. Science *336*, 1578-1581.

185. Sauka-Spengler, T., and Bronner-Fraser, M. (2008). A gene regulatory network orchestrates neural crest formation. Nat Rev Mol Cell Biol *9*, 557-568.

186. Savagner, P. (2001). Leaving the neighborhood: molecular mechanisms involved during epithelial-mesenchymal transition. Bioessays *23*, 912-923.

187. Savagner, P. (2010). The epithelial-mesenchymal transition (EMT) phenomenon. Ann Oncol *21 Suppl 7*, vii89-92.

188. Scarpa, E., Szabo, A., Bibonne, A., Theveneau, E., Parsons, M., and Mayor, R. (2015). Cadherin Switch during EMT in Neural Crest Cells Leads to Contact Inhibition of Locomotion via Repolarization of Forces. Dev Cell *34*, 421-434.

189. Schilling, T.F., and Kimmel, C.B. (1994). Segment and cell type lineage restrictions during pharyngeal arch development in the zebrafish embryo. Development *120*, 483-494.

190. Schmitz, B., Papan, C., and Campos-Ortega, J.A. (1993). Neurulation in the anterior trunk region of the zebrafish Brachydanio rerio. Roux Arch Dev Biol *202*, 250-259.

191. Schoenwolf, G.C. (1984). Histological and ultrastructural studies of secondary neurulation in mouse embryos. Am J Anat *169*, 361-376.

192. Schoenwolf, G.C., and Delongo, J. (1980). Ultrastructure of secondary neurulation in the chick embryo. Am J Anat *158*, 43-63.

193. Schoenwolf, G.C., and Larsen, W.J. (2009). Larsen's human embryology, 4th edn (Philadelphia: Churchill Livingstone/Elsevier).

194. Sepich, D.S., Usmani, M., Pawlicki, S., and Solnica-Krezel, L. (2011). Wnt/PCP signaling controls intracellular position of MTOCs during gastrulation convergence and extension movements. Development *138*, 543-552.

195. Sharp, K.A., and Axelrod, J.D. (2016). Prickle isoforms control the direction of tissue polarity by microtubule independent and dependent mechanisms. Biol Open *5*, 229-236.

196. Shiau, C.E., and Bronner-Fraser, M. (2009). N-cadherin acts in concert with Slit1-Robo2 signaling in regulating aggregation of placode-derived cranial sensory neurons. Development *136*, 4155-4164.

197. Shnitsar, I., and Borchers, A. (2008). PTK7 recruits dsh to regulate neural crest migration. Development *135*, 4015-4024.

198. Shulman, J.M., Perrimon, N., and Axelrod, J.D. (1998). Frizzled signaling and the developmental control of cell polarity. Trends Genet *14*, 452-458.

199. Sienknecht, U.J., Anderson, B.K., Parodi, R.M., Fantetti, K.N., and Fekete, D.M. (2011). Non-cell-autonomous planar cell polarity propagation in the auditory sensory epithelium of vertebrates. Dev Biol *352*, 27-39.

200. Simoes-Costa, M., and Bronner, M.E. (2015). Establishing neural crest identity: a gene regulatory recipe. Development *142*, 242-257.

201. Simoes-Costa, M., Tan-Cabugao, J., Antoshechkin, I., Sauka-Spengler, T., and Bronner, M.E. (2014). Transcriptome analysis reveals novel players in the cranial neural crest gene regulatory network. Genome Res *24*, 281-290.

202. Simoes-Costa, M.S., McKeown, S.J., Tan-Cabugao, J., Sauka-Spengler, T., and Bronner, M.E. (2012). Dynamic and differential regulation of stem cell factor FoxD3 in the neural crest is Encrypted in the genome. PLoS Genet *8*, e1003142.

203. Sittaramane, V., Pan, X., Glasco, D.M., Huang, P., Gurung, S., Bock, A., Li, S., Wang, H., Kawakami, K., Matise, M.P., *et al.* (2013). The PCP protein Vangl2 regulates migration of hindbrain motor neurons by acting in floor plate cells, and independently of cilia function. Dev Biol *382*, 400-412.

204. Smith, J.L., and Schoenwolf, G.C. (1991). Further evidence of extrinsic forces in bending of the neural plate. J Comp Neurol *307*, 225-236.

205. Solomon, K.S., Kudoh, T., Dawid, I.B., and Fritz, A. (2003). Zebrafish foxi1 mediates otic placode formation and jaw development. Development *130*, 929-940.

206. Steventon, B., Mayor, R., and Streit, A. (2014). Neural crest and placode interaction during the development of the cranial sensory system. Dev Biol *389*, 28-38.

207. Stewart, R.A., Arduini, B.L., Berghmans, S., George, R.E., Kanki, J.P., Henion, P.D., and Look, A.T. (2006). Zebrafish foxd3 is selectively required for neural crest specification, migration and survival. Dev Biol *292*, 174-188.

208. Stockinger, P., Maitre, J.L., and Heisenberg, C.P. (2011). Defective neuroepithelial cell cohesion affects tangential branchiomotor neuron migration in the zebrafish neural tube. Development *138*, 4673-4683.

209. Strahle, U., and Blader, P. (1994). Early neurogenesis in the zebrafish embryo. FASEB J *8*, 692-698.

210. Strutt, D.I. (2001). Asymmetric localization of frizzled and the establishment of cell polarity in the Drosophila wing. Mol Cell *7*, 367-375.

211. Strutt, H., and Strutt, D. (2009). Asymmetric localisation of planar polarity proteins: Mechanisms and consequences. Semin Cell Dev Biol *20*, 957-963.

212. Strutt, H., and Strutt, D. (2015). Planar polarity: forcing cells into line. Curr Biol *25*, R1032-R1034.

213. Strutt, H., Thomas-MacArthur, V., and Strutt, D. (2013). Strabismus promotes recruitment and degradation of farnesylated prickle in Drosophila melanogaster planar polarity specification. PLoS Genet *9*, e1003654.

214. Szabo, A., and Mayor, R. (2016). Modelling collective cell migration of neural crest. Curr Opin Cell Biol *42*, 22-28.

215. Szabo, A., Melchionda, M., Nastasi, G., Woods, M.L., Campo, S., Perris, R., and Mayor, R. (2016). In vivo confinement promotes collective migration of neural crest cells. J Cell Biol *213*, 543-555.

216. Tada, M., and Smith, J.C. (2000). Xwnt11 is a target of Xenopus Brachyury: regulation of gastrulation movements via Dishevelled, but not through the canonical Wnt pathway. Development *127*, 2227-2238.

217. Tahtakran, S.A., and Selleck, M.A. (2003). Ets-1 expression is associated with cranial neural crest migration and vasculogenesis in the chick embryo. Gene Expr Patterns *3*, 455-458.

218. Takeuchi, M., Nakabayashi, J., Sakaguchi, T., Yamamoto, T.S., Takahashi, H., Takeda, H., and Ueno, N. (2003). The prickle-related gene in vertebrates is essential for gastrulation cell movements. Curr Biol *13*, 674-679.

219. Taneyhill, L.A., and Schiffmacher, A.T. (2017). Should I stay or should I go? Cadherin function and regulation in the neural crest. Genesis *55*.

220. Tawk, M., Araya, C., Lyons, D.A., Reugels, A.M., Girdler, G.C., Bayley, P.R., Hyde, D.R., Tada, M., and Clarke, J.D. (2007). A mirror-symmetric cell division that orchestrates neuroepithelial morphogenesis. Nature *446*, 797-800.

221. Taylor, J., Abramova, N., Charlton, J., and Adler, P.N. (1998). Van Gogh: a new Drosophila tissue polarity gene. Genetics *150*, 199-210.

222. Theveneau, E., Marchant, L., Kuriyama, S., Gull, M., Moepps, B., Parsons, M., and Mayor, R. (2010). Collective chemotaxis requires contact-dependent cell polarity. Dev Cell *19*, 39-53.

223. Theveneau, E., and Mayor, R. (2011a). Can mesenchymal cells undergo collective cell migration? The case of the neural crest. Cell Adh Migr *5*, 490-498.

224. Theveneau, E., and Mayor, R. (2011b). Collective cell migration of the cephalic neural crest: the art of integrating information. Genesis *49*, 164-176.

225. Theveneau, E., and Mayor, R. (2012). Neural crest delamination and migration: from epithelium-to-mesenchyme transition to collective cell migration. Dev Biol *366*, 34-54.

226. Theveneau, E., Steventon, B., Scarpa, E., Garcia, S., Trepat, X., Streit, A., and Mayor, R. (2013). Chase-and-run between adjacent cell populations promotes directional collective migration. Nat Cell Biol *15*, 763-772.

227. Thiery, J.P., and Sleeman, J.P. (2006). Complex networks orchestrate epithelial-mesenchymal transitions. Nat Rev Mol Cell Biol *7*, 131-142.

228. Thompson, E.W., and Williams, E.D. (2008). EMT and MET in carcinoma--clinical observations, regulatory pathways and new models. Clin Exp Metastasis *25*, 591-592.

229. Torban, E., Patenaude, A.M., Leclerc, S., Rakowiecki, S., Gauthier, S., Andelfinger, G., Epstein, D.J., and Gros, P. (2008). Genetic interaction between members of the Vangl family causes neural tube defects in mice. Proc Natl Acad Sci U S A *105*, 3449-3454.

230. Trainor, P.A. (2010). Craniofacial birth defects: The role of neural crest cells in the etiology and pathogenesis of Treacher Collins syndrome and the potential for prevention. Am J Med Genet A *152A*, 2984-2994.

231. Trainor, P.A., Sobieszczuk, D., Wilkinson, D., and Krumlauf, R. (2002). Signalling between the hindbrain and paraxial tissues dictates neural crest migration pathways. Development *129*, 433-442.

232. Tree, D.R., Shulman, J.M., Rousset, R., Scott, M.P., Gubb, D., and Axelrod, J.D. (2002). Prickle mediates feedback amplification to generate asymmetric planar cell polarity signaling. Cell *109*, 371-381.

233. Usui, T., Shima, Y., Shimada, Y., Hirano, S., Burgess, R.W., Schwarz, T.L., Takeichi, M., and Uemura, T. (1999). Flamingo, a seven-pass transmembrane cadherin, regulates planar cell polarity under the control of Frizzled. Cell *98*, 585-595.

234. Vallin, J., Thuret, R., Giacomello, E., Faraldo, M.M., Thiery, J.P., and Broders, F. (2001). Cloning and characterization of three Xenopus slug promoters reveal direct regulation by Lef/beta-catenin signaling. J Biol Chem *276*, 30350-30358.

235. Veeman, M.T., Slusarski, D.C., Kaykas, A., Louie, S.H., and Moon, R.T. (2003). Zebrafish prickle, a modulator of noncanonical Wnt/Fz signaling, regulates gastrulation movements. Curr Biol *13*, 680-685.

236. Vladar, E.K., Bayly, R.D., Sangoram, A.M., Scott, M.P., and Axelrod, J.D. (2012). Microtubules enable the planar cell polarity of airway cilia. Curr Biol *22*, 2203-2212.

237. Wada, H., Tanaka, H., Nakayama, S., Iwasaki, M., and Okamoto, H. (2006). Frizzled3a and Celsr2 function in the neuroepithelium to regulate migration of facial motor neurons in the developing zebrafish hindbrain. Development *133*, 4749-4759.

238. Walker, M.B., and Trainor, P.A. (2006). Craniofacial malformations: intrinsic vs extrinsic neural crest cell defects in Treacher Collins and 22q11 deletion syndromes. Clin Genet *69*, 471-479.

239. Wallingford, J.B., and Harland, R.M. (2001). Xenopus Dishevelled signaling regulates both neural and mesodermal convergent extension: parallel forces elongating the body axis. Development *128*, 2581-2592.

240. Wallingford, J.B., Rowning, B.A., Vogeli, K.M., Rothbacher, U., Fraser, S.E., and Harland, R.M. (2000). Dishevelled controls cell polarity during Xenopus gastrulation. Nature *405*, 81-85.

241. Wang, J., Hamblet, N.S., Mark, S., Dickinson, M.E., Brinkman, B.C., Segil, N., Fraser, S.E., Chen, P., Wallingford, J.B., and Wynshaw-Boris, A. (2006). Dishevelled genes mediate a conserved mammalian PCP pathway to regulate convergent extension during neurulation. Development *133*, 1767-1778.

242. Wanner, S.J., and Prince, V.E. (2013). Axon tracts guide zebrafish facial branchiomotor neuron migration through the hindbrain. Development *140*, 906-915.

243. Weston, J.A., and Thiery, J.P. (2015). Pentimento: Neural Crest and the origin of mesectoderm. Dev Biol *401*, 37-61.

244. Wheelock, M.J., Shintani, Y., Maeda, M., Fukumoto, Y., and Johnson, K.R. (2008). Cadherin switching. J Cell Sci *121*, 727-735.

245. Wilson, A.L., Shen, Y.C., Babb-Clendenon, S.G., Rostedt, J., Liu, B., Barald, K.F., Marrs, J.A., and Liu, Q. (2007). Cadherin-4 plays a role in the development of zebrafish cranial ganglia and lateral line system. Dev Dyn *236*, 893-902.

246. Wong, L.L., and Adler, P.N. (1993). Tissue polarity genes of Drosophila regulate the subcellular location for prehair initiation in pupal wing cells. J Cell Biol *123*, 209-221.

247. Wurdak, H., Ittner, L.M., and Sommer, L. (2006). DiGeorge syndrome and pharyngeal apparatus development. Bioessays *28*, 1078-1086.

248. Yen, W.W., Williams, M., Periasamy, A., Conaway, M., Burdsal, C., Keller, R., Lu, X., and Sutherland, A. (2009). PTK7 is essential for polarized cell motility and convergent extension during mouse gastrulation. Development *136*, 2039-2048.

249. Yin, C., Kiskowski, M., Pouille, P.A., Farge, E., and Solnica-Krezel, L. (2008). Cooperation of polarized cell intercalations drives convergence and extension of presomitic mesoderm during zebrafish gastrulation. J Cell Biol *180*, 221-232.

250. Yu, H.H., and Moens, C.B. (2005). Semaphorin signaling guides cranial neural crest cell migration in zebrafish. Dev Biol *280*, 373-385.

251. Zadran, S., Arumugam, R., Herschman, H., Phelps, M.E., and Levine, R.D. (2014). Surprisal analysis characterizes the free energy time course of cancer cells undergoing epithelial-to-mesenchymal transition. Proc Natl Acad Sci U S A *111*, 13235-13240.

252. Zallen, J.A. (2007). Planar polarity and tissue morphogenesis. Cell *129*, 1051-1063.

253. Zhu, H., and Owen, M.R. (2013). Damped propagation of cell polarization explains distinct PCP phenotypes of epithelial patterning. Sci Rep *3*, 2528.